A DISSERTATION FOR THE DEGREE OF DOCTOR OF PHILOSOPHY

Molecular mechanisms of *Phytophthora infestans* RXLR effectors in plant immunity

감자역병균 RXLR 이펙터의 식물 면역 반응에 대한 작용기작 연구

AUGUST 2023

SOEUI LEE

MAJOR IN HORTICULTURAL SCIENCE AND BIOTECHNOLOGY

DEPARTMENT OF AGRICULTURE, FORESTY AND BIORESOURCES

COLLEGE OF AGRICULTURE AND LIFE SCIENCES

THE GRADUATE SCHOOL OF SEOUL NATIONAL UNIVERSITY

Molecular mechanisms of *Phytophthora infestans* RXLR effectors in plant immunity

UNDER THE DIRECTION OF DR. DOIL CHOI
SUBMITTED TO THE FACULTY OF THE GRADUATE SCHOOL OF SEOUL NATIONAL UNIVERSITY

BY
SOEUI LEE

MAJOR IN HORTICULTURAL SCIENCE AND BIOTECHNOLOGY
DEPARTMENT OF AGRICULTURE, FORESTY AND BIORESOURCES

AUGUST 2023

APPROVED AS A QUALIFIED DISSERTATION OF SOEUI LEE
FOR THE DEGREE OF DOCTOR OF PHILOSOPHY
BY THE COMMITTEE MEMBERS

CHAIRMAN	**Cecile Segonzac, Ph.D.**
VICE-CHAIRMAN	**Doil Choi, Ph.D.**
MEMBER	**Sun Tae Kim, Ph.D.**
MEMBER	**Joo Hyun Lee, Ph.D.**
MEMBER	**Hyun Ah Lee, Ph.D.**

Molecular mechanisms of *Phytophthora infestans* RXLR effectors in plant immunity

SOEUI LEE

Department of Agriculture, Foresty and Bioresources,

Seoul National University

ABSTRACT

Plants have evolved a multilayered immune system capable of recognizing most pathogen classes. To overcome this, pathogenic organisms have evolved virulence factors known as effectors, some of which are delivered inside host cells to interfere with immune perception and take nutrients, eventually facilitate colonization. As hemibiotrophic pathogen, *Phytophthora infestans* delivers RXLR effector proteins into host cells for its biphasic infection cycle. The regulation of infection stage and detailed mechanisms that modulate host defense are still unclear, although effector proteins are thought to play a key role. In this study, nucleolar inflation was observed in host *N. benthamiana*

during the transition between *P. infestans* infection stages. Similary, the nucleolar localized *P. infestans* RXLR effector Pi23226 causes nucleolar inflation and triggers strong cell death in *N. benthamiana*. In nucleolus, RNA pull down showed that Pi23226 directly binds to 25S rRNA precursors and inhibits the 27S pre-rRNA processing leading to nucleolar stress. Moreover, Pi23226 also inhibits the global protein translation by binding with ribosome proteins. Despite of cell death phenotype, Pi23226 enhances the *P. infestans* pathogenicity, implying that effector activities and cell death induced by Pi23226 positive effect on pathogen infection. Meanwhile, at the plasma membrane, transient elevation of cytosolic Ca^{2+} upon pathogen recognition in the early infection stage is essential for plant pathogen-associated molecular pattern (PAMP)-triggered immunity (PTI). Through overexpression assay, the RXLR effector Pi20300 (AVRblb2) showed strong inhibition of PAMP-induced Ca^{2+} influx and downstream PTI response. Based on the interactor screening of Pi20300, a subset of *N. benthamiana* plasma membrane-localized cyclic nucleotide-gated channels (CNGC) 18/19/20 was identified as a target of Pi20300, suggesting that Pi20300 interacts with NbCNGCs to regulate their activity at the plasma membrane. Moreover, *in vivo* and *in vitro* assays confirmed that calmodulin (CaM) and calmodulin-like protein (CML) are required for Pi20300-NbCNGC interaction, forming complex to regulate

CNGC activity. In addition, NbCNGC18 forms heteromers with other NbCNGCs to generate Ca^{2+} influx in response to PAMP recognition. Consequently, gene silencing assay confirmed that full effector activity of Pi20300 is dependent on multiple NbCNGCs. Although further investigation is required, our findings improve our understanding about various type of effector's action mechanisms for manipulating host immune system.

Keywords: *P. infestans*, effector, nucleolar, calmodulin, cyclic-nucleotide gated channel

Student number: 2016-32844

CONTENTS

LIST OF TABLES

CHAPTER 1

CHAPTER 2

LIST OF FIGURES

CHAPTER 1

CHAPTER 2

LIST OF ABBREVIATIONS

CaM	Calmodulin
CHX	cycloheximide
CML	Calmodulin-like protein
CNGC	Cyclic nucleotide-gated channel
ETI	Effector-triggered immunity
HR	Hypersensitive response
MAPK	Mitogen-activated protein kinase
PAMP	Pathogen-associated molecular pattern
PTI	PAMP-triggered immunity
PRR	Pattern recognition receptor
RXLR	Arg-any amino acid-Leu-Arg
TOE	Transient overexpression
uHPLC	Ultra-High Performance Liquid Chromatography

Literature review

Plant immune system

Plants encounter a wide range of microbial pathogens throughout their lifetime. In order to respond to various pathogenic microorganisms, plants have developed an innate immune system based on the mechanism induced by the microbes and exhibit defense responses (Boller & Felix, 2009; Jones & Dangl, 2006). Plants have a sophisticated immune response system that can be constitutive or induced by a pathogen attack (Pieterse et al., 2014).

The pathogens that successfully overcome these barriers have to encounter the efficient plant immune system terminating the progression of microbial colonization (Boller & Felix, 2009; Jones & Dangl, 2006). Initially, plants utilize the cell surface-anchored pattern recognition receptors (PRRs) to recognize the microbe or pathogen or damage-associated molecular patterns (MAMP/PAMP/DAMP) and trigger a set of responses (Upson et al., 2018). This leads to the activation of defenses against invading pathogens, known as pattern triggered immunity (PTI) and thus to limit pathogen growth (Melotto et al., 2006).

To counteract PTI, pathogen releases effector protein into the host cell to inhibit host defense responses and promote pathogenesis. Pathogen effectors

have been shown by many studies to be important pathogenic factors, suppressing PTI signaling or preventing detection by the host (Rocafort et al., 2020; Xin et al., 2018). In turn, as pathogens evolved effectors that inhibited the first layer of immunity, plants evolved nucleotide-binding domain and leucine-rich repeat protein (NLR) receptors that recognized the effectors, thus leading to a second layer of immunity (ETI) (Jones & Dangl, 2006). The activation of these immune responses triggers a cascade of complex signaling events, leading to suppression of pathogen attacks.

Although the two classes of immune receptors are involved with different activation mechanisms, increasing evidence suggests that PTI and ETI are functionally linked with many similar downstream responses (Cui et al., 2015). For example, PTI and ETI lead to a number of overlapping downstream events such as mitogen-activated protein kinase (MAPK) cascades, calcium flux, nitric oxide and ROS production, transcriptional reprograming, alteration in membrane trafficking and phytohormone signaling, suggesting several linkage points between two signaling cascades (Thulasi Devendrakumar et al., 2018; Tsuda & Katagiri, 2010).

Molecular mechanisms of pathogen effectors during infection

Microbial plant pathogens have adapted to colonize plants using effectors

as their molecular weapons. Intracellular effectors are delivered by the pathogens into the host cell cytoplasm where they interfere with normal plant physiology (Galan & Wolf-Watz, 2006).

In order to facilitate infection, plant pathogens secrete numerous effector proteins directly or indirectly into the plant cytoplasm (McCann & Guttman, 2008; Panstruga & Dodds, 2009). Most of typical effectors are proteins but also include small molecules that alter the structure and function of host cells (Collemare et al., 2019). The effectors of filamentous pathogens such as fungi or oomycetes contain canonical secretion signal to translocate in their host cell (Whisson et al., 2007). In case of the oomycete pathogen *Phytophthora infestans*, they have RLXR effector family candidates in their genome, named for the presence of a conserved arginine-X-leucine-arginine motif. Many RXLR genes were detected during early stages of infection by *P. infestans*, indicating that they translocated inside the host cell and may act in concert to suppress host immunity for the successful infection (Schornack et al., 2009).

During pathogen invasion, PAMPs and DAMPs can be recognized by plant PRRs and induce host immunity. Consequently, pathogens secrete a range of different effectors to suppress PTI. For example, maintaining cell wall integrity and molecular status is a conserved strategy for pathogens. In this situation, effectors target receptor-like kinase and downstream signaling

molecules (Gimenez-Ibanez et al., 2009; Zeng & He, 2010) or scavenge free chitinous oligosaccharides in the apoplast to avoid triggering PTI (De Jonge et al., 2010; Li et al., 2020).

Moreover, effector proteins can interfere with host cell physiological activities. Effectors localized in host nucleus function as transcription factors or regulate RNA degradation to reprogram the host defense pathway (Kay & Bonas, 2009; Sun et al., 2015). There are also some effectors that target functional proteins in the host plant cytosol, causing functional abnormalities and thus pathogenic effects, for example, alterations of autophagy and protein-ubiquitin systems (Banfield, 2015; Langin et al., 2020) or protein localization (Qi et al., 2019).

In plant-pathogen interactions, recognition of pathogens by NLRs and PRRs generates signals to implement systemic resistance that leads to HR, and eventually restricts the pathogen growth (Coll et al., 2011). But some effectors of biotrophic or hemibiotrophic pathogen could suppress HR cell death to promote infection (Koeck et al., 2011). Therefore, pathogen effectors act in multiple ways on different targets, thus promoting pathogen infection.

Importance of nucleus and nucleolus in plant immunity

In plants, several studies on the localization of R proteins, pathogen

effectors and host factors have revealed that dynamic responses of multiple cellular components are required for the recognition and signaling events during defense (Deslandes & Rivas, 2011; Liu et al., 2009; Wiermer et al., 2010). In particular, a large number of effector proteins from different pathogenic microorganisms, including viruses, bacteria, oomycetes and fungi are translocated into the nucleus of host cells. This observation suggests the crucial role played by nuclear dynamics, and nucleo-cytoplasmic protein trafficking during pathogen infection (Noel et al., 2013).

The fact that a significant number of effector proteins is translocated into the host cell nucleus, suggests that effectors may manipulate host transcription or directly target essential nuclear host components for the benefit of the pathogen (Quentin et al., 2013). Along these lines, it has been proposed that some effectors affect histone modification and chromatin remodeling, regulating essential cellular processes such as DNA replication, DNA repair, and transcription (Clapier & Cairns, 2009; Kay & Bonas, 2009). Other nuclear effectors target transcription factors or even function as transcription factor themselves (Qi et al., 2019; Yang et al., 2006). Moreover, inhibition of nucleo-cytoplasmic trafficking process by pathogen effectors is also reported (Kanneganti et al., 2007; Palma et al., 2005).

In nucleus, the nucleolus is the largest structure where ribosomal RNAs

(rRNAs) are synthesized and assembled with the rRNA-ribosomal protein subunits (Boisvert et al., 2007; Olson, 2006). The nucleolus also reported as cellular component that is involved in plant immunity. Recently, several studies about virus, bacterial and filamentous effector proteins were reported that they target the nucleolus proteins during infection and subvert the host cell for enhance susceptibility (Caillaud et al., 2013; Rajamäki & Valkonen, 2009; Seo et al., 2019). But their detail mechanisms in nucleolar during infection largely unexplored.

Ca^{2+} signaling during pathogen infection

One of the common and early cellular responses in plant immunity is the transient increase of cytosolic calcium concentration ($[Ca^{2+}]$cyt). Plants generate Ca^{2+} fluxes upon PAMP perception, along with decoding systems that transduce downstream signaling events during pathogen invasion (Grant et al., 2000).

Theses Ca^{2+} signaling downstream events are largely facilitated by proteins that contain a conserved EF-hand domain. The activation of these proteins through Ca^{2+} binding leads to events such as altered gene expression and regulation of the plant immune responses (Marcec et al., 2019).

Recent studies revealed that pathogen-induced Ca^{2+} influx is decoded by

various Ca^{2+}-binding proteins. Among them, calmodulin (CaM) is a conserved eukaryotic protein that has four EF-hand motifs (Gifford et al., 2007). Upon Ca^{2+} binding, CaM regulates the activity and protein-protein interactions of a range of targets such as CaM-dependent kinases and transcription factors. Other Ca^{2+} sensors including CaM-like proteins (CMLs), calcineurin B-like proteins (CBLs), and Ca^{2+} dependent protein kinases (CPKs) are also primary Ca^{2+} sensors and have been reported to be involved in PTI and systemic acquired resistance (Marcec et al., 2019).

The elevation of cytosolic Ca^{2+} upon PAMP perception is mainly conducted by plasma membrane localized Ca^{2+} channels. In Arabidopsis, the Ca^{2+} influx to the cytosol related to plant wounding and immune signaling occurs through Ca^{2+}-permeable channels, such as the voltage-gated two pore channel 1 (TPC1), cyclic nucleotide-gated channels (CNGCs), and GLRs (Tian et al., 2019).

CNGCs are non-selective cation channels, some of which have been shown to be engaged in directing the Ca^{2+} current inward across the plasma membrane to the cytosol for plant immune signaling. For example, *dnd1* and *dnd2*, the mutants of AtCNGC2 and AtCNGC4, respectively, exhibited autoimmune phenotypes, in which the PAMP-induced Ca^{2+} response was weakened (Clough et al., 2000). These observations suggest that AtCNGCs

are involved in the formation of a Ca^{2+} signature for plant defense responses. Moreover, AtCNGC2 and AtCNGC4 form heteromeric channels that are important for proper PRR signaling and required for defense response (Tian et al., 2019). Further, heteromeric channels AtCNGC19/20 and AtCNGC11/12 are also reported to be involved in plant defense responses, suggesting multiple channels acting in a coordinated fashion to tailor the Ca^{2+} signature (Jogawat et al., 2020; Yuan, Ngou, et al., 2021).

Hypersensitive response during pathogen infection

Pathogen recognition by the plant immune system activates defense signals that often induction of a hypersensitive response (HR). An array of pathogenic elicitors including PAMPs and effectors can be recognized by plant specific receptors to activate plant immunity. The number of cytoplasmic NLRs recognize effector molecules and initiate defense signaling cascades that often leads to HR cell death (Jones & Dangl, 2006). Moreover, some secreted proteins were proved as an elicitor that can trigger PTI response and induce HR cell death (Nie et al., 2019; Seidl & Van den Ackerveken, 2019). This type of HR cell death can be concomitant with series of immune responses including calcium influxes, oxidative bursts, mitogen-activated protein kinases, and transcriptional reprogramming. In addition, HR cell death could

be explained as a result of surpassing certain signaling thresholds (Adachi & Tsuda, 2019).

However, HR plays differential roles in defense responses based on the life style of pathogens. The hemibiotrophic pathogen *P. infestans* facilitates the development of infection by secreting a cell death suppressor during its biotrophic phase and producing cell death inducers in its necrotrophic phase (Kelley et al., 2010). The virulence of *Botrytis cinerea*, a necrotrophic pathogen, is conducted by a number of lytic enzymes, toxins, and high levels of reactive oxygen species and necrosis-inducing factors (Choquer et al., 2007). Thus, HR cell death resists biotroph infection by disconnecting nutrient supplies resulting in limiting pathogen growth, however, it may provide growth substrates for invasive necrotrophs (Choquer et al., 2007).

Because induced HR cell death was frequently induced by elicitors from adapted biotroph or hemibiotroph pathogens, HR cell death is often considered as an immune strategy to inhibit pathogen infection However, it has also been reported that HR cell death does not have any impact on the growth of pathogens (Coll et al., 2010; Lapin et al., 2019; Menna et al., 2015), indicating that HR cell death necessarily indicates resistance to pathogen infection.

REFERENCES

Adachi, H., & Tsuda, K. (2019). Convergence of cell-surface and intracellular immune receptor signalling. *The New Phytologist*, *221*(4), 1676-1678.

Banfield, M. J. (2015). Perturbation of host ubiquitin systems by plant pathogen/pest effector proteins. *Cell Microbiol.*, *17*(1), 18-25.

Berridge, M. J., Lipp, P., & Bootman, M. D. (2000). The versatility and universality of calcium signalling. *Nature reviews Mol. Cell. Biol.*, *1*(1), 11-21.

Boisvert, F. M., van Koningsbruggen, S., Navascues, J., & Lamond, A. I. (2007). The multifunctional nucleolus. *Nat. Rev. Mol. Cell. Biol.*, *8*(7), 574-585.

Boller, T., & Felix, G. (2009). A renaissance of elicitors: perception of microbe-associated molecular patterns and danger signals by pattern-recognition receptors. *Annu. Rev. Plant Biol.*, *60*, 379-406.

Bozkurt, T. O., Schornack, S., Win, J., Shindo, T., Ilyas, M., Oliva, R., Cano, L. M., Jones, A. M., Huitema, E., van der Hoorn, R. A., & Kamoun, S. (2011). Phytophthora infestans effector AVRblb2 prevents secretio n of a plant immune protease at the haustorial interface. *Proc. Natl. Acad. Sci. U S A*, *108*(51), 20832-20837.

Brost, C., Studtrucker, T., Reimann, R., Denninger, P., Czekalla, J., Krebs, M., Fabry, B., Schumacher, K., Grossmann, G., & Dietrich, P. (2019). Multiple cyclic nucleotide-gated channels coordinate calcium oscillations and polar growth of root hairs. *Plant J.*, *99*(5), 910-923.

Caillaud, M. C., Asai, S., Rallapalli, G., Piquerez, S., Fabro, G., & Jones, J. D. (2013). A downy mildew effector attenuates salicylic acid-triggered immunity in Arabidopsis by interacting with the host mediator complex. *PLoS Biol.*, *11*(12), e1001732.

Chin, K., DeFalco, T. A., Moeder, W., & Yoshioka, K. (2013). The Arabidopsis cyclic nucleotide-gated ion channels AtCNGC2 and AtCNGC4 work in the same signaling pathway to regulate pathogen defense and floral transition. *Plant Physiol.*, *163*(2), 611-624.

Choquer, M., Fournier, E., Kunz, C., Levis, C., Pradier, J. M., Simon, A., & Viaud, M. (2007). Botrytis cinerea virulence factors: new insights into a necrotrophic and polyphageous pathogen. *FEMS Microbiol. Lett.*, *277*(1), 1-10.

Chung, E., Seong, E., Kim, Y. C., Chung, E. J., Oh, S. K., Lee, S., & Choi, D. (2004). A Method of High Frequency Virus-induced Gene Silencing in Chili Pepper. *Mol. Cells*, *17*(2), 377-380.

Clapier, C. R., & Cairns, B. R. (2009). The biology of chromatin remodeling complexes. *Annu. Rev. Biochem.*, *78*, 273-304.

Clough, S. J., Fengler, K. A., Yu, I. C., Lippok, B., Smith Jr, R. K., & Bent, A. F. (2000). The Arabidopsis dnd1 "defense, no death" gene encodes a mutated cyclic nucleotide-gated ion channel. *Proc. Natl. Acad. Sci. U S A*, *97*(16), 9323-9328.

Coll, N. S., Epple, P., & Dangl, J. L. (2011). Programmed cell death in the plant immune system. *Cell Death Differ.*, *18*(8), 1247-1256.

Coll, N. S., Vercammen, D., Smidler, A., Clover, C., Van Breusegem, F., Dangl, J. L., & Epple, P. (2010). Arabidopsis type I metacaspases control cell death. *Science*, *330*(6009), 1393-1397.

Collemare, J., O'Connell, R., & Lebrun, M. H. (2019). Nonproteinaceous effectors: the terra incognita of plant-fungal interactions. *New Phytol.*, *223*(2), 590-596.

Cui, H., Tsuda, K., & Parker, J. E. (2015). Effector-triggered immunity: from pathogen perception to robust defense. *Annu. Rev. Plant Biol.*, *66*, 487-511.

Curran, A., Chang, I. F., Chang, C. L., Garg, S., Miguel, R. M., Barron, Y. D., Li, Y., Romanowsky, S., Cushman, J. C., Gribskov, M., Harmon, A. C., & Harper, J. F. (2011). Calcium-dependent protein kinases from Arabidopsis show substrate specificity differences in an analysis of 103 substrates. *Front. Plant Sci.*, *2*, 36.

De Jonge, R., Peter van Esse, H., Kombrink, A., Shinya, T., Desaki, Y., Bours, R., & Thomma, B. P. (2010). Conserved fungal LysM effector Ecp6 prevents chitin-triggered immunity in plants. *Science*, *329*(5994), 953-955.

DeFalco, T. A., Marshall, C. B., Munro, K., Kang, H. G., Moeder, W., Ikura, M., Snedden, W. A., & Yoshioka, K. (2016). Multiple Calmodulin-Binding Sites Positively and Negatively Regulate Arabidopsis CYCLIC NUCLEOTIDE-GATED CHANNEL12. *Plant Cell*, *28*(7), 1738-1751.

Deslandes, L., & Rivas, S. (2011). The plant cell nucleus: a true arena for the fight between plants and pathogens. *Plant Signal Behav*, *6*(1), 42-48.

Dietrich, P., Moeder, W., & Yoshioka, K. (2020). Plant Cyclic Nucleotide-Gated Channels: New Insights on Their Functions and Regulation. *Plant Physiol.*, *184*(1), 27-38.

Du, Y., Chen, X., Guo, Y., Zhang, X., Zhang, H., Li, F., Huang, G., Meng, Y., & Shan, W. (2021). Phytophthora infestans RXLR effector PITG20303 targets a potato MKK1 protein to suppress plant immunity. *New*

Phyto.l, *229*(1), 501-515.
Fischer, C., DeFalco, T. A., Karia, P., Snedden, W. A., Moeder, W., Yoshioka, K., & Dietrich, P. (2017). Calmodulin as a Ca2+-Sensing Subunit of Arabidopsis Cyclic Nucleotide-Gated Channel Complexes. *Plant Cell Physiol*, *58*(7), 1208-1221.
Galan, J. E., & Wolf-Watz, H. (2006). Protein delivery into eukaryotic cells by type III secretion machines. *Nature*, *444*(7119), 567-573.
Gifford, J. L., Walsh, M. P., & Vogel, H. J. (2007). Structures and metal-ion-binding properties of the Ca2+-binding helix-loop-helix EF-hand motifs. *Biochem. J.*, *405*(2), 199-221.
Gimenez-Ibanez, S., Hann, D. R., Ntoukakis, V., Petutschnig, E., Lipka, V., & Rathjen, J. P. (2009). AvrPtoB targets the LysM receptor kinase CERK1 to promote bacterial virulence on plants. *Curr. Biol.*, *19*(5), 423-429.
Grant, M., Brown, I., Adams, S., Knight, M., Ainslie, A., & Mansfield, J. (2000). The RPM1 plant disease resistance gene facilitates a rapid and sustained increase in cytosolic calcium that is necessary for the oxidative burst and hypersensitive cell death. *Plant J.*, *23*(4), 441-450.
Guo, M., Kim, P., Li, G., Elowsky, C. G., & Alfano, J. R. (2016). A Bacterial Effector Co-opts Calmodulin to Target the Plant Microtubule Network. *Cell Host Microbe.*, *19*(1), 67-78.
Heese, A., Hann, D. R., Gimenez-Ibanez, S., J., M., A., He, K., Li, J., & Rathjen, J. P. (2007). The receptor-like kinase SERK3/BAK1 is a central regulator of innate immunity in plants. *Proc. Natl. Acad. Sci. U S A*, *104*(29), 12217-12222.
Jegla, T., Busey, G., & Assmann, S. M. (2018). Evolution and Structural Characteristics of Plant Voltage-Gated K(+) Channels. *Plant Cell*, *30*(12), 2898-2909.
Jogawat, A., Meena, M. K., Kundu, A., Varma, M., & Vadassery, J. (2020). Calcium channel CNGC19 mediates basal defense signaling to regulate colonization by Piriformospora indica in Arabidopsis roots. *J. Exp. Bot.*, *71*(9), 2752-2768.
Jones, J. D., & Dangl, J. L. (2006). The plant immune system. *Nature*, *444*(7117), 323-329.
Kadota, Y., Liebrand, T. W. H., Goto, Y., Sklenar, J., Derbyshire, P., Menke, F. L. H., Torres, M. A., Molina, A., Zipfel, C., Coaker, G., & Shirasu, K. (2019). Quantitative phosphoproteomic analysis reveals common regulatory mechanisms between effector- and PAMP-triggered immunity in plants. *New Phytol.*, *221*(4), 2160-2175.

Kanneganti, T. D., Lamkanfi, M., & Nunez, G. (2007). Intracellular NOD-like receptors in host defense and disease. *Immunity*, *27*(4), 549-559.

Kay, S., & Bonas, U. (2009). How Xanthomonas type III effectors manipulate the host plant. *Curr. Opin. Microbiol.*, *12*(1), 37-43.

Kelley, B. S., Lee, S. J., Damasceno, C. M., Chakravarthy, S., Kim, B. D., Martin, G. B., & Rose, J. K. (2010). A secreted effector protein (SNE1) from Phytophthora infestans is a broadly acting suppressor of programmed cell death. *Plant J.*, *62*(3), 357-366.

Koeck, M., Hardham, A. R., & Dodds, P. N. (2011). The role of effectors of biotrophic and hemibiotrophic fungi in infection. *Cell Microbiol.*, *13*(12), 1849-1857.

Ladwig, F., Dahlke, R. I., Stuhrwohldt, N., Hartmann, J., Harter, K., & Sauter, M. (2015). Phytosulfokine Regulates Growth in Arabidopsis through a Response Module at the Plasma Membrane That Includes CYCLIC NUCLEOTIDE-GATED CHANNEL17, H+-ATPase, and BAK1. *Plant Cell*, *27*(6), 1718-1729.

Langin, G., Gouguet, P., & Ustun, S. (2020). Microbial Effector Proteins - A Journey through the Proteolytic Landscape. *Trends Microbiol.*, *28*(7), 523-535.

Lapin, D., Kovacova, V., Sun, X., Dongus, J. A., Bhandari, D., von Born, P., Bautor, J., Guarneri, N., Rzemieniewski, J., Stuttmann, J., Beyer, A., & Parker, J. E. (2019). A Coevolved EDS1-SAG101-NRG1 Module Mediates Cell Death Signaling by TIR-Domain Immune Receptors. *Plant Cell*, *31*(10), 2430-2455.

Li, Y., Liu, X., Liu, M., Wang, Y., Zou, Y., You, Y., Yang, L., Hu, J., Zhang, H., Zheng, X., Wang, P., & Zhang, Z. (2020). Magnaporthe oryzae Auxiliary Activity Protein MoAa91 Functions as Chitin-Binding Protein To Induce Appressorium Formation on Artificial Inductive Surfaces and Suppress Plant Immunity. *mBio.*, *11*(2).

Liu, J., Elmore, J. M., Fuglsang, A. T., Palmgren, M. G., Staskawicz, B. J., & Coaker, G. (2009). RIN4 functions with plasma membrane H+-ATPases to regulate stomatal apertures during pathogen attack. *PLoS Biol.*, *7*(6), e1000139.

Luker, G. D., & Luker, K. E. (2011). Luciferase protein complementation assays for bioluminescence imaging of cells and mice. *Methods Mol. Biol.*, *680*, 29-43.

Marcec, M. J., Gilroy, S., Poovaiah, B. W., & Tanaka, K. (2019). Mutual interplay of Ca(2+) and ROS signaling in plant immune response. *Plant Sci.*, *283*, 343-354.

McCann, H. C., & Guttman, D. S. (2008). Evolution of the type III secretion system and its effectors in plant-microbe interactions. *New Phytol.*, *177*(1), 33-47.

Melotto, M., Underwood, W., Koczan, J., Nomura, K., & He, S. Y. (2006). Plant stomata function in innate immunity against bacterial invasion. *Cell*, *126*(5), 969-980.

Menna, A., Nguyen, D., Guttman, D. S., & Desveaux, D. (2015). Elevated Temperature Differentially Influences Effector-Triggered Immunity Outputs in Arabidopsis. *Front. Plant Sci.*, *6*, 995.

Moeder, W., Phan, V., & Yoshioka, K. (2019). Ca(2+) to the rescue - Ca(2+)channels and signaling in plant immunity. *Plant Sci.*, *279*, 19-26.

Monshausen, G. B., Messerli, M. A., & Gilroy, S. (2008). Imaging of the Yellow Cameleon 3.6 indicator reveals that elevations in cytosolic Ca2+ follow oscillating increases in growth in root hairs of Arabidopsis. *Plant Physiol.*, *147*(4), 1690-1698.

Naveed, Z. A., Bibi, S., & Ali, G. S. (2019). The Phytophthora RXLR Effector Avrblb2 Modulates Plant Immunity by Interfering With Ca(2+) Signaling Pathway. *Front. Plant Sci.*, *10*, 374.

Nie, J., Yin, Z., Li, Z., Wu, Y., & Huang, L. (2019). A small cysteine-rich protein from two kingdoms of microbes is recognized as a novel pathogen-associated molecular pattern. *New Phytol*, *222*(2), 995-1011.

Noel, L. D., Denance, N., & Szurek, B. (2013). Predicting promoters targeted by TAL effectors in plant genomes: from dream to reality. *Front. Plant Sci.*, *4*, 333.

Oh, S. K., Young, C., Lee, M., Oliva, R., Bozkurt, T. O., Cano, L. M., Win, J., Bos, J. I., Liu, H. Y., van Damme, M., Morgan, W., Choi, D., Van der Vossen, E. A., Vleeshouwers, V. G., & Kamoun, S. (2009). In planta expression screens of Phytophthora infestans RXLR effectors reveal diverse phenotypes, including activation of the Solanum bulbocastanum disease resistance protein Rpi-blb2. *Plant Cell*, *21*(9), 2928-2947.

Ohbayashi, I., Lin, C. Y., Shinohara, N., Matsumura, Y., Machida, Y., Horiguchi, G., Tsukaya, H., & Sugiyama, M. (2017). Evidence for a Role of ANAC082 as a Ribosomal Stress Response Mediator Leading to Growth Defects and Developmental Alterations in Arabidopsis. *Plant Cell*, *29*(10), 2644-2660.

Oliva, R. F., Cano, L. M., Raffaele, S., Win, J., Bozkurt, T. O., Belhaj, K., Oh, S. K., Thines, M., & Kamoun, S. (2015). A Recent Expansion of the

RXLR Effector Gene Avrblb2 Is Maintained in Global Populations of Phytophthora infestans Indicating Different Contributions to Virulence. *Mol. Plant Microbe. Interact.*, *28*(8), 901-912.

Olson, M. O. J. (2006). Nucleolus: Structure and Function. In *eLS*.

Palma, K., Zhang, Y., & Li, X. (2005). An importin alpha homolog, MOS6, plays an important role in plant innate immunity. *Curr. Biol.*, *15*(12), 1129-1135.

Pan, Y., Chai, X., Gao, Q., Zhou, L., Zhang, S., Li, L., & Luan, S. (2019). Dynamic Interactions of Plant CNGC Subunits and Calmodulins Drive Oscillatory Ca(2+) Channel Activities. *Dev Cell*, *48*(5), 710-725 e715.

Panstruga, R., & Dodds, P. N. (2009). Terrific protein traffic: the mystery of effector protein delivery by filamentous plant pathogens. *Science*, *324*(5928), 748-750.

Pieterse, C. M., Zamioudis, C., Berendsen, R. L., Weller, D. M., Van Wees, S. C., & Bakker, P. A. (2014). Induced systemic resistance by beneficial microbes. *Annu. Rev. Phytopathol.*, *52*, 347-375.

Qi, T., Guo, J., Liu, P., He, F., Wan, C., Islam, M. A., Tyler, B. M., Kang, Z., & Guo, J. (2019). Stripe Rust Effector PstGSRE1 Disrupts Nuclear Localization of ROS-Promoting Transcription Factor TaLOL2 to Defeat ROS-Induced Defense in Wheat. *Mol. Plant*, *12*(12), 1624-1638.

Quentin, M., Abad, P., & Favery, B. (2013). Plant parasitic nematode effectors target host defense and nuclear functions to establish feeding cells. *Front. Plant Sci.*, *4*, 53.

Rajamäki, M.-L., & Valkonen, J. P. T. (2009). Control of Nuclear and Nucleolar Localization of Nuclear Inclusion Protein a of Picorna-LikePotato virus AinNicotianaSpecies. *Plant Cell*, *21*(8), 2485-2502.

Rao, X., Huang, X., Zhou, Z., & Lin, X. (2013). An improvement of the 2ˆ (– delta delta CT) method for quantitative real-time polymerase chain reaction data analysis. *Biostat. bioinforma. biomath.*, *3*(3), 71.

Rocafort, M., Fudal, I., & Mesarich, C. H. (2020). Apoplastic effector proteins of plant-associated fungi and oomycetes. *Curr. Opin. Plant Biol.*, *56*, 9-19.

Saand, M. A., Xu, Y. P., Li, W., Wang, J. P., & Cai, X. Z. (2015). Cyclic nucleotide gated channel gene family in tomato: genome-wide identification and functional analyses in disease resistance. *Front. Plant Sci.*, *6*, 303.

Schornack, S., Huitema, E., Cano, L. M., Bozkurt, T. O., Oliva, R., Van Damme, M., Schwizer, S., Raffaele, S., Chaparro-Garcia, A., Farrer,

R., Segretin, M. E., Bos, J., Haas, B. J., Zody, M. C., Nusbaum, C., Win, J., Thines, M., & Kamoun, S. (2009). Ten things to know about oomycete effectors. *Mol. Plant Pathol.*, *10*(6), 795-803.

Seidl, M. F., & Van den Ackerveken, G. (2019). Activity and Phylogenetics of the Broadly Occurring Family of Microbial Nep1-Like Proteins. *Annu. Rev. Phytopathol.*, *57*, 367-386.

Seo, J. S., Diloknawarit, P., Park, B. S., & Chua, N. H. (2019). ELF18-INDUCED LONG NONCODING RNA 1 evicts fibrillarin from mediator subunit to enhance PATHOGENESIS-RELATED GENE 1 (PR1) expression. *New Phytol.*, *221*(4), 2067-2079.

Sun, T., Zhang, Y., Li, Y., Zhang, Q., Ding, Y., & Zhang, Y. (2015). ChIP-seq reveals broad roles of SARD1 and CBP60g in regulating plant immunity. *Nat. Commun.*, *6*, 10159.

Thomma, B. P., Nurnberger, T., & Joosten, M. H. (2011). Of PAMPs and effectors: the blurred PTI-ETI dichotomy. *Plant Cell*, *23*(1), 4-15.

Thulasi Devendrakumar, K., Li, X., & Zhang, Y. (2018). MAP kinase signalling: interplays between plant PAMP- and effector-triggered immunity. *Cell Mol. Life Sci.*, *75*(16), 2981-2989.

Tian, W., Hou, C., Ren, Z., Wang, C., Zhao, F., Dahlbeck, D., Hu, S., Zhang, L., Niu, Q., Li, L., Staskawicz, B. J., & Luan, S. (2019). A calmodulin-gated calcium channel links pathogen patterns to plant immunity. *Nature*, *572*(7767), 131-135.

Tian, W., Wang, C., Gao, Q., Li, L., & Luan, S. (2020). Calcium spikes, waves and oscillations in plant development and biotic interactions. *Nat. Plants*, *6*(7), 750-759.

Tsuda, K., & Katagiri, F. (2010). Comparing signaling mechanisms engaged in pattern-triggered and effector-triggered immunity. *Curr. Opin. Plant Biol.*, *13*(4), 459-465.

Upson, J. L., Zess, E. K., Białas, A., Wu, C. H., & Kamoun, S. (2018). The coming of age of EvoMPMI: evolutionary molecular plant–microbe interactions across multiple timescales. *Curr. Opin. Plant Biol.*, *44*, 108-116.

Wang, J., Liu, X., Zhang, A., Ren, Y., Wu, F., Wang, G., Xu, Y., Lei, C., Zhu, S., Pan, T., Wang, Y., Zhang, H., Wang, F., Tan, Y. Q., Wang, Y., Jin, X., Luo, S., Zhou, C., Zhang, X., . . . Wan, J. (2019). A cyclic nucleotide-gated channel mediates cytoplasmic calcium elevation and disease resistance in rice. *Cell Res.*, *29*(10), 820-831.

Whisson, S. C., Boevink, P. C., Moleleki, L., Avrova, A. O., Morales, J. G., Gilroy, E. M., Armstrong, M. R., Grouffaud, S., van West, P., Chapman,

S., Hein, I., Toth, I. K., Pritchard, L., & Birch, P. R. (2007). A translocation signal for delivery of oomycete effector proteins into host plant cells. *Nature*, *450*(7166), 115-118.

Wiermer, M., Germain, H., Cheng, Y. T., Garcia, A. V., Parker, J. E., & Li, X. (2010). Nucleoporin MOS7/Nup88 contributes to plant immunity and nuclear accumulation of defense regulators. *Nucleus*, *1*(4), 332-336.

Xin, X. F., Kvitko, B., & He, S. Y. (2018). Pseudomonas syringae: what it takes to be a pathogen. *Nat. Rev. Microbiol.*, *16*(5), 316-328.

Xu, G., Moeder, W., Yoshioka, K., & Shan, L. (2022). A Tale of Many Families: Calcium Channels in Plant Immunity. *Plant Cell*.

Yang, B., Sugio, A., & White, F. F. (2006). Os8N3 is a host disease-susceptibility gene for bacterial blight of rice. *Proc. Natl. Acad. Sci. U S A*, *103*(27), 10503-10508.

Yoshioka, K., Moeder, W., Kang, H. G., Kachroo, P., Masmoudi, K., Berkowitz, G., & Klessig, D. F. (2006). The chimeric Arabidopsis CYCLIC NUCLEOTIDE-GATED ION CHANNEL11/12 activates multiple pathogen resistance responses. *Plant Cell*, *18*(3), 747-763.

Yu, X., Xu, G., Li, B., de Souza Vespoli, L., Liu, H., Moeder, W., Chen, S., de Oliveira, M. V. V., Ariadina de Souza, S., Shao, W., Rodrigues, B., Ma, Y., Chhajed, S., Xue, S., Berkowitz, G. A., Yoshioka, K., He, P., & Shan, L. (2019). The Receptor Kinases BAK1/SERK4 Regulate Ca(2+) Channel-Mediated Cellular Homeostasis for Cell Death Containment. *Curr. Biol.*, *29*(22), 3778-3790 e3778.

Yuan, M., Jiang, Z., Bi, G., Nomura, K., Liu, M., Wang, Y., Cai, B., Zhou, J. M., He, S. Y., & Xin, X. F. (2021). Pattern-recognition receptors are required for NLR-mediated plant immunity. *Nature*, *592*(7852), 105-109.

Yuan, M., Ngou, B. P. M., Ding, P., & Xin, X. F. (2021). PTI-ETI crosstalk: an integrative view of plant immunity. *Curr Opin Plant Biol*, *62*, 102030.

Zeng, W., & He, S. Y. (2010). A prominent role of the flagellin receptor FLAGELLIN-SENSING2 in mediating stomatal response to Pseudomonas syringae pv tomato DC3000 in Arabidopsis. *Plant Physiol.*, *153*(3), 1188-1198.

Zhao, C., Tang, Y., Wang, J., Zeng, Y., Sun, H., Zheng, Z., Su, R., Schneeberger, K., Parker, J. E., & Cui, H. (2021). A mis-regulated cyclic nucleotide-gated channel mediates cytosolic calcium elevation and activates immunity in Arabidopsis. *New Phytol.*, *230*(3), 1078-1094.

Zhao, Y., Liu, W., Xu, Y. P., Cao, J. Y., & Braam, J. C., X. Z. (2013). Genome-

wide identification and functional analyses of calmodulin genes in Solanaceousspecies. *BMC Plant Biol.*, *13*(1), 1-15.

Zheng, X., McLellan, H., Fraiture, M., Liu, X., Boevink, P. C., Gilroy, E. M., Chen, Y., Kandel, K., Sessa, G., Birch, P. R., & Brunner, F. (2014). Functionally redundant RXLR effectors from Phytophthora infestans act at different steps to suppress early flg22-triggered immunity. *PLoS Pathog.*, *10*(4), e1004057.

Zheng, X., Wagener, N., McLellan, H., Boevink, P. C., Hua, C., Birch, P. R. J., & Brunner, F. (2018). Phytophthora infestans RXLR effector SFI5 requires association with calmodulin for PTI/MTI suppressing activity. *New Phytol.*, *219*(4), 1433-1446.

Zhou, L., Lan, W., Jiang, Y., Fang, W., & Luan, S. (2014). A calcium-dependent protein kinase interacts with and activates a calcium channel to regulate pollen tube growth. *Mol. Plant*, *7*(2), 369-376.

CHAPTER 1

A *Phytophthora* nucleolar effector, Pi23226, targets host ribosome biogenesis to promote necrotrophic cell death

The research described in this chapter has been published in Plant communication.
DOI: https://doi.org/10.1016/j.xplc.2023.100606

ABSTRACT

Pathogen effectors target diverse subcellular compartments to manipulate the plant immune system. Although the nucleolus has emerged as a stress marker, and several effectors are localized in the nucleolus, the roles of nucleolar-targeted effectors remain elusive. In this study, we showed that *P. infestans* infection of *N. benthamiana* results in nucleolar inflation during the transition from biotrophic to necrotrophic phase. Multiple *P. infestans* effectors were localized in the nucleolus; Pi23226 induced cell death in *N. benthamiana* and nucleolar inflation similar to that observed in the necrotrophic stage of infection, whereas its homolog Pi23015 and a deletion mutant (Pi23226ΔC) did not induce cell death nor affect the nucleolus size. RNA immunoprecipitation and individual nucleotide resolution of crosslinked RIP(iCLIP)-seq analysis indicated that Pi23226 bound to the 3′-end of 25S rRNA precursors, resulting in the accumulation of unprocessed 25S pre-rRNAs. The nucleolar stress marker NAC082 was strongly upregulated under Pi23226-expressing conditions. Pi23226 subsequently inhibited global protein translation in host cells by interacting with ribosomes. Pi23226 enhanced *P. infestans* pathogenicity, indicating that Pi23226-induced ribosome malfunction and cell death was beneficial for pathogenesis in the

host. Our results provide evidence for the molecular mechanism underlying RNA-binding effector activity in host ribosome biogenesis, and lead to new insights into the nucleolar action of effectors in pathogenesis.

INTRODUCTION

Although plants lack an adaptive immune system, they developed a unique innate immune system against pathogen infection (Jones and Dangl, 2006; Jones et al., 2016). Plant contains plasma membrane-localized pattern recognition receptors (PRRs) that recognize pathogen-associated molecular patterns (PAMPs) and initiate pattern-triggered immunity (PTI) (Chisholm et al., 2006). During pathogen invasion of host cells, specialized secreted molecules called effectors are delivered to modulate the host immune response and enhance pathogenicity. As a result of the long arms-race history between hosts and pathogens, plants have evolved polymorphic pathogen resistance (R) genes that contain a nucleotide-binding site and a leucine-rich repeat domain (NLR) to recognize cognate pathogen effectors. Effector recognition induces a more durable and robust defense response called effector-triggered immunity (ETI) (Cui et al., 2015). ETI often results in a hypersensitive cell death response (HR) that restricts further pathogen invasion at the infection site (Dangl et al., 2013).

Recent research has focused on completing the whole genome sequences of pathogens and understanding the molecular mechanisms of effector action

in pathogenesis and host defense (Dean et al., 2005; Haas et al., 2009). RXLR (Arg-any amino acid-Leu-Arg)-type effectors are ubiquitous in most oomycete pathogens and are a major virulence factors (Rehmany et al., 2005; Birch et al., 2006; Dou and Zhou, 2012; He et al., 2020). After pathogen effectors are translocated into plant cells, they target diverse subcellular organelles to manipulate the plant immune system. For example, the *P. infestans* effector Pi04314 modulates the activity of protein phosphatase I in the nucleus and suppresses JA- and SA-induced transcription of defense-related genes (Boevink et al., 2016). The *Phytophthora sojae* (hereafter *P. sojae*) RXLR effector, PsAvh262 associates with endoplasmic reticulum (ER)-luminal binding immunoglobulin proteins and suppresses ER stress-related cell death (Jing et al., 2016).

The nucleolus is a eukaryotic subcellular organelle that has critical functions in ribosome biogenesis, initiating rDNA transcription, and processing pre-rRNAs to assemble mature rRNA-ribosomal protein translation complexes (Boisvert et al., 2007; Kalinina et al., 2018; Sáez-Vásquez and Delseny, 2019). RNA polymerase I mediates the transcription of rRNA genes, and nascent pre-rRNAs are processed by numerous ribonucleoproteins to produce 18S, 5.8S, and 25S rRNAs. The assembly of ribosome subunits requires more than 200 accessory factors known as

ribosome biogenesis factors. Finally, mature rRNAs are assembled with ribosomal proteins to form small (40S) and large (60S) subunits in the nucleoplasm and in the cytoplasm (Weis et al., 2015). Disruption of ribosome biogenesis factors causes severe defects in development. For example, homozygous knockout mutants of 40S ribosome biogenesis factors were embryo lethal in Arabidopsis (Harscoët et al., 2010; Missbach et al., 2013).

The nucleolus also has an emerging role in plant immunity against diverse pathogens. For example, a number of plant viral proteins target nucleolar methyltransferase fibrillarin (FIB) for the long-distance movement of viruses (Kim et al., 2007; Rajamäki and Valkonen, 2009; Chang et al., 2016). Plant nucleoli also respond to the invasion of bacterial, fungal, and oomycete pathogens (Seo et al., 2019). Under normal conditions, FIB2 interacts with Mediator subunit 19a (MED19a), a component of the Mediator complex, and functions as a negative regulator of immune-related gene expression. However, infection with the bacterial pathogen *Pseudomonas syringae* or treatment with elf18 causes FIB2 dissociation from the complex and release the gene promoter to enhance the expression of immune-responsive genes (Seo et al., 2019). The *Hyaloperonospora arabidopsidis* RXLR effector HaRxL44 interacts with MED19a to modulate the interactions between transcriptional regulators and RNA polymerase II, which shifts the balance of

transcription from SA-responsive to JA/ethylene-responsive genes, and enhances plant susceptibility (Caillaud et al., 2013). The fungal ribonuclease-like effector CSEP0064/BEC1054 of a biotrophic pathogen, *Blumeria graminis* associates with total RNA and suppresses the activity of host ribosome-inactivating proteins (RIP) which leads to cell death (Pennington et al., 2019). Although recent research has achieved significant progress in mapping the interactions of nuclear/nucleolar-localizing pathogen effectors, the molecular roles of nucleolar targeting effectors in pathogenicity and host defense are still elusive.

In this study, we observed the morphological changes of plant nucleoli during transition of *P. infestans* life cycle from biotrophic to necrotrophic stage. We also investigated the molecular activity in host ribosome biogenesis of the *P. infestans* effector Pi23226, which is conserved in diverse *P. infestans* strains and is localized in the host nucleolus. We found that Pi23226 inflated the size of the nucleolus, subverted 25S pre-rRNA processing by binding immature 27S rRNA, and subsequently suppressed protein translation leading to host cell death. Our results provide new insights into the mechanisms of action of a nucleolar-localized pathogen effector that induces necrotic host cell death and enhances host susceptibility by subverting ribosome biogenesis and protein synthesis in the host cell.

MATERIALS AND METHODS

Plant growth conditions and Agrobacterium-mediated transient overexpression in plants

Plants were grown and maintained in a walk-in chamber with an ambient temperature of 23–24°C and 16 h : 8 h (light : dark) cycle. For *in planta* expression, *A. tumefaciens*-mediated transient expression was performed on 4-week-old *N. benthamiana* plants. An overnight culture of *A. tumefaciens* strain GV3101 was centrifuged, resuspended in buffer (10 mM $MgCl_2$, 10 mM MES-KOH pH 5.7, 200 μM acetosyringone) and incubated for 1 h at room temperature. The bacterial suspension was adjusted to OD_{600} = 0.4 and pressure-infiltrated into the abaxial surface of *N. benthamiana* leaves using a needleless syringe. For coexpression experiments, Agrobacteria harboring each construct were mixed 1:1 and adjusted to OD_{600} = 0.4 in the same suspension and infiltrated. Leaf tissues were collected at 1.5~2 days post inoculation.

Plasmid constructs

For N-terminal GFP fusions, RXLR effector genes (Pi23226, Pi23015,

Pi07550, and Pi04089) and other mutants were synthesized without the signal peptide and the RXLR regions, then amplified with primers containing the NruI restriction site, and then ligated into the PZP212 vector using enzyme digestion. Fibrillarin was amplified with the attB site from cDNA of *N. benthamiana* and fused to RFP using pB7WGF2 in the GATEWAY system. To detect the protein level of effectors, the amplicons of 3FLAG-Pi23226 and 3FLAG-mutants were cloned into the pkw-LIC vector containing the cauliflower mosaic virus 35S promoter using the ligation-independent cloning (LIC) method (Oh et al., 2010). Generated vector constructs were transformed into *A. tumefaciens* GV3101 for transient expression. The primer sequences used in this study are presented in Table 1-1.

Confocal microscopy

To determine the subcellular localization of GFP-tagged Pi23226 in *N. benthamiana* leaves, samples were observed using a Leica SP8 X (USA) confocal microscope equipped with a ×40 water immersion objective. GFP fluorescence was visualized using a 488 nm laser line for excitation, and emission was collected between 455 and 480 nm. For imaging mRFP fluorescence, excitation was at 532 nm, and emission was observed between 580 and 650 nm. To minimize spectral bleed-through between fluorescence

channels during colocalization experiments, images were acquired by sequential scanning with alternation between frames. Plant nuclei were stained using DAPI (4′,6-diamidino-2-phenylindole, 10 μg ml^{-1} in water) that was pressure-infiltrated into the abaxial side of the leaf 10 min before observation. DAPI fluorescence was excited at 405 nm and observed between 450 and 480 nm. Nucleolar size was measured and analyzed using Image J software.

Protein isolation and immunoblot analyses

Total proteins are extracted using extraction buffer [10% (v/v) glycerol, 25 mM Tris-HCl (pH 7.5), 1 mM EDTA, 150 mM NaCl, 1% (w/v) polyvinylpolypyrrolidone, and 1× protease inhibitor cocktail], mixed with SDS/PAGE sample buffer, and analyzed by immunoblotting. For western blotting, protein samples were separated on SDS-PAGE gels and transferred to PVDF membranes (Bio-Rad, 88585) using a Trans-Blot Turbo Transfer System (Bio-Rad, 1704150). Membranes were blocked with 6% milk prepared in Tris-buffered saline with 0.1% Tween 20 (TBST) and incubated with primary anti-FLAG (1:12000, Sigma-Aldrich, F3165) or anti-GFP (1:12000, Invitrogen, A10260) antibodies at room temperature for 1 h. The membrane was washed twice with PBST for 10 min each before the addition of the secondary anti-mouse Ig-HRP antibody (1: 15,000, Abcam, ab6708) or

anti-rabbit Ig-HRP antibody (1:15,000, Abcam, ab6702) for 1 h. ECL (Bio-Rad, 1705061) detection was performed according to the manufacturer's instructions.

In vitro and *in vivo* translation assay

In vitro translation was carried out using a wheat germ protein expression system (Promega, USA) following the manufacturer's instruction. In brief, 2 μg of GFP pk7FWG, 1 μg of GST-tagged effector proteins and 2 μl of FluoroTect™ GreenLys tRNA (Promega, USA) were gently mixed with High-Yield Wheat Germ Master Mix, followed by incubation at 25°C for 2 h. Recombinant GST-strawberry was used as a negative control for comparison with other GST recombinant proteins. The final protein products were analyzed by SDS-PAGE and immunoblotting with anti-GFP, and the level of tRNA was detected using an Azure 400 chemiluminescence imager (Azure Biosystems, USA) as an equal loading control. For cycloheximide (CHX) treatment, CHX (Amresco, 94271) at the indicated concentrations was added together with Wheat Germ Master Mix before incubation. *De novo* protein synthesis was examined *in planta* using a modified surface sensing of translation (SUnSET) assay (Van Hoewyk, 2016). Briefly, *N. benthamiana* leaf discs were incubated with 100 μM puromycin for 2 h in 1/2 MS medium under vacuum. Then, 30 μg of total protein extract was loaded onto a 4–20%

gradient SDS-PAGE gel, and puro-polypeptides were detected by western blotting with an anti-puromycin antibody (Millipore, MABE343) at a dilution of 1:10,000. Newly synthesized proteins were detected using an Azure 400 chemiluminescence imager (Azure Biosystems, USA), and the intensity of *de novo* protein synthesis was calculated using ImageJ. For CHX treatment, leaf discs were incubated with CHX in 1/2 MS medium at 25°C for 4 h before puromycin treatment.

Polysome isolation and profiling

The polysome fractionation method Ribo Mega-SEC was modified for polysome profiling (Yoshikawa et al., 2018). Approximately one-half of the *N. benthamiana* leaves were ground in liquid nitrogen, homogenized in 500 µl of polysome isolation buffer (200 mM Tris-HCl pH 8.5, 50 mM KCl, 25 mM $MgCl_2$, 1% sodium deoxycholate, 1% CHAPS, 50 µg/ml chloramphenicol, 50 µg/ml cycloheximide, 1 x protease inhibitor cocktail, 400 U/ml SUPERase In RNase Inhibitor), and incubated for 15 min on ice. Then, the homogenate was clarified by centrifugation at 17,000 x g for 10 min at 4°C. The supernatant was passed through a 0.45 µm Ultrafree-MC-HV centrifugal filter (UFC30HVNB, Merck Millipore, USA) followed by centrifugation at 12,000 x g for 2 min at 4°C. Then, 25 µg of ribosome isolate

was injected with SEC buffer (20 mM Hepes-NaOH pH 7.4, 130 mM NaCl, 10 mM $MgCl_2$, 1% CHAPS, 2.5 mM DTT, 50 mg/ml cycloheximide, 20 U SUPERase In RNase Inhibitor, complete EDTA-free Protease Inhibitor Cocktail) and analyzed by chromatography system (UltiMate 3000 UHPLC, Thermo Fisher Scientific) using Agilent Bio SEC-5 2,000 Å columns (7.8 x 300 mm with 5-mm particles). The gradient was collected with simultaneous measurement of UV absorbance at 260 nm (flow rate 0.4 ml/min). Fractionated proteins were isolated with MeOH/chloroform and detected by western blotting with the 60S ribosomal protein L13-1 antibody (Agrisera, AS132650, Sweden) at a dilution of 1:4,000.

UV crosslinking and immunoprecipitation (iCLIP)-seq and RNA-immunoprecipitation (RIP)

For iCLIP-seq, four-week-old *N. benthamiana* leaves were irradiated three times with UV at 0.500 J/cm2, and leaf samples were ground in liquid nitrogen. Total protein extracts were filtered through a 0.45 μm filter and sonicated in an ice bath using a bioruptor (Sonifier SFX 550, USA) at 30-s on/30-s off for 15 min. Samples were centrifuged at 16,000 × g for 20 min, and the supernatant was collected. For RIP, the protocol from Gagliardi and Matarazzo was modified (Gagliardi and Matarazzo, 2016). In brief, plant

tissues were crosslinked with 1% formaldehyde in crosslinking buffer (10 mM Tris-HCl, pH 8.0, 0.4 M Sucrose, 1 mM EDTA, 1 mM PMSF, and 1 x complete protease inhibitor) via vacuum infiltration for 20 min. Crosslinking reaction was quenched by adding 2M glycine (final concentration 200 mM) and continuously incubating for 10 min. Crosslinked tissues were washed for four times in cold and sterile water for 1 min. Total protein was extracted as described above and filtered through a 0.45μm filter. After measuring protein concentration, 1.2 μg of total protein was sonicated with a micro-needle (3 min total, 30 s on/ 1min off at amplitude 10%). Samples were centrifuged at 16,000 × g for 20 min, and the supernatant was collected. Supernatants were treated with 4 μL of DNAse I (NEB, EN0521) and incubated for 10 min at 37°C with shaking at 1,200 rpm. For RNA digestion, 40 U of RNase I was added for 10 min at 37°C with shaking at 1,200 rpm. The sample was precleared with agarose beads in IP buffer [10% (v/v) glycerol, 25 mM Tris–HCl pH 7.5, 1 mM EDTA, 150 mM NaCl, 1× protease inhibitor cocktail] for 1 h at 4°C. The sample was centrifuged, and the supernatant was incubated with a-FLAG-affinity agarose beads (BioLegend, USA) for 2 h at 4°C. The beads were washed four times with IP buffer followed by elution with 130 μl of elution buffer (1% SDS, 0.1 M $NaHCO_3$, 5 units of SUPERase In RNase Inhibitor) by rotating for 30 min at 4°C. For reverse crosslinking, 10 μl

proteinase K (20 mg/ml) was added and incubated at 60°C for 1 h. RNA was recovered with TRIzol reagent according to the manufacturer's instructions. The genome sequences and annotations for genes and repeats in *N. benthamiana* were downloaded from the Sol Genomics Network (https://solgenomics.net/ftp/genomes/Nicotiana_benthamiana/) (Bombarely et al., 2012). The raw reads from iCLIP-seq were trimmed to remove sequences with low quality and adaptors using fastp v 0.20.1 (-l 71 -q 30) (Chen et al., 2018). The filtered reads were mapped to the reference genome in *N. benthamiana* using Hisat2 v 2.1.0 with the default parameter (Kim et al., 2019). The BAM files from aligned reads were sorted using Samtools v 1.10 (Li et al., 2009) and converted into raw and RPKM-normalized bed files using bamCoverage implemented in Deeptools v 3.5.0 (Ramírez et al., 2016). The raw and RPKM-normalized bed files were visualized in IGV v 2.8.4 (Robinson et al., 2011).

Circular RT-PCR analysis

Circular RT-PCR analysis was performed using 10 μg of RNA extracted from nuclei of *N. benthamiana* leaves. For this, 1g of frozen leaves was suspended in nuclear isolation buffer (10 mM Tris-HCl, pH 8.0, 10 mM $MgCl_2$, 400 mM sucrose, 10 mM β-mercaptoethanol, 0.2 mM PMSF, and 1 x

protease inhibitor cocktail). The solution was filtered using a cell strainer and centrifuged at 4°C for 20 minutes at 1,900 x g. The pellet was resuspended in storage buffer [10 mM Tris-HCl, pH 8.0, 10 mM $MgCl_2$, 250 mM sucrose, 0.15% (w/v) Triton X-100, 5 mM β-mercaptoethanol, 0.1 mM PMSF, and 1 x protease inhibitor cocktail]. The quality and quantity of nuclei were confirmed under a microscope. RNA was extracted using TRIzol reagent (MRC, USA) and ligated with T4 RNA ligase 1 (NEB, USA) at 37 °C for 1 h. First-strand cDNA was reverse-transcribed from ligated RNAs using SuperScript III reverse transcriptase (Invitrogen, USA) and primers 18c, 5.8c, and 25c. The rRNA intermediates were amplified with specific primer sets (Table 1-1), and amplified PCR fragments were determined by sequencing.

RNA extraction and gene expression analyses

Total RNA was extracted from *N. benthamiana* leaves using TRIzol reagent (MRC, USA). To investigate the level of rDNA transcription, samples expressing each construct were collected before the cell death phenotype was observed using the same amounts of leaf tissues. The same volumes of RNA were loaded on 1.5% agarose gel.

For gene expression analysis, reverse transcription was performed using SuperScript III reverse transcriptase (Invitrogen, USA) and random hexamer

priming. Quantitative RT-PCR assays were conducted using PowerUP SYBR green master mix (Thermo, USA) according to the manufacturer's instructions. The expression levels of genes were calculated using the $2^{-\Delta\Delta Ct}$ algorithm (KJ and TD, 2001). Primer pairs were designed for each of the selected genes (Table 1-1). The *N. benthamiana* elongation factor 1α (*NbEF1α*) gene was used as an internal control.

Phytophthora **infection assays**

The virulence function of effectors was evaluated using *A. tumefaciens* infiltration of *N. benthamiana* leaves. Each GFP-fused effector was transiently overexpressed on one-half of the leaf, and GFP was overexpressed on the other half of the same 4-week-old leaf. *P. infestans* isolate T30-4 was cultured on Rye agar at 19°C for 10 days. Plates were flooded with 5 ml cold H_2O and scraped with a cell scraper to release sporangia. The zoospore solution was collected and diluted to 50,000 spores/ml. Infection assays were performed using droplet inoculations (10 μl of a zoospore solution) on detached leaves after 24 from agroinfiltration. The lesion size was measured 5 days after inoculation. Each lesion size was photographed using Cy5 and Cy3 channels in an Azure 400 (Azure Biosystems, USA). Autofluorescent areas were analyzed using Image J software.

Detection of cell death intensity

Cell death intensity was quantified by measuring chlorophyll fluorescence (Lee et al., 2021; Wen et al., 2019). Detached *N. benthamiana* leaves were exposed to a measuring beam, and the minimal (Fv) and maximal (Fm) fluorescence were determined using FluorCam 800MF (Photon Systems Instruments, Czechia). The Fv/Fm parameter was visualized spatially with Fluorcam 7.0 software according to the protocol provided by Photon Systems Instruments.

Virus-induced gene silencing assay (VIGS)

The cloned pTRV2-SGT1, pTRV2-NRC2/3/4, pTRV2-NRG1/ADR1, pTRV2-EDS1, pTRV2-NDR1, pTRV2-RAR1 vector constructs were agroinfiltrated as previously described (Chung et al., 2004). Briefly, two-week-old *N. benthamiana* plants were infiltrated with 1:1 mixtures of pTRV1 and pTRV2 constructs using infiltration buffer (10 mM 2-[N-morpholine]-ethanesulfonic acid [MES]; 10 mM $MgCl_2$; and 150 μM acetosyringone, pH 5.6) to a final OD_{600} = 0.25. All plants were grown in the same growth chamber at 24°C (day/night), with a 16 hr light/8 hr dark photoperiod. About three weeks after inoculation, the upper leaves were used for further assays

and evaluation of silenced efficiency.

TRV-mediated host-induced gene silencing assay (HIGS)

The TRV based VIGS system was employed for HIGS of effector genes Pi23226 and Pi23015 in *N. benthamiana* plants. The cDNA fragments of Pi23226 and Pi23015 genes of *P. infestans* were cloned into a pTRV2 vector. A TRV2-GFP was used as a negative control. Strains of *A. tumefaciens* GV3101 harboring pTRV1 and pTRV2-Pi23226 or pTRV2-Pi23015 were resuspended in the infiltration buffer (OD_{600} = 0.25) mixed with an equal volume and infiltrated into the 2-week-old *N. benthamiana* plants. Two weeks after agroinfiltration, *N. benthamiana* plants described above were used for the pathogen infection assay to confirm the efficiency of TRV-mediated HIGS in *N. benthamiana* plants against *P. infestans.*

Table 1-1. Primers used in this study.

primer name	Primer 5'-3'
pPZP-Pi23226-NruI-F	TCGCGAATGGCAGGTACTGCTTTG
pPZP-Pi23226-NruI-R	TCGCGATCAGTCCCTGCATCCCAC
pPZP-Pi23226ΔC-NruI-R	TCGCGATCAGTAGAACTTGATGTACCTA
pPZP-Pi23015-NruI-F	TCGCGAATGAGCAAGCTATTCTATGC
pPZP-Pi23015-NruI-R	TCGCGATCATTTAGTTTGCACACGGA
pPZP-Pi07550-NruI-F	TCGCGAATGGCAGGTAAGATCCAGA
pPZP-Pi07550-NruI-R	TCGCGATCATCCAGATGGGTTAAGTGAGTG
pPZP-Pi04089-NruI-F	TCGCGAATGGCAGGTGTGAGGGT
pPZP-Pi04089-NruI-R	TCGCGATCACTTAGCAGGCTTCTTG
pkw-Pi23226-LIC-F	CCAATCCCTCTACGGATGGCAGGTACTGCTTTG
pkw-Pi23226-LIC-R	TATCCTCCTACGTCAGTCCCTGCATCCCAC
pkw- Pi23226ΔC-LIC-R	TATCCTCCTACGTCAGTAGAACTTGATGTACCTA
pkw-Pi23015-LIC-F	CCAATCCCTCTACGGATGAGCAAGCTATTCTATGC
pkw-Pi23015-LIC-R	TATCCTCCTACGTCATTTAGTTTGCACACGGA
pET28a-mStrawberry-F	GGATCCATGGTGAGCAAGGGCGAGGAGA
pET28a-mStrawberry-R	GAATTCCTTGTACAGCTCGTCCATGC
pET28a-Pi23226-F	GGATCCATGGCAGGTACTGCTTTG
pET28a-Pi23226-R	GAATTCGTCCCTGCATCCCACTCC
pET28a-Pi23226ΔC-R	GAATTCGTAGAACTTGATGTACCTA
pET28a-Pi23015-F	GGATCCATGAGCAAGCTATTCTATGC
pET28a-Pi23015-R	GAATTCTTTAGTTTGCACACGGA
qRT-EF1a-F	GTATGCCTGGGTGCTTGAC
qRT-EF1a-R	ACAGGGACAGTTCCAATACCA
qRT-5ETS-F	CGGTCGCCTTTCTCCCTTCG
qRT-5ETS-R	GCCCGAGCATGCTAAGTCGT
qRT-18S-F	TTCAGACTGTGAAACTGCGA
qRT-18S-R	GAATCATCGCAGCAACGGGC
qRT-ITS1-F	AGAACGACCCGCGAACTTGT
qRT-ITS1-R	CGTTAATCACCCGGCACGCA
qRT-5.8S-F	GCAACGGATATCTCGGCT
qRT-5.8S-R	CAGGCAGACGTGCCCT
qRT-ITS2-F	GATACTGGCCTCCCGTGCTC
qRT-ITS2-R	CCGTCGCTGTGGACTTGCAT
qRT-25S-F	AGTTCTATCGGGTAAAGCCAA
qRT-25S-R	TTCCGGTTCATCCCGCAT
qRT-3ETS-F	CCGTGGCCATGGCAAGAGTT
qRT-3ETS-R	GTCCTGCGACGTCCTGACAC
qRT-NAC082-1-F	CTAACAATAAGAACTACTCAATA
qRT-NAC082-1-R	GGAAAGACGCGGTTCACC

qRT-NAC082-2-F	GAGCAGATTCTTGGGACT
qRT-NAC082-2-R	GATCAAATGATTCCTTATCGT
qRT-NAC082-3-F	AATGTGAACTCTGAAGATGTG
qRT-NAC082-3-R	GGTACTCCTCAAGCATGT
qRT-NAC082-4-F	AATTTCTGATCAAGCACTGC
qRT-NAC082-4-R	GGATACTGACGATCTGATCC
qRT-RIP-18S-1-F	TATGGGTGGTGGTGCATGGC
qRT-RIP-18S-1-R	TAAGAAGCTGGCCGCGAAGG
qRT-RIP-18S-2-F	TGGTAATTGGAATGAGTACAAT
qRT-RIP-18S-2-R	TCCCAAAGTCCAACTACG
qRT-RIP-5.8S-1-F	ACGGATATCTCGGCTCTCGCA
qRT-RIP-5.8S-1-R	CCCTCGGCCTAATGGCTTCG
qRT-RIP-25S-1-F	CGCAACGCCCTCGACCTTAT
qRT-RIP-25S-1-R	TTCCGGTTCATCCCGCATCG
qRT-RIP-25S-2-F	GCGGGTAAACGGCGGAAGTA
qRT-RIP-25S-2-R	CCGTTCCCTTGGCTGTGGTT
qRT-iCLIP-25S-3-F	TCTGATTCGTCCATCCCCCT
qRT-iCLIP-25S-3-R	GCATCAAGGTAGGAGTGAACCT
qRT-iCLIP-25S-4-F	CACGTGTCGTTGGCTAAGTC
qRT-iCLIP-25S-4-R	ATTGTACTTCAAGGCGGCCA
qRT-iCLIP-25S-5-F	ACAATTTCCATCGAGCGGCG
qRT-iCLIP-25S-5-R	TGGCAGCAATGCCACTCTAC
qRT-cRT-r1	TACTTACACATGCATGGCT
qRT-cRT-r2	CTCGGCCTAATGGCTTCG
qRT-cRT-r3	CGCAGTTTCACAGTCTGAA
qRT-cRT-r4	AGGAGAAGTCGTAACAAGGT
qRT-cRT-r5	GCACGTCTGCCTGGGCGTCA
qRT-cRT-r6	AGCCCTTTGTCGCTCTGATTCGT

RESULTS

P. infestans infection leads to inflation of host nucleoli before the initiation of necrosis

To investigate the impact of pathogen infection on host nucleolar morphology in the progress of disease, we tracked the size of nucleolus using RFP-tagged fibrillarin (Fib2-RFP) as a nucleolar marker (Loza-Muller et al., 2015) after inoculating *P. infestans* zoospores (500 spores/drop) onto detached *N. benthamiana* leaves (Figure 1-1 A). Inoculated leaf tissues were collected and observed for 5 days after inoculation. The progress of disease was determined with the transcript levels of a biotrophic (IpIO) and necrotrophic (NPP1.1) marker (Van West et al., 1998; Kanneganti et al., 2007). IpIO expression dramatically increased at 2- and 3-days post-infection (dpi) compared to 0 dpi, and then subsequently decreased. By contrast, NPP1.1 expression sharply increased from 4 dpi (Figure 1-1 B). These results suggested that the transition from biotrophic to necrotrophic phase occurred around 4 dpi in *N. benthamiana.* During the biotrophic stage (ca. 1-3 dpi), no significant change in the nuclear or nucleolar size was observed, whereas the size of nucleolus was increased at 4 dpi with a slight increase of nuclear size (Figure 1-1 A). Nuclear shrinkage and a reduction in nucleolar size occurred

along with the progression of necrotic cell death. These results suggest that the pathogen modulates the host nucleolar activities during the switch of the disease cycle from the biotrophic to necrotrophic stage.

Several pathogen effectors have been reported to localize in the nucleolus, including Pi23226, Pi23015, Pi07550, and Pi04089 (Wang et al., 2019). The subcellular localization of the four effectors (Pi23226, Pi23015, Pi07550, and Pi04089) was confirmed by transient coexpression of N-terminal GFP-tagged effector constructs along with RFP-Fib2 as nucleolar marker in *N. benthamiana* leaves. Protein expression levels of constructs were confirmed using α-GFP immunoblotting assay (Figure 1-2). All of the effectors colocalized with RFP-Fib2 primarily in the nucleolus (Figure 1-1 C). Pi23226 was reported to localize in nucleocytoplasm and occasionally nucleolar (Wang et al., 2019); however, we observed accumulation of Pi23226 mainly in nucleoli. Enhanced CaMV 35S promoter used in this study probably increased the transcriptional level of Pi23226 leading to its accumulation in the nucleolus. Among nucleolus targeting effectors, Pi23015 and Pi23226 have almost identical amino acid sequences except for the C-terminal variation (Figure 1-3); therefore, we generated a deletion mutant containing only the conserved sequence (Pi23226ΔC). We observed that Pi23226ΔC was localized in the nucleolus, similar to Pi23226 and Pi23015, indicating that

Pi23226ΔC still contains the ability of nucleolar localization. A nuclear localization signal was detected in N-terminal region (aa. 12–29) of the effector domain in subcellular localization prediction using LOCALIZER (Sperschneider et al., 2017) (Figure 1-3). To determine whether Pi23226's nucleolar localization is required for its nucleolar inflation activity, we drove Pi23226 out of the nucleolus by inserting a nuclear export signal (NES) at the C-terminus of Pi23226 (Pi23226-NES). Pi23226-NES remained localized in the nucleus but not in the nucleolus and did not increase nucleolar size (Figure 1-1 C).

We examined the nucleolar morphology in the effector-expressing *N. benthamiana* cells. Nucleolar size inflation was observed only in Pi23226-expressing cells (Figure 1-1 C). To investigate the effect of Pi23226 on *P. infestans* virulence, we inoculated *P. infestans* under host-induced gene silencing (HIGS) and effector-overexpression conditions. The virulence of *P. infestans* was reduced when Pi23226 expression was suppressed (Figure 1-4), while Pi23226 enhanced pathogen growth, consistent with previous report (Lee et al., 2018) (Figure 1-5). Pi23226ΔC or Pi23226-NES did not significantly enhance pathogen growth when compared to Pi23226, indicating that the nucleolar localization and nucleolar inflation of Pi23226 affect the virulence of pathogen (Figure 1-5). We also performed HIGS on Pi23015 and

found that it reduced *P. infestans* virulence, implying that nucleolar localized effectors play a variety of roles in pathogen colonization. Additionally, as Pi23226 has been reported to enhance *P. infestans* virulence in *N. benthamiana* (Lee et al., 2018), we hypothesized that Pi23226 could modulate the general functions of its host nucleolar. We investigated the timing of expression of these nucleolar-localizing effectors during infection by measuring their transcript levels using qRT-PCR. The transcripts of Pi04089, Pi07550, Pi23015, and Pi23226 gradually increased during the biotrophic stage and reached maximum levels at 4 to 5 dpi (Figure 1-1 B), which is considered as the time for transition to the necrotrophic phase. These results suggested that Pi23226 could function in the host nucleolus for the transition of pathogen life cycle from the biotrophic to necrotrophic phase.

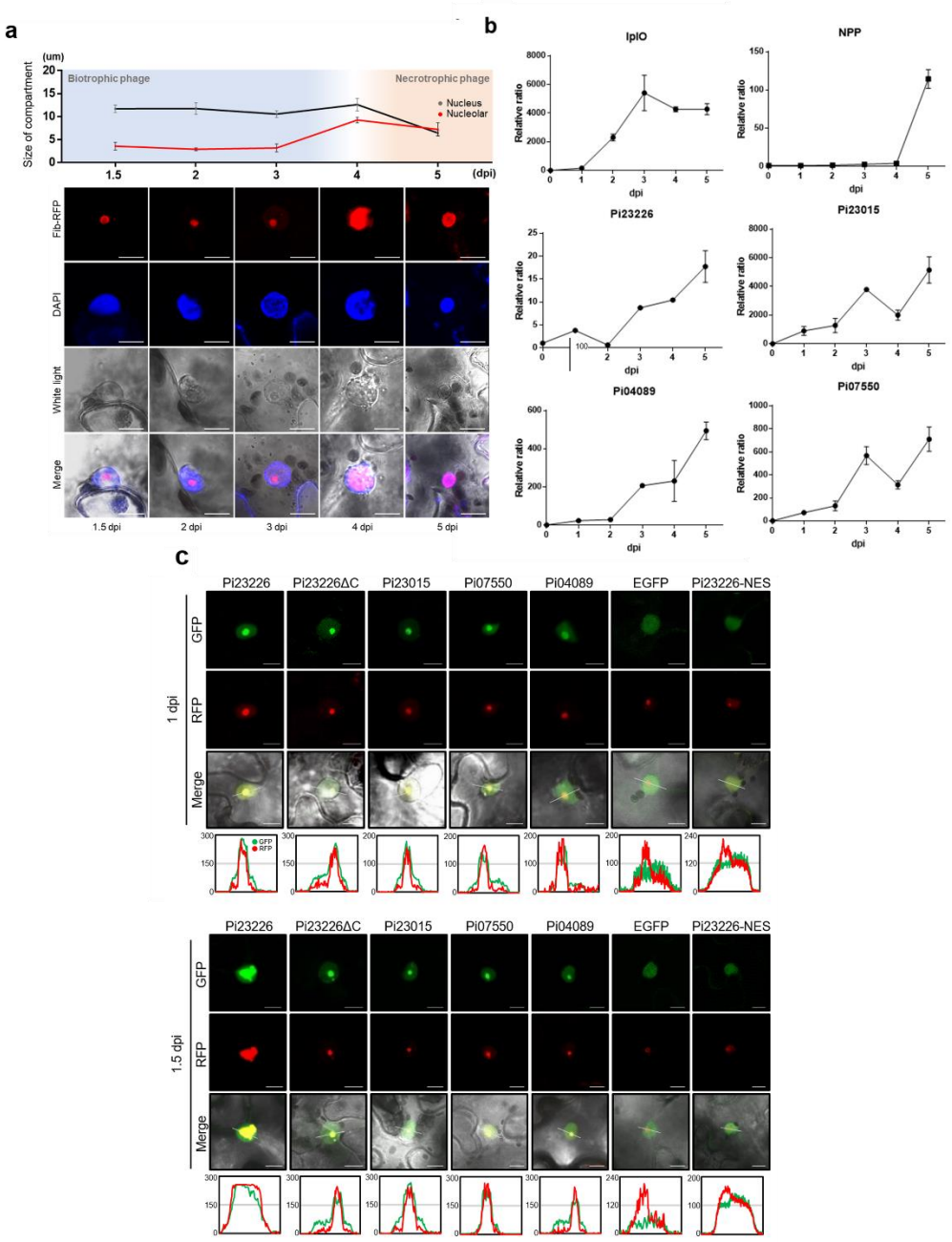

Figure 1-1. Inflation of host nucleoli before the initiation of necrosis following infection of *P. infestans.*

(A) Morphology of host nucleolus during infection of *P. infestans*. RFP-fibrillarin2 (RFP-Fib2, red) was detected by confocal microscopy (SP8 X, Leica, Germany) as a nucleolar marker. DAPI staining (blue) was used to track nuclear and nucleolar sizes. Images were captured for 5 days after infection under red, blue, and white light, and subsequently merged. Top panel shows the sizes of nuclear and nucleolar sizes. Representative confocal images from three independent experiments are presented. (B) Transcript accumulation of IpIO and NPP1.1, and nucleolar-localizing effectors were measured by qRT-PCR. Each transcript level was normalized to each gene at the initiation of infection (0 dpi). Representative fold changes are depicted as the mean values ± SD from three biological replicates. (C) Nucleolar localization of *P. infestans* effectors. Each GFP-fused effector was detected by confocal microscopy along with RFP-Fib2 as a nucleolar marker. Images were captured at 1 and 1.5 dpi under green, red, and white light, and subsequently merged. GFP signals from each effector construct were overlaid with those of RFP-Fib2 in the histogram. Representative confocal images from 5 independent experiments are presented.

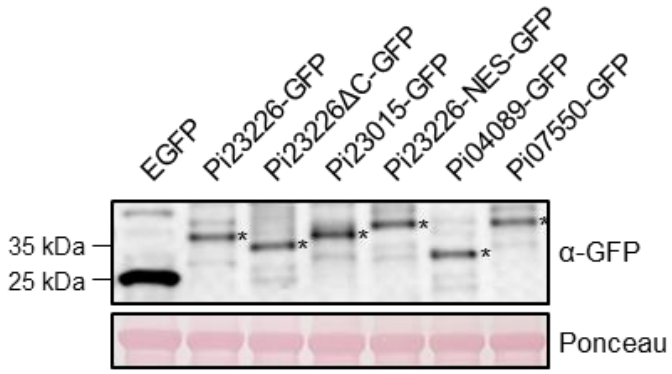

Figure 1-2. Western blot analysis of selected C-terminus GFP tagged proteins after transient expression. Leaf discs were harvested at 1.5 dpi. The blots are revealed after incubation with the anti-GFP specific antibodies.

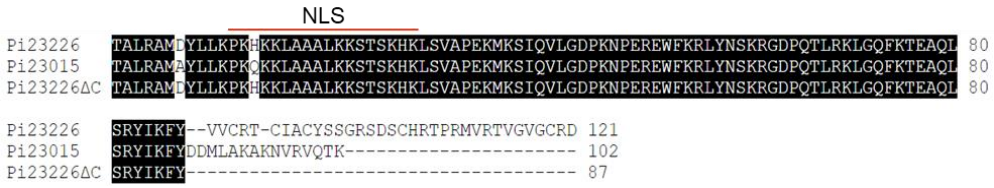

Figure 1-3. Sequence alignment of Pi23226, Pi23226ΔC, and Pi23015. The effector domain sequences of each effector were aligned. Residues with the identical or similar biochemical properties were shown in black. Nuclear localization signal was predicted with LOCALIZER.

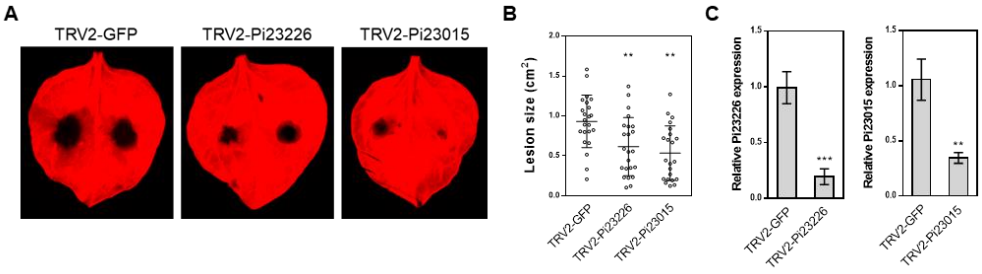

Figure 1-4. Effects of Pi23226 and Pi23015 HIGS on resistance to *P. infestans* infection. (A) Disease symptoms of the Pi23226 or Pi23015 silenced *N. benthamiana* plants compared with GFP control. Pictures were taken at 7 days after infection. (B) Lesion size of Pi23226 or Pi23015 silenced leaves. These experiments were repeated for three times using at least 20 leaves per treatment. Error bars show the standard deviation of three biological replicates. Asterisks indicate statistically significant differences determined by Student's t-tests (**P < 0.01). (C) Expression levels of Pi23226 and Pi23015 in *P. infestans* infected leaves respectively. Error bars show ± SE (n=3).

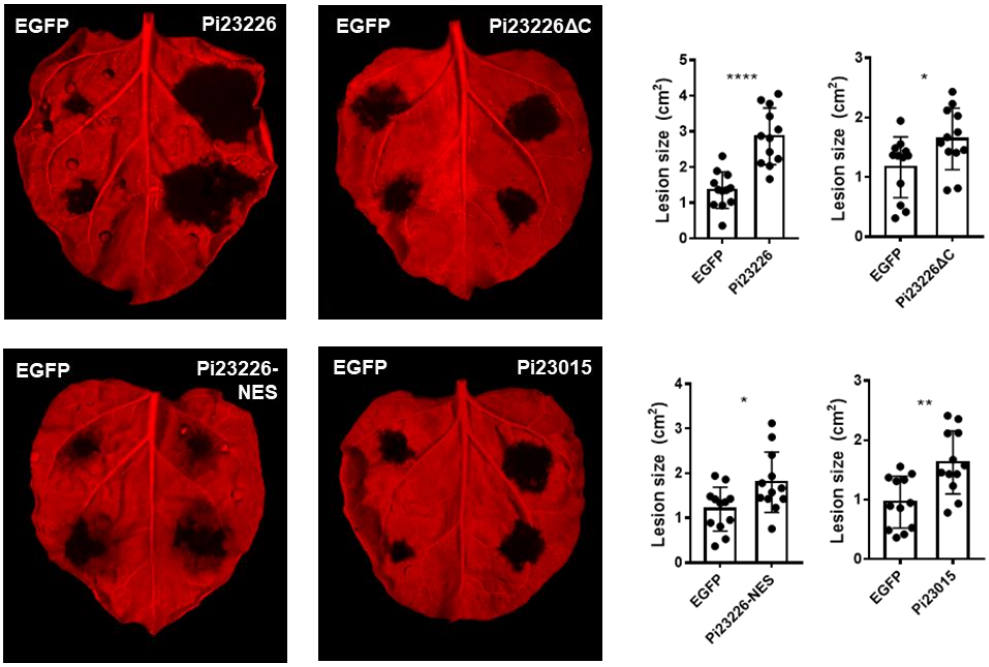

Figure 1-5. Pi23226 enhances pathogenicity of *P. infestans*. FLAG-effectors were expressed on one-half of the *N. benthamiana* leave and GFP expressed on the other half as a negative control. *P. infestans* (T30-4) was inoculated on the detached leaves after 1 day after infiltration. The lesion size was measured 5 days after inoculation. Each lesion size was photographed using Cy5 channels in Azure 400 (Azure biosystem, USA).

Nucleolar inflation coincides with Pi23226-induced necrotrophic cell death

To investigate whether Pi23226-induced cell death is the result of the canonical ETI pathway, we silenced several ETI components in *N. benthamiana* and expressed Pi23226 by agroinfiltration. SGT1, and RAR1 mediate R gene-activated disease resistance (Azevedo et al., 2002; Azevedo et al., 2006); EDS1 and NDR1 function in TNL and CNL-mediated defense signaling, respectively (Moreau et al., 2012; McNeece et al., 2017); NRC2/3/4, and NRG/ADR1 function as helper NLRs (Bonardi et al., 2011; Wu et al., 2017). In all tested ETI component-silenced plants, Pi23226 induced cell death similar to GFP-silenced plants (Figure 1-6). Additionally, when we tested Pi23226's cell death activity in other Solanaceae species, it induced cell death in host species *S. lycopersicum* and nonhost species *N. tabacum* and *Capsicum annuum* (Figure 1-7). These results indicate that the Pi23226-induced cell death is likely canonical ETI pathway independent.

Because Pi23226 induces host cell death concomitantly with nucleolar size inflation, we tested the cell death-inducing activities of other nucleolar effectors. However, none of the other transiently expressed nucleolar effectors induced cell death in *N. benthamiana* leaves. Additionally, Pi23226-NES also did not induce cell death, indicating that the nucleolar localization of Pi23226

is required for its cell death activity (Figure 1-8). The inflation of nucleolar size observed in Pi23226-expressing cells occurred before visible cell death. We investigated whether nucleolar size inflation could result from the cell death by observing nucleolar morphology in cells expressing cell death-inducers INF1 and CC309. INF1 and CC309 induce cell death by plasma membrane-mediated signal transduction in *N. benthamiana* (Lee et al., 2021). We observed that both INF1 and CC309 induced a gradual decrease in nuclear size and a slight increase in nucleolar size as the cell death progressed. However, Pi23226 showed a slightly increased nuclear size and a significantly greater increase in nucleolar size at 1.2 dpi. In fact, the nucleolus expressing Pi23226 inflated 3.3-fold, which is much greater than the 1.6-fold and 1.9-fold increase observed for INF1 and CC309, respectively (Figure 1-8 B and C). We concluded that nuclear shrinkage occurs commonly under cell death-inducing conditions whereas nucleolar size inflation occurred specifically in cell death induced by Pi23226. Because nucleoli primarily function in ribosome biogenesis, we postulated that Pi23226 could affect ribosome biogenesis and protein translation.

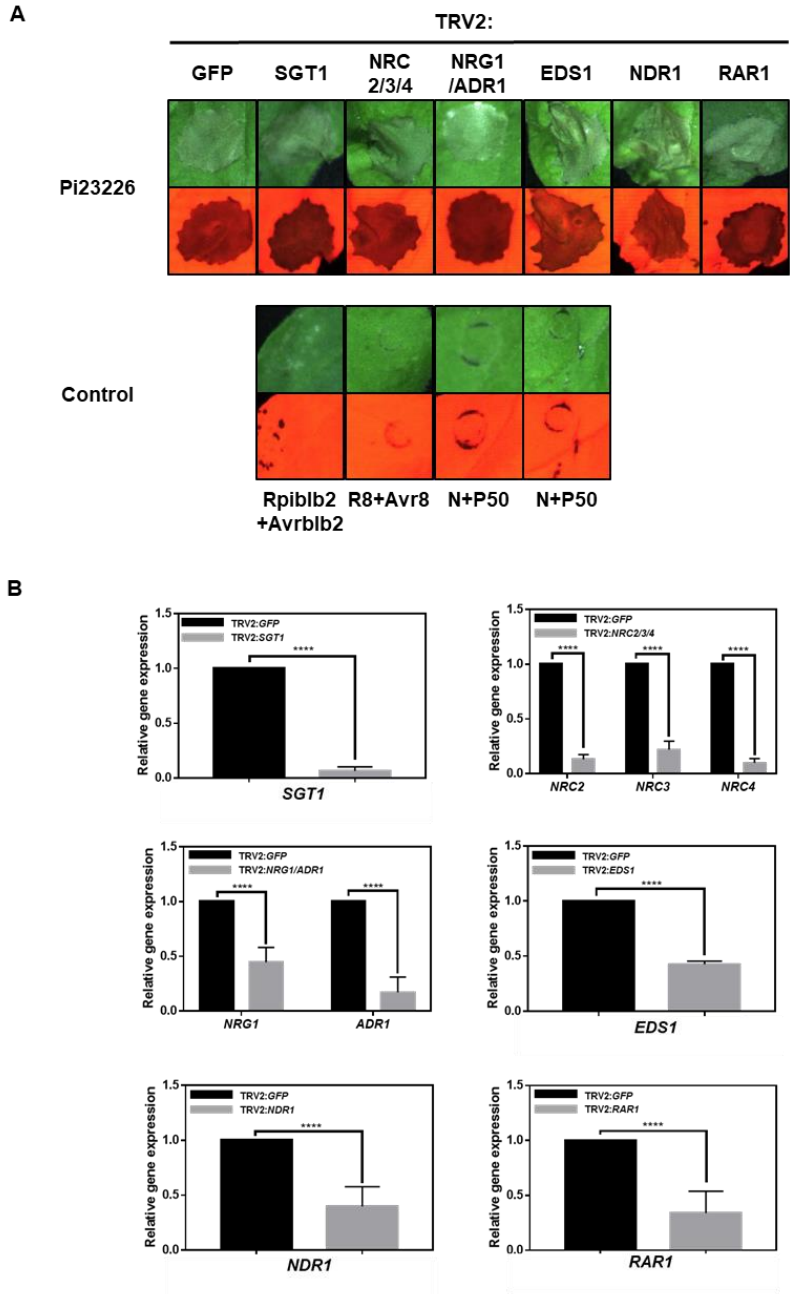

Figure 1-6. Pi23226 induced cell death in ETI component-silenced plants. (A) Three-week-old *N. benthamiana* silenced by TRV:GFP, TRV:SGT1,

TRV:RAR1, TRV:NRC2/3/4, TRV:NRG1/ADR1, TRV:EDS1, or TRV:NDR1 were agro-infiltrated with Pi23226. Rpiblb2+Avrblb2, R8+Avr8 and N+P50 were used as controls for efficiently silenced each component. The leaves were photographed at 4 dpi using white and Cy5 and Cy3 channels in Azure 400 (Azure biosystem, USA). (B) Transcript levels of silenced plants. The transcript level of each component was measured by qRT-PCR at 3 weeks after VIGS. Representative fold changes are depicted as the mean values ± SD from three biological replicates.

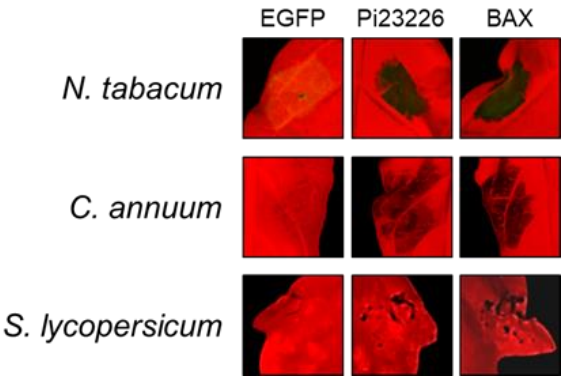

Figure 1-7. Induction of cell death by Pi23226 in Solanaceae plants. Plants including *N. tabacum* (Samsun), *C. annuum* (CM334), *S. lycopersicum* (Heinz) leaves were agroinfiltrated with construct expressing Pi23226. EGFP and BAX were used as a negative and positive control, respectively. Representative images were taken 5 days after infiltration.

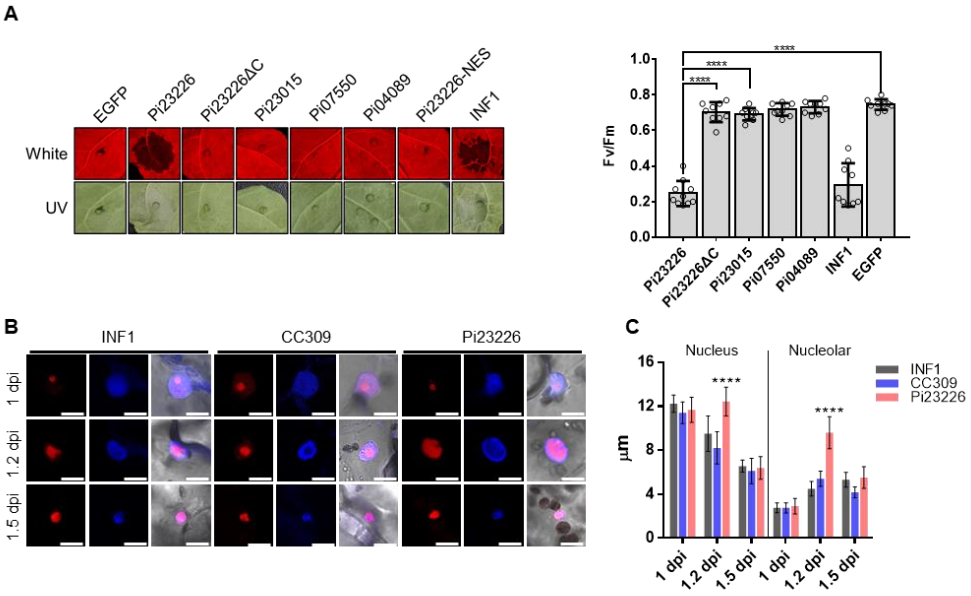

Figure 1-8. Nucleolar inflation coincides with Pi23226-induced cell death. (A) Cell death induced by the Pi23226 nucleolar effector. Cell death was observed under white and UV light. INF1 and EGFP were used as positive and negative controls, respectively. Representative images are presented. The quantum yield of photosystem II (Fv/Fm) was measured (Closed FluorCam FC 800-1010GFP, Photon Systems Instruments, Czechia) to represent the intensity of cell death. Data are mean values ± SD of five biological replicates. Significance was determined using one-way ANOVA (**** $p<0.0001$). (B) Nucleolar morphology in cells expressing Pi23226, INF1, and CC309. Each construct was co-infiltrated with RFP-Fib2 into *N. benthamiana*, and the nucleus and nucleolus were observed during the progression of cell death.

Images were captured for two days after infection under red, blue, and white light, and subsequently merged. Representative confocal images from three independent experiments are presented. (C) Changes in nuclear and nucleolar sizes in cells expressing Pi23226, INF1 or CC309. Each Pi23226, INF1 or CC309 construct was co-infiltrated with RFP-Fib2 into *N. benthamiana* leaves. Nuclear and nucleolar diameters were measured using ImageJ at 1, 1.2, and 1.5 dpi. For oval shapes, the semi-major axis was measured. Data are mean values ± SD for three biological replicates. Significance was determined using one-way ANOVA with Dunnett's test (**** $p<0.0001$).

Pi23226 directly binds 25S rRNA

To test whether Pi23226 binds rRNA and interferes with ribosome biogenesis, we examined the binding of Pi23226 to rRNA-RNP complexes using RNA immunoprecipitation (RIP) of FLAG-tagged effectors transiently expressed in *N. benthamiana*. RNA-protein complexes were crosslinked with formaldehyde, precipitated with anti-FLAG affinity gels, and followed by reverse crosslinking. The amount of precipitated RNA was measured by qRT-PCR analysis using primers amplifying 18S, 5.8S, and 25S rRNA and normalized to the input, which was similarly treated as RIP but without the precipitation step (Figure 1-9). The 25S rRNA region was enriched 20- to 30-fold in cells expressing Pi23226, whereas no amplification of the 25S rRNA region was observed in cells expressing Pi23226ΔC or Pi23015. By contrast, the 18S and 5.8S regions were not enriched in any of the samples (Figure 1-10 A). To analyze whether Pi23226 contains RNA-binding motif, we conducted PRIdictor using the amino acid sequence (Tuvshinjargal et al., 2016). Three motifs were predicted to bind with RNA: among them, two sites were located at the C-terminal region which is different with Pi23015 (Figure 1-11). To identify the Pi23226 binding region rRNA, we performed individual-nucleotide resolution UV crosslinking and immunoprecipitation (iCLIP), which utilizes UV to crosslink RNA-protein complex, but not

protein-protein interaction, followed by next-generation sequencing (NGS) to precisely identify the Pi23226-binding sequence on 25S rRNA. Consistent with the RIP results, iCLIP-NGS analyses identified the sequence covering the 3′-end of the 25S rRNA gene as the Pi23226-binding region (Figure 1-10 C and 1-5). To verify the NGS results, we designed primer sets to amplify the exact 3′-end region identified in the NGS results (primer 25S-4) and covering the peripheral area (primer 25S-3 and 25S-5) (Figure 1-12). The qRT-PCR results showed that the 25S-4 amplicon was enriched in Pi23226-expressing cells but not in Pi23226ΔC- or Pi23015-expressing cells (Figure 1-10 D). Amplicons at the peripheral area (primers 25S-3 and 25S-5) were not enriched in any of the construct-expressing samples. To investigate whether Pi23226 directly interacts with 25S-4 amplicon, we conducted RNA electrophoretic mobility gel shift assay. The 25S-4 amplicon shifted with gradually increased GST:Pi23226 (Figure 1-13 and 1-14). Whereas, the 25S-2 region was not shifted by either Pi23226 or Pi23015. These results indicate that Pi23226 directly binds to rRNA, especially the 3′-end of the 25S rRNA region (Figure 1-10 B). Thus, we postulated that Pi23226 binding to the 25S rRNA sequence could interfere with 25S rRNA processing from the precursor.

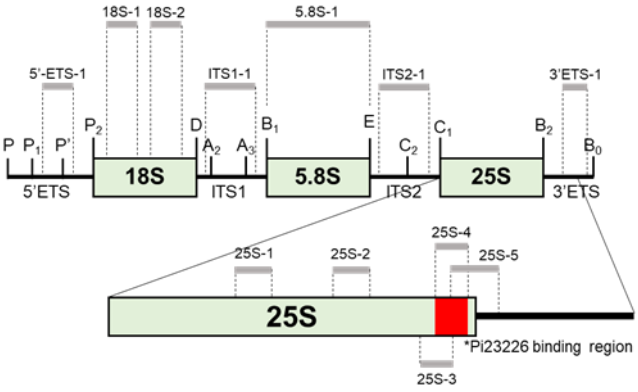

Figure 1-9. Information of primers used in Figure 2 and 3 was indicated on the 45S rRNA.

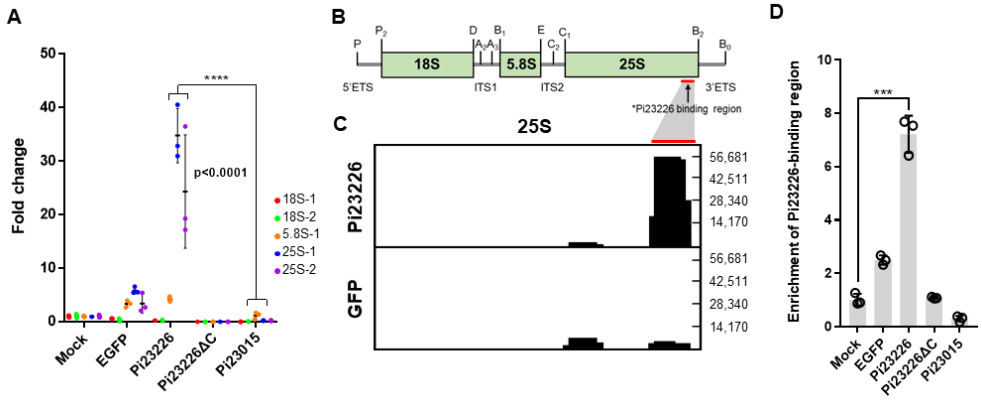

Figure 1-10. Pi23226 directly binds to 25S rRNA. (A) RIP using FLAG-fused effector constructs. FLAG-effector constructs were expressed in *N. benthamiana* using agroinfiltration. The abundance of RNAs associated with FLAG-fused effectors was measured and normalized relative to inputs which were processed identically as RIP except for precipitation. Specific primers to amplify 18S, 5.8S, and 25S rRNAs were used in qRT-PCR. Data represents mean values ±SD, and significance was determined using Student's t-test (**** $p<0.0001$). (B) 45S rRNA transcript containing 18S, 5.8S, and 25S rRNAs. Exonucleolytic and endonucleolytic cleavage sites are indicated. The Pi23226 binding region on 25S rRNA from iCLIP is marked with a red bar. (C) Pi23226 specifically binds to the 3′-end of 25S rRNA. iCLIP-seq data were mapped on the *N. benthamiana* genome (v1.0.1). The normalized mapped reads on 25S rRNA gene region are presented as Integrative Genomics Viewer. iCLIP-seq data from FLAG:GFP-expressing *N.*

benthamiana are used as a negative control. (D) iCLIP-qRT-PCR for validation of iCLIP-seq. FLAG-effector constructs were expressed in *N. benthamiana*. iCLIP-qRT-PCR was performed using primers derived from the 3′-region of 25S rRNA (Figure 1-9B). RNA abundance was measured and normalized relative to inputs, which were processed identically as iCLIP except for precipitation. Representative fold changes of amplicons are depicted as mean values ±SD from five biological replicates and significance was determined using Student's t-test (*** $p<0.001$).

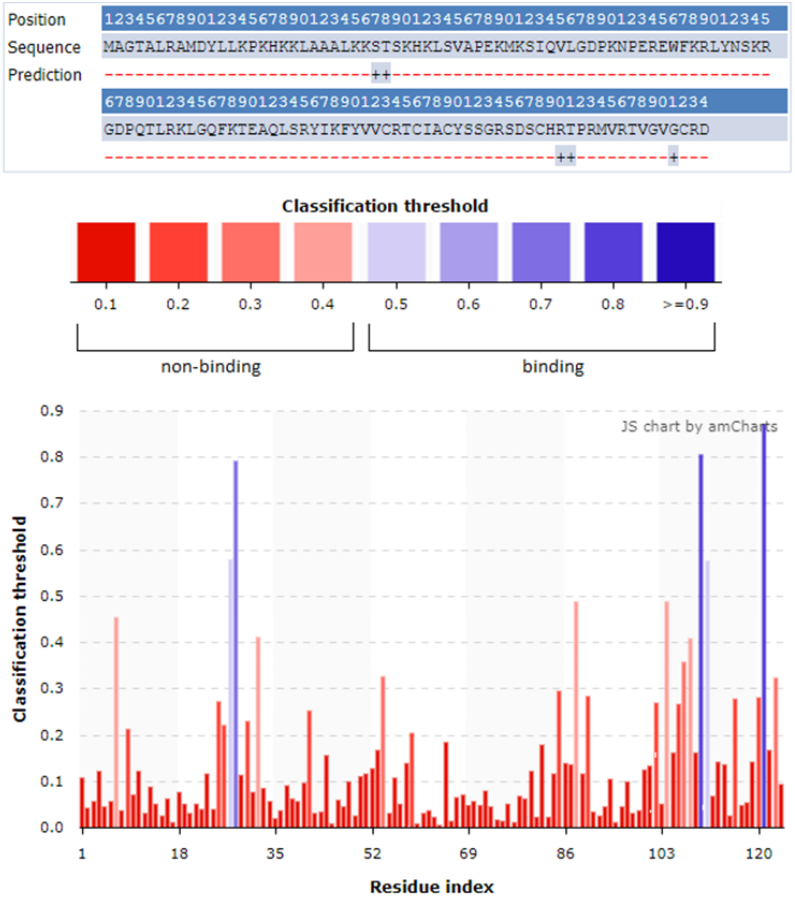

Figure 1-11. Information about RNA binding site in Pi23226 provided by PRIdictor. Indicated single amino acids are predicted to bind with RNA.

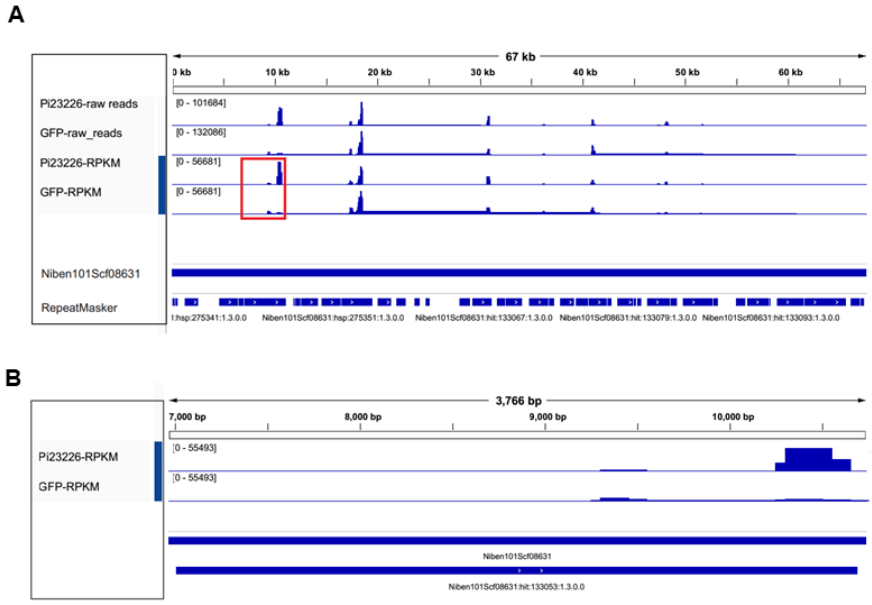

Figure 1-12. Genomic landscape of the rRNA locus for Pi23226- and GFP-iCLIP analyses (A) The raw and RPKM normalized read coverages were visualized using IGV for the Niben101Scf 08631 scaffold in *N. benthamiana*. (B) Expanded view of red box in (A).

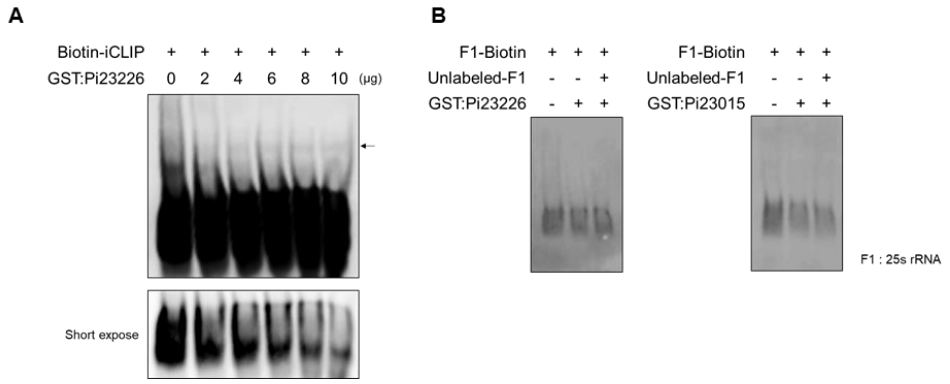

Figure 1-13. Electrophoretic mobility shift assay (EMSA) of Pi23226 binding to the 25S rRNA *in vitro*. (A) Biotinlabeled RNA probe from the 25S rRNA region which were identified in iCLIP-seq was incubated with Pi23226 protein. Concentrations (μM) of Pi23226 protein in reactions are indicated above. Arrowhead indicates protein-bound RNA. - and + represent the absence or presence of the indicated constructs. (B) Gel image of binding assay of Pi23226 or Pi23015 with 25S rRNA fragment (F1). 25S rRNA fragment was used as a negative control.

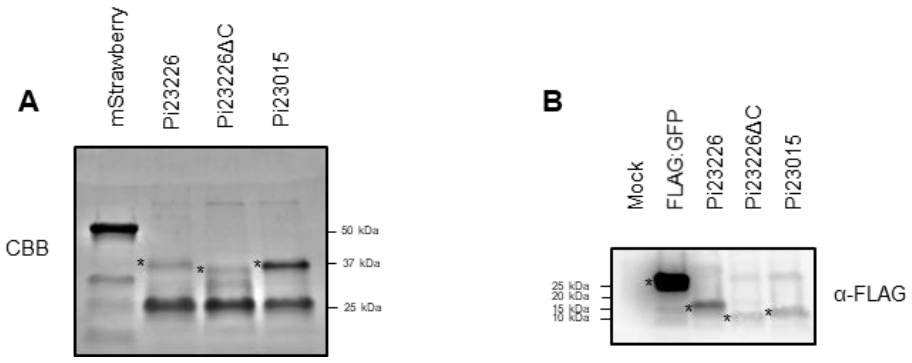

Figure 1-14. Protein expression of recombinant proteins (A) GST-fused effectors were expressed in *E. coli* (BL21). Recombinant proteins were detected on SDS-PAGE followed by Coomassie blue staining. (B) Protein expression of FLAG-effectors in *N. benthamiana*. Leave tissues were collected at 1.5 dpi after agroinfiltration of FLAG-fused effectors. Total protein was extracted and the protein levels of FLAG-effectors were measured using anti-FLAG.

Pi23226 disrupts pre-rRNA processing and induces nucleolar stress

To investigate whether Pi23226 binding to 25S rRNA affects rRNA processing, we measured the accumulated levels of rRNAs using qRT-PCR. Unexpectedly, all 18S, 5.8S, and 25S rRNA fragments were highly accumulated in cells expressing Pi23226, Pi23226ΔC, and Pi23015 compared to the EGFP control, whereas the 5′-ETS, ITS1, and ITS2 regions did not show a significant difference. There was no abnormal accumulation of rRNA in cells expressing INF1 compared to the EGFP control, indicating that rRNA accumulation was not a result of cell death (Figure 1-15). This suggests that Pi23226, Pi23015 and Pi23226ΔC could increase mature rRNA accumulation by an unknown mechanism. A 10-fold higher accumulation of 3′-ETS was observed only in cell expressing Pi23226 (Figure 1-15A). In addition, the ratio of untrimmed 27S rRNA precursor/25S rRNA also increased only in cells expressing Pi23226 (Figure 1-15B). These results suggested that Pi23226 binding to the 3′-end of the 27S rRNA precursor could interfere with the cleavage of the 3′-ETS from the 27S rRNA precursor. To confirm that Pi23226 disrupted pre-rRNA maturation, we performed circular RT-PCR (cRT-PCR). Each fragment of 18S, 5.8S, and 25S was circularized by reverse primers, designed as 18C, 5.8C, and 25C, respectively, subjected to PCR with the indicated primer sets, and detected in agarose gels (Figure 1-15 C-1). Two

abnormal bands were detected only for 25S cRT-PCR in cells expressing Pi23226, whereas no significant differences were observed in cells expressing other effector constructs (Figure 1-15 C-2). To investigate which rRNA processing was disrupted by Pi23226, the abnormal bands were collected and sequenced. Sequencing analysis of the abnormal bands indicated that one contained 27SB including 5.8S, ITS2, and 25S rRNA sequences, and the other contained 27SA3 and part of 3′-ETS (3′-ETSp) (Figure 1-15 C-1, lower box). During pre-rRNA processing step in ribosome biogenesis, premature 35S is trimmed in multiple steps to be finalized in 18S, 5.8S, and 25S. In the maturation of 25S rRNA, 35S rRNA is cleaved by nuclease to remove 3'-ETS (Weis et al., 2015). This indicated that ectopic expression of Pi23226 caused inefficient processing in the maturation steps from 27SA3 and 27SB rRNA to 25S rRNA precursors and the removal step of 3′-ETS from 25S rRNA precursors. This also suggests that Pi23226 binding on the 3′-end of 25S may interfere with the early stage of the ITS1-first pathway in pre-rRNA processing and result in the accumulation of malprocessed pre-rRNA.

These observations of Pi23226-induced enlargement of nucleolar size and accumulation of malprocessed rRNA prompted us to investigate the activation of nucleolar stress. The p53 transcription factor is a key regulator of the ribosomal stress response in mammals, although no p53 ortholog has been

reported in plants (Ohbayashi et al., 2017). The Arabidopsis NAC082 transcription factor (ANAC082, AT5G09330) has been reported as an essential biomarker that is upregulated under nucleolar stress conditions (Ohbayashi et al., 2017). Therefore, we examined the transcript levels of the NAC082 transcription factor by qRT-PCR. We selected four NAC082 transcription factor candidates from *N. benthamiana* (designated as NbNAC082-1 to -4 according to the degree of similarity to ANAC082). NbNAC082-1, the closest homolog of ANAC082, was specifically upregulated only in Pi23226-overexpressing cells (Figure 1-16). Furthermore, we measured the transcript levels of NAC092 and SOG1, which are responsive to DNA damage and oxidative stress, respectively (Ohbayashi and Sugiyama, 2018), and found that Pi23226 did not activate those genes (Figure 1-15 D). These results indicate that Pi23226 binding to the 3′-end of the 25S rRNA sequence may lead to the accumulation of untrimmed 25S rRNA by inappropriate processing from 27S to 25S rRNA, which eventually affects ribosome biogenesis and causes nucleolar stress.

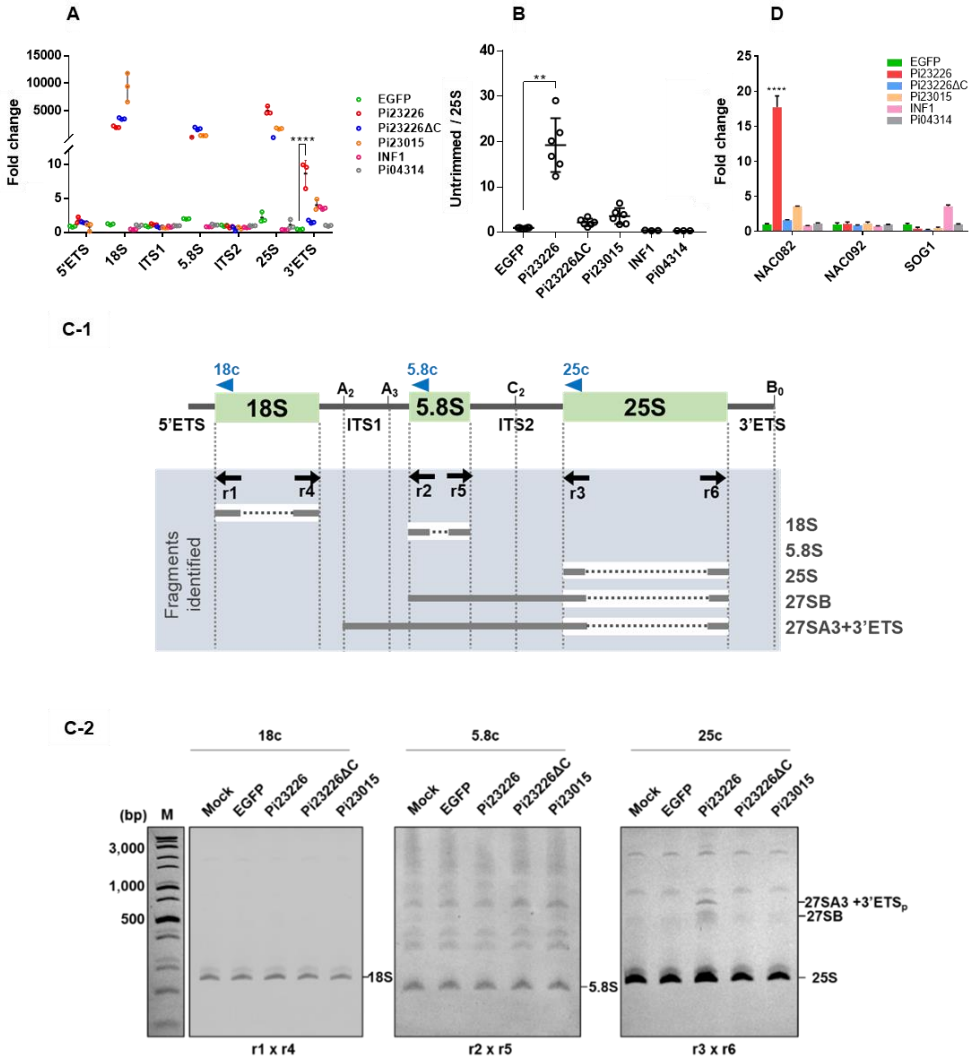

Figure 1-15. Pi23226 disrupts pre-rRNA processing and induces nucleolar stress. (A) The rRNA fragments are accumulated in FLAG-fused effector constructs and INF1 expresssing leaves. The abundance of rRNA was measured after the expression of Pi23226, Pi23226ΔC, Pi23015, and INF1 using qRT-PCR. The graph depicts the relative ratios of amplified fragments

normalized to the level of ubiquitin (UBQ) transcripts. RNA samples from eGFP-expressing *N. benthamiana* cells were used as a negative control. A representative graph from four biological replicates is presented, and the significance was determined using one-way ANOVA with Dunnett's test (**** $p<0.0001$). (B) Pi23226-induced accumulation of unprocessed 27S rRNAs. The untrimmed 3′-region of 25S rRNA was quantified by qRT-PCR using primers covering 25S and 3′-ETS. The relative ratio was calculated from the amplicons covered from the end of 25S rRNA to 3′-ETS normalized by the level of 25S rRNA transcripts. RNA samples from eGFP-expressing *N. benthamiana* cells were used as a negative control. A representative graph from six biological replicates is presented (one-way ANOVA (*** $p<0.001$)). (C-1) Primers designed for cRT-PCR to amplify the pre-rRNA fragments. Nuclear RNA samples from effector-expressing *N. benthamiana* cells were circularized by RNA ligation; 18S, 5.8S, and 25S intermediate cDNAs were synthesized using specific primers (arrows without bars); and each intermediate was amplified by PCR (arrows with bars). Amplicons in Figure 4C-2 are depicted as black bars. Gray bars in 27SB and 27SA3+3′ETSp indicate sequencing results from abnormal bands in C-2. (C-2) Gels showing the rRNA processing intermediates using cRT-PCR with different primer sets as indicated in Figure 1-15 under effector-expressing

conditions. Bands at the bottom present the minimal size, which can be amplified with each primer set following cRT-PCR. Abnormal bands shown in the cRT-PCR by 25c under Pi23226-expressing conditions represent 27SA3 and 27SB. Representative images from three biological replicates are shown. (D) Transcript levels of cellular stress marker gene candidates measured by qRT-PCR. Each transcript level was normalized to *EF1-α* as a reference gene and compared to EGFP as a negative control. Significance was determined using one-way ANOVA (*** $p<0.001$).

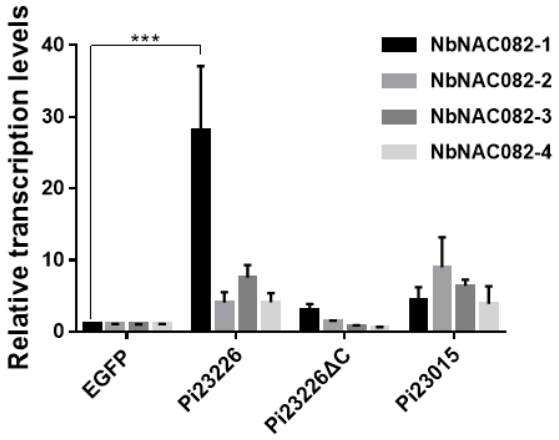

Figure 1-16. Transcript levels of NAC082 transcription factor candidates measured by quantitative RT-PCR. Each transcript level was normalized by *EF1-α* as a reference gene and compared to EGFP as a negative control. The significance was determined using one-way ANOVA test (***, $p<0.001$).

Pi23226 disrupts protein synthesis by suppressing global translation

We performed polysome profiling using ultra-High Performance Liquid Chromatography (uHPLC) (Yoshikawa et al., 2018) to investigate whether Pi23226-induced defects in pre-rRNA processing perturb ribosome assembly. Polysomes were isolated from leaf tissues expressing FLAG:Pi23226, FLAG: Pi23226 ΔC, or FLAG:Pi23015, and then collected in 27 fractions with a column flow rate of 0.4 ml/min with monitoring by measuring UV absorbance at 260 nm (Figure 1-17 A and Figure 1-18). Polysomes isolated from untreated and FLAG:GST-expressing leaf tissues were used as negative controls. The 40S and 60S subunit, monosome and n-mer polysomes eluted at ~33min, 32min, 31min and 29min, respectively. Pi23226 expressing cells showed increased levels of 60S, 40S subunit and small protein complex with a distinct increase in the peaks (Figure 1-17 A). To validate the relevant protein distribution in polysome profiling, proteins were extracted from each fractions and immunoblotted using ribosomal protein large subunit 13 antibody (α-RPL13). Pi23226 caused a significant increase in 60S and reduced the 80S/60S ratio, whereas Pi23226ΔC and Pi23015 did not affect the distribution of ribosomes (Figure 1-17 A and1-18). To investigate whether Pi23226 associated with ribosome subunits, we performed western blotting using α-FLAG. The results showed that Pi23226, but not Pi23226ΔC or

Pi23015, was detected in fractions representing polysomes and 60S subunits. We postulated that Pi23226 association with polysomes and rRNA may affect pre-rRNA processing and assembly; thus, we investigated the effect of Pi23226 on protein translation activity. First, we adapted the wheat germ extract system for *in vitro* translation experiments. Recombinant GFP plasmid DNA was used as a template for translation. We validated the system by inhibiting the *in vitro* translation of GFP using the translation inhibitor cycloheximide (CHX). The translated GFP products were significantly reduced according to the CHX concentration (Figure 1-17 B, lower panel). Subsequently, the recombinant GST:Pi23226, GST:Pi23226ΔC, and GST:Pi23015 proteins were incubated with wheat germ extract in the presence of GFP plasmid constructs. GFP protein was not translated in the presence of GST:Pi23226, whereas neither GST:Pi23226ΔC nor GST:Pi23015 affected the translation of GFP (Figure 1-17 B, upper panel). Next, we examined *de novo* protein synthesis *in planta* using a surface sensing of translation (SUnSET) assay (Van Hoewyk, 2016). Similar to the *in vitro* translation system, *de novo* protein was barely detected by treatment with a high concentration of CHX (Figure 1-17 C, left panel). Consistent with the *in vitro* analysis, *de novo* protein translation was significantly reduced under Pi23226-expressing conditions, whereas no significant change in total protein

synthesis was observed under Pi23226ΔC or Pi23015-exxpressing conditions (Figure 1-17 C, right panel). These combined results suggest that Pi23226 but not Pi23226ΔC or Pi23015 disrupts protein synthesis, probably by associating with functional polysomes and the 60S subunit, thereby resulting in translation inhibition.

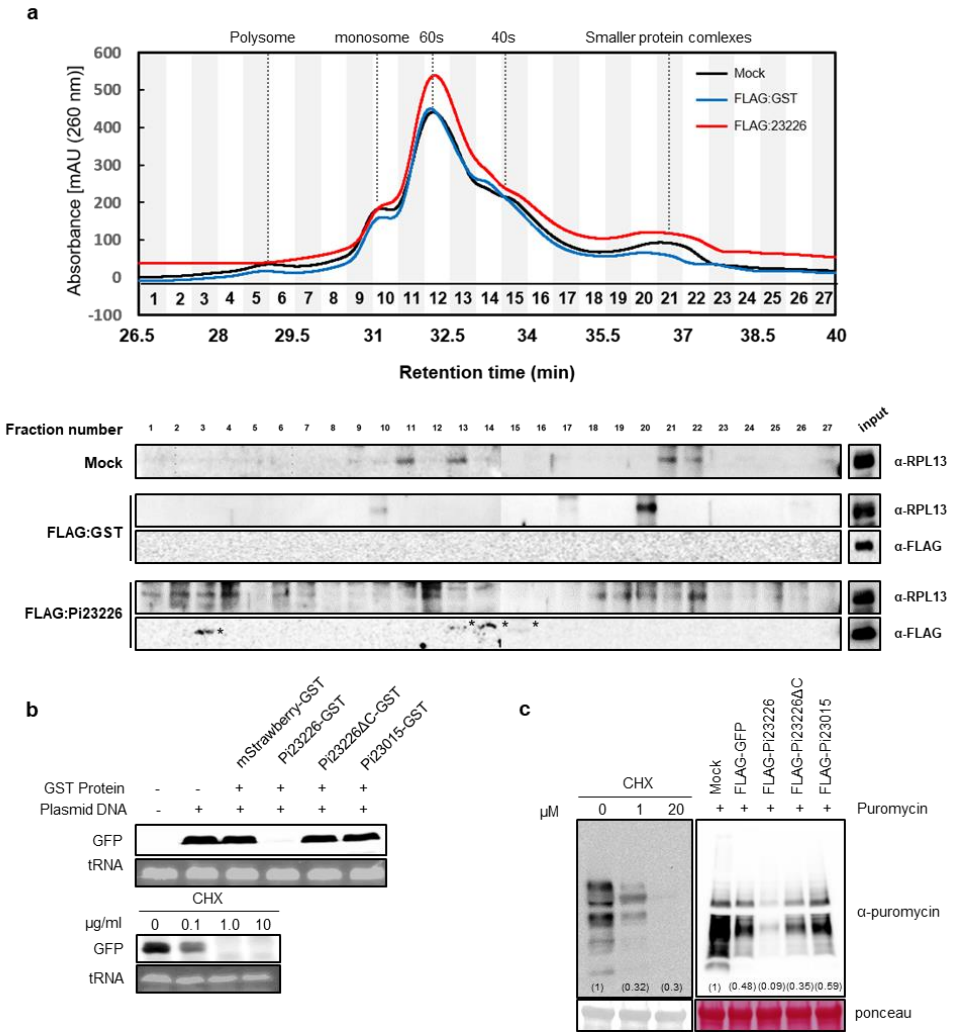

Figure 1-17. Pi23226-induced interruption of protein synthesis suppresses global translation. (A) Pi23226 affected the polysome profile. Ribosomes were isolated from leaf tissues expressing FLAG:Pi23226. Untreated or FLAG:GST-expressing conditions were used as negative controls. Ribosomes were collected into 27 fractions with a column flow rate of 0.4 ml/min with

monitoring absorbance at 260 nm. Fractionated proteins were extracted and detected with anti-RPL13 or anti-FLAG antibodies and compared with input. Representative images from three biological replicates are shown. (B) Pi23226 inhibits *in vitro* translation of GFP using wheat germ extract. Lower panel: CHX-dependent inhibition of *in vitro* GFP translation. Upper panel: GFP translation *in vitro* following incubation with GST-fused recombinant effector proteins. GFP was detected with an anti-GFP antibody. Equal loading was controlled by adding ε-labeled biotinylated lysine tRNA. Representative images from five independent experiments are shown. (C) Pi23226 inhibits *de novo* protein synthesis in the SUnSET assay. The level of newly synthesized protein from effector-expressing *N. benthamiana* following puromycin treatment was measured using an anti-puromycin antibody. Left panel: CHX-dependent inhibition of *de novo* protein synthesis. Protein samples were extracted after puromycin treatment following CHX supplementation. Right panel: SUnSET assay for the detection of newly synthesized protein in FLAG-effector-expressing *N. benthamiana*. FLAG:GFP-expressing and untreated leaf tissues were used as negative controls. The loading control was visualized by Ponceau staining.

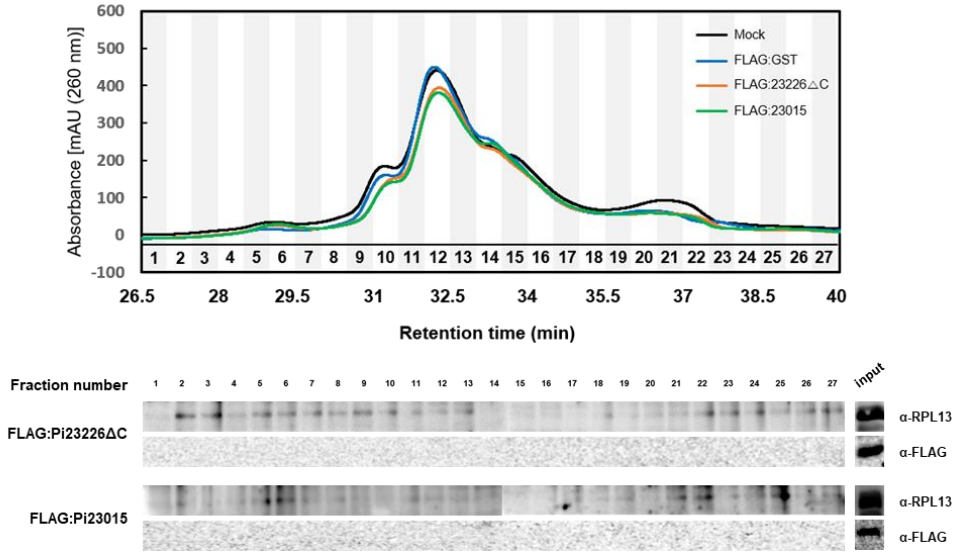

Figure 1-18. Polysome profiling in FLAG:Pi23226ΔC and Pi23015-expressing *N. benthamiana* using HPLC. Distribution of ribosomes was monitored at absorbance 260nm and fractions were collected in 27 columns with flow rate of 0.4ml/min. Proteins from each fraction was extracted and immunoblots were performed using α-RPL13 or α-FLAG.

DISCUSSION

In the hemibiotrophic life cycle of pathogen infection, cell death can be harmful or beneficial to pathogens depending on the timing of cell death. Plant immune receptors can recognize effector activities and induce HR cell death as an immune response. Most of the disease-resistant HR cell death induced by immune receptor recognition is associated with the plasma membrane and cytosol (Lee et al., 2021; Bi et al., 2021; Lee et al., 2022). Pathogens also facilitate host cell death to gain benefits from the dying tissue by transiting from the biotrophic to the necrotrophic phase. Thus, they utilize cell death by hijacking essential components of the host cell in diverse subcellular organelles without immune receptor recognition. However, it is not clear when and how pathogens shift their lifestyle from the biotrophic to the necrotrophic phase. In this study, we observed nucleolar inflation concurrently with the switch from biotrophic to necrotrophic stage during *P. infestans* infection. This suggests that cell death signaling initiated from the nucleolus could be a strategy mediating the transitioning of the disease cycle. The nucleolar-localized Pi23226 induced a similar nucleolar morphology as that induced by the disease cycle transition when expressed in *N. benthamiana*.

(Figure 1-5). When Pi23226 was translocated from the nucleolus by adding a nuclear export signal (NES), it was unable to enhance *P. infestans* pathogenicity, indicating that the subcellular localization of Pi23226 is essential for virulence activity. We also observed that Pi23226 suppressed global protein translation *in vitro* and *in planta*, suggesting that Pi23226 may enhance pathogen virulence by hijacking ribosomes and inducing nucleolar stress responses. Our results and previous studies suggested that *P. infestans* may utilize nucleolar-localizing effectors to induce the disease transition in host cells.

As genome sequences of major plant pathogens become available, hundreds of pathogen effectors have been identified and their functions in host cells have been reported (Gao et al., 2020; He et al., 2020). Most of the effector targets are host proteins, and only a few effectors are localized in nuclei and directly bind to host DNA, such as the transcription activator-like effectors (TALEs) (Szurek et al., 2001; Kay et al., 2007). A small number of effectors from bacterial and filamentous pathogens are localized in the nucleus and nucleolus (Boevink et al., 2016; Kim et al., 2020). A recent study tried to identify RNA-binding effectors from a collection of animal and plant pathogen effectors; however, only a small number of effectors were reported that were theoretically predicted to carry RNA binding domains (Tawk et al.,

2017). The current study demonstrated that the *P. infestans* effector Pi23226 directly associated with rRNA, especially at the 3′-end of 25S rRNA, affects ribosome biogenesis, and inhibits translation to enhance pathogenicity. The binding of Pi23226 to 25S rRNA precursors appeared to interfere with the processing of 27S pre-rRNA to 25S rRNA because the quantity of untrimmed 3′-ETS increased in cells expressing Pi23226. Furthermore, detection of 27SB and 27SA3+3′-ETSp in Pi23226-expressing conditions suggested that Pi23226 interfered with the processing step of 25S rRNA maturation. It is unlikely that Pi23226 had endonuclease activity, as it did not contain any domain identified in RNase. Pi23226 is a relatively small protein (123 amino acids) with no known functional motif, and appears to act as a small interfering adaptor. Thus, Pi23226 binding on the end of 25S rRNA precursors may block the access of RNase to the cleavage site in the 3′-ETS. A ribonuclease involved in cleavage of the 3′-ETS in *N. benthamiana* has not been identified, but RNASE THREE LIKE2 (RTL2) is required for cleavage of the pre-rRNA in the 3′-ETS in Arabidopsis (Comella et al., 2008). Therefore, it would be interesting to further investigate whether Pi23226 binding on the 25S rRNA precursors affects the activity of RTL2 or a homolog on the cleavage of 3′-ETS in *N. benthamiana*. The accumulation of the 27SA3+3′-ETSp and 27SB pre-rRNAs under Pi23226-expressing conditions

suggests that the increase in untrimmed 3′-ETS could suppress further processing of 27S rRNA to 25S rRNA, which is recognized by the ribosome biogenesis surveillance system and induce nucleolar stress responses leading to cell death.

Although we showed that Pi23226 had the RNA-binding activity, we do not rule out the possibility that Pi23226 also associated and functioned with yet-unidentified host proteins. The polysome profiling analyses detected Pi23226 on the polysome fraction (fraction 3, Figure 1-17A), suggesting that Pi23226 may function on polysomes by associating with rRNA or other proteins. We previously reported that Pi23226 is associated with heat shock protein 70 (HSP70) and MAPK are involved in Pi23226-induced cell death signaling (Lee et al., 2018). In mammals, HSP70 modulate tumor necrosis factor (TNF)-related apoptosis-inducing ligand, inducing cell death together with up-regulating expression of p53, indicating that HSP70 is on the cell death pathway (Clemons and Anderson, 2006). Furthermore, during ribosome biogenesis, a variety of proteins are folded correctly and translocated through the nuclear pore complex. Thus, HSP70 and MAPK may participate in the ribosome biogenesis surveillance system, recognizing activation of Pi23226-induced nucleolar stress. However, the molecular mechanism of HSP70 activity in Pi23226-inducing cell death remains to be elucidated.

In conclusion, our results provide the first *in vivo* evidence of RNA-binding pathogen effectors, and extend our knowledge of the nucleolar action of pathogen effectors that disrupt ribosome biogenesis.

REFERENCES

Azevedo, C., Sadanandom, A., Kitagawa, K., Freialdenhoven, A., Shirasu, K., and Schulze-Lefert, P. (2002). The RAR1 interactor SGT1, an essential component of R gene-triggered disease resistance. Science **295**:2073–2076.

Azevedo, C., Betsuyaku, S., Peart, J., Takahashi, A., Noël, L., Sadanandom, A., Casais, C., Parker, J., and Shirasu, K. (2006). Role of SGT1 in resistance protein accumulation in plant immunity. EMBO J. **25**:2007.

Bi, G., Su, M., Li, N., Liang, Y., Dang, S., Xu, J., Hu, M., Wang, J., Zou, M., Deng, Y., et al. (2021). The ZAR1 resistosome is a calcium-permeable channel triggering plant immune signaling. Cell **184**(13), 3528–3541.

Birch, P. R. J., Rehmany, A. P., Pritchard, L., Kamoun, S., and Beynon, J. L. (2006). Trafficking arms: Oomycete effectors enter host plant cells. Trends Microbiol.. **14**:8–11.

Boevink, P. C., Wang, X., McLellan, H., He, Q., Naqvi, S., Armstrong, M. R., Zhang, W., Hein, I., Gilroy, E. M., Tian, Z., et al. (2016). A Phytophthora infestans RXLR effector targets plant PP1c isoforms that promote late blight disease. Nat. Commun. **7**, 10311.

Boisvert, F. M., Van Koningsbruggen, S., Navascués, J., and Lamond, A. I. (2007). The multifunctional nucleolus. Nat. Rev. Mol. Cell Biol. **8**:574–585.

Bombarely, A., Rosli, H. G., Vrebalov, J., Moffett, P., Mueller, L. A., and Martin, G. B. (2012). A draft genome sequence of Nicotiana benthamiana to enhance molecular plant-microbe biology research. Mol. Plant-Microbe Interact. **25**:1523–1530.

Bonardi, V., Tang, S., Stallmann, A., Roberts, M., Cherkis, K., and Dangl, J. L. (2011). Expanded functions for a family of plant intracellular immune receptors beyond specific recognition of pathogen effectors. Proc. Natl. Acad. Sci. U.S.A. **108**:16463–16468.

Caillaud, M. C., Asai, S., Rallapalli, G., Piquerez, S., Fabro, G., and Jones, J. D. G.

(2013). A Downy Mildew Effector Attenuates Salicylic Acid-Triggered Immunity in Arabidopsis by Interacting with the Host Mediator Complex. PLoS Biol. **14**(3), e1002408.

Chang, C. H., Hsu, F. C., Lee, S. C., Lo, Y. S., Wang, J. Da, Shaw, J., Taliansky, M., Chang, B. Y., Hsu, Y. H., and Lin, N. S. (2016). The nucleolar fibrillarin protein is required for helper virus-independent long-distance trafficking of a subviral satellite RNA in plants. Plant cell **28**(10), 2586–2602.

Chen, S., Zhou, Y., Chen, Y., and Gu, J. (2018). fastp: an ultra-fast all-in-one FASTQ preprocessor. Bioinformatics **34**:i884–i890.

Chisholm, S. T., Coaker, G., Day, B., and Staskawicz, B. J. (2006). Host-microbe interactions: Shaping the evolution of the plant immune response. Cell **124**:803–814.

Chung, E., Seong, E., Kim, Y. C., Chung, E. J., Oh, S. K., Lee, S., and Choi, D. (2004). A method of high frequency virus induced gene silencing in chili pepper (Capsicum annuum L. cv. Bukang). Mol. Cells. **17**(2), 377-80.

Clemons, N. J., and Anderson, R. L. (2006). TRAIL-induced apoptosis is enhanced by heat shock protein 70 expression. Cell Stress and Chaperones **11**:343.

Comella, P., Pontvianne, F., Lahmy, S., Vignols, F., Barbezier, N., DeBures, A., Jobet, E., Brugidou, E., Echeverria, M., and Sáez-Vásquez, J. (2008). Characterization of a ribonuclease III-like protein required for cleavage of the pre-rRNA in the 3′ETS in Arabidopsis. Nucleic Acids Res. Spec. Publ. **36**(4), 1163–1175

Cui, H., Tsuda, K., and Parker, J. E. (2015). Effector-triggered immunity: From pathogen perception to robust defense. Annu. Rev. Plant Biol. **66**:487–511.

Dangl, J. L., Horvath, D. M., and Staskawicz, B. J. (2013). Pivoting the plant immune system from dissection to deployment. Science **16**;341(6147):746-51

Dean, R., Talbot, N., Ebbole, D. et al. (2005) The genome sequence of the rice blast fungus Magnaporthe grisea. Nature 434, 980–986

Dou, D., and Zhou, J. M. (2012). Phytopathogen effectors subverting host immunity:

Different foes, similar battleground. Cell Host Microbe **12**:484–495.

Gagliardi, M., and Matarazzo, M. R. (2016). RIP: RNA immunoprecipitation. Methods Mol. Biol. **1480**:73–86.

Gao, C., Xu, H., Huang, J., Sun, B., Zhang, F., Savage, Z., Duggan, C., Yan, T., Wu, C. H., Wang, Y., et al. (2020). Pathogen manipulation of chloroplast function triggers a light-dependent immune recognition. Proc. Natl. Acad. Sci. U.S.A. **117**(17), 9613–9620.

Haas, B., Kamoun, S., Zody, M. et al. (2009) Genome sequence and analysis of the Irish potato famine pathogen Phytophthora infestans. Nature 461, 393–398

Harscoët, E., Dubreucq, B., Palauqui, J. C., and Lepiniec, L. (2010). NOF1 encodes an arabidopsis protein involved in the control of rRNA expression. PLoS One **5**:1–12.

He, Q., McLellan, H., Boevink, P. C., and Birch, P. R. J. (2020). All Roads Lead to Susceptibility: The Many Modes of Action of Fungal and Oomycete Intracellular Effectors. Plant Commun. **1**(4), 100050.

Jing, M., Guo, B., Li, H., Yang, B., Wang, H., Kong, G., Zhao, Y., Xu, H., Wang, Y., Ye, W., et al. (2016). A Phytophthora sojae effector suppresses endoplasmic reticulum stress-mediated immunity by stabilizing plant Binding immunoglobulin Proteins. Nat. Commun. **7**, 11685,

Jones, J. D. G., and Dangl, J. L. (2006). The plant immune system. Nature **444**:323–329.

Jones, J. D. G., Vance, R. E., and Dangl, J. L. (2016). Intracellular innate immune surveillance devices in plants and animals. Science Dec 354(6316), aaf6395.

Kalinina, N. O., Makarova, S., Makhotenko, A., Love, A. J., and Taliansky, M. (2018). The multiple functions of the nucleolus in plant development, disease and stress responses. Front. Plant Sci. **9**:1–19.

Kanneganti, T. D., Huitema, E., Cakir, C., and Kamoun, S. (2007). Synergistic interactions of the plant cell death pathways induced by Phytophthora infestans Nepl-like protein PiNPP1.1 and INF1 elicitin. Mol. Plant-Microbe Interact. 19(8), 854–863.

Kay, S., Hahn, S., Marois, E., Hause, G., and Bonas, U. (2007). A bacterial effector acts as a plant transcription factor and induces a cell size regulator. Science 318(5850), 648–651.

Kim, S. H., Ryabov, E. V., Kalinina, N. O., Rakitina, D. V., Gillespie, T., MacFarlane, S., Haupt, S., Brown, J. W. S., and Taliansky, M. (2007). Cajal bodies and the nucleolus are required for a plant virus systemic infection. EMBO j., *26(8), 2169–2179.*

Kim, D., Paggi, J. M., Park, C., Bennett, C., and Salzberg, S. L. (2019). Graph-based genome alignment and genotyping with HISAT2 and HISAT-genotype. Nat. Biotech. **37**:907–915.

Kim, S., Kim, C. Y., Park, S. Y., Kim, K. T., Jeon, J., Chung, H., Choi, G., Kwon, S., Choi, J., Jeon, J., et al. (2020). Two nuclear effectors of the rice blast fungus modulate host immunity via transcriptional reprogramming. Nat. commun.11(1), 5845.

KJ, L., and TD, S. (2001). Analysis of relative gene expression data using real-time quantitative PCR and the 2(-Delta Delta C(T)) Method. Methods **25**:402–408.

Lee, J. H., Lee, S. E., Oh, S., Seo, E., and Choi, D. (2018). HSP70s enhance a phytophthora infestans effector-induced cell death via an MAPK cascade in Nicotiana benthamiana. Mol. Plant-Microbe Interact. 31(3), 356–362.

Lee, H. Y., Mang, H., Choi, E., Seo, Y. E., Kim, M. S., Oh, S., Kim, S. B., and Choi, D. (2021). Genome-wide functional analysis of hot pepper immune receptors reveals an autonomous NLR clade in seed plants. New Phytol. **229**:532–547.

Lee, H. Y., Seo, Y. E., Lee, J. H., Lee, S. E., Oh, S., Kim, J., Jung, S., Kim, H., Park, H., Kim, S., et al. (2022). Plasma membrane-localized plant immune receptor targets H+-ATPase for membrane depolarization to regulate cell death. New Phytol. **233**:934–947.

Li, H., Handsaker, B., Wysoker, A., Fennell, T., Ruan, J., Homer, N., Marth, G., Abecasis, G., and Durbin, R. (2009). The Sequence Alignment/Map format and SAMtools. Bioinformatics **25**:2078–2079.

Loza-Muller, L., Rodríguez-Corona, U., Sobol, M., Rodríguez-Zapata, L. C., Hozak, P., and Castano, E. (2015). Fibrillarin methylates H2A in RNA polymerase I trans-active promoters in Brassica oleracea. Front. Plant Sci. **6**:976.

McNeece, B. T., Pant, S. R., Sharma, K., Niruala, P., Lawrence, G. W., and Klink, V. P. (2017). A Glycine max homolog of NON-RACE SPECIFIC DISEASE RESISTANCE 1 (NDR1) alters defense gene expression while functioning during a resistance response to different root pathogens in different genetic backgrounds. Plant Physiol. Biochem. **114**:60–71.

Missbach, S., Weis, B. L., Martin, R., Simm, S., Bohnsack, M. T., and Schleiff, E. (2013). 40S Ribosome Biogenesis Co-Factors Are Essential for Gametophyte and Embryo Development. PLoS One **8**:54084.

Moreau, M., Degrave, A., Vedel, R., Bitton, F., Patrit, O., Renou, J., Barny, M., Fagard, M., Vi, U. P., and Bernard, C. (2012). EDS1 Contributes to Nonhost Resistance of Arabidopsis thaliana Against Erwinia amylovora Mol. Plant-Microbe Interact. **25**:421–430.

Oh, S. A., Park, K. S., Twell, D., and Park, S. K. (2010). The SIDECAR POLLEN gene encodes a microspore-specific LOB/AS2 domain protein required for the correct timing and orientation of asymmetric cell division. Plant J. **64**:839–850.

Ohbayashi, I., Lin, C. Y., Shinohara, N., Matsumura, Y., Machida, Y., Horiguchi, G., Tsukaya, H., and Sugiyama, M. (2017). Evidence for a role of ANAC082 as a ribosomal stress response mediator leading to growth defects and developmental alterations in arabidopsis. Plant cell **29**(10), 2644–2660.

Ohbayashi, I., and Sugiyama, M., (2018) Plant Nucleolar Stress Response, a New Face in the NAC-Dependent Cellular Stress Responses. Front. Plant Sci. 8:2247.

Pennington, H. G., Jones, R., Kwon, S., Bonciani, G., Thieron, H., Chandler, T., Luong, P., Morgan, S. N., Przydacz, M., Bozkurt, T., et al. (2019). The fungal ribonuclease-like effector protein CSEP0064/BEC1054 represses plant immunity and interferes with degradation of host ribosomal RNA. PLoS Pathog. **15**:e1007620.

Qiao, Y., Shi, J., Zhai, Y., Hou, Y., & Ma, W. (2015). Phytophthora effector targets a novel component of small RNA pathway in plants to promote infection. Proc. Natl. Acad. Sci. U. S. A. **112**(18), 5850-5855.

Rajamäki, M. L., and Valkonen, J. P. T. (2009). Control of nuclear and nucleolar localization of nuclear inclusion protein a of picorna-like potato virus a in nicotiana species. Plant cel **21**(8), 2485–2502.

Ramírez, F., Ryan, D. P., Grüning, B., Bhardwaj, V., Kilpert, F., Richter, A. S., Heyne, S., Dündar, F., and Manke, T. (2016). deepTools2: a next generation web server for deep-sequencing data analysis. Nucleic Acids Res. **44**:W160–W165.

Rehmany, A., Gordon, A., Rose, L., Allen, R., and Armstrong, M. (2005). Differential recognition of highly divergent downy mildew avirulence gene alleles by RPP1 resistance genes from two Arabidopsis lines. Plant cell **17**(6), 1839–1850.

Robinson, J. T., Thorvaldsdóttir, H., Winckler, W., Guttman, M., Lander, E. S., Getz, G., and Mesirov, J. P. (2011). Integrative genomics viewer. Nat. Biotechnol. **29**:24–26.

Sáez-Vásquez, J., and Delseny, M. (2019). Ribosome biogenesis in plants: From functional 45S ribosomal DNA organization to ribosome assembly factors. Plant cell **31**(9), 1945–1967.

Seo, J. S., Diloknawarit, P., Park, B. S., and Chua, N. H. (2019). ELF18-INDUCED LONG NONCODING RNA 1 evicts fibrillarin from mediator subunit to enhance PATHOGENESIS-RELATED GENE 1 (PR1) expression. New phytol. **221**(4), 2067–2079.

Sperschneider, J., Catanzariti, A. M., Deboer, K., Petre, B., Gardiner, D. M., Singh, K. B., Dodds, P. N., and Taylor, J. M. (2017). LOCALIZER: subcellular localization prediction of both plant and effector proteins in the plant cell. Sci. Rep. **7**:1–14.

Szurek, B., Marois, E., Bonas, U., and Van den Ackerveken, G. (2001). Eukaryotic features of the Xanthomonas type III effector AvrBs3: protein domains involved in transcriptional activation and the interaction with nuclear import receptors from

pepper. Plant J. **26**:523–534.

Tawk, C., Sharan, M., Eulalio, A., and Vogel, J. (2017). A systematic analysis of the RNA-targeting potential of secreted bacterial effector proteins. Sci. Rep. **7**(1), 9328.

Tuvshinjargal, N., Lee, W., Park, B., and Han. K. (2016) PRIdictor: protein–RNA interaction predictor. Biosystems 139:17-22.

Van Hoewyk, D. (2016). Use of the non-radioactive SUnSET method to detect decreased protein synthesis in proteasome inhibited Arabidopsis roots. Plant Methods **12**:20.

Van West, P., De Jong, A. J., Judelson, H. S., Emons, A. M. C., and Govers, F. (1998). The ipiO gene of Phytophthora infestans is highly expressed in invading hyphae during infection. Fungal Genet. Biol. **23**:126–138.

Wang, S., McLellan, H., Bukharova, T., He, Q., Murphy, F., Shi, J., Sun, S., Van Weymers, P., Ren, Y., Thilliez, G., et al. (2019). Phytophthora infestans RXLR effectors act in concert at diverse subcellular locations to enhance host colonization. J. Exp. Bot. **70**:343–356.

Weis, B. L., Kovacevic, J., Missbach, S., and Schleiff, E. (2015). Plant-Specific Features of Ribosome Biogenesis. Trends Plant Sci. **20**(11), 729–740.

Wen, Z., Raffaello, T., Zeng, Z., Pavicic, M., and Asiegbu, F. O. (2019). Chlorophyll fluorescence imaging for monitoring effects of Heterobasidion parviporum small secreted protein induced cell death and in planta defense gene expression. Fungal Genet. Biol. **126**:37-49.

Wu, C. H., Abd-El-Haliem, A., Bozkurt, T. O., Belhaj, K., Terauchi, R., Vossen, J. H., and Kamoun, S. (2017). NLR network mediates immunity to diverse plant pathogens. Proc. Natl. Acad. Sci. U.S.A. **114**:8113–8118.

Yoshikawa, H., Larance, M., Harney, D. J., Sundaramoorthy, R., Ly, T., Owen-Hughes, T., and Lamond, A. I. (2018). Efficient analysis of mammalian polysomes in cells and tissues using ribo mega-SEC. Elife **7**, e36530.

CHAPTER 2

The oomycete effector AVRblb2 targets cyclic nucleotide-gated channels through calcium sensors to suppress pattern-triggered immunity

ABSTRACT

Transient, rapid increase of cytosolic Ca^{2+} upon pathogen infection is essential for plant pathogen-associated molecular pattern (PAMP)-triggered immunity (PTI). Several cyclic nucleotide-gated channels (CNGCs) have been implicated; however, their regulatory mechanisms remain elusive. Here, the *Phytophthora infestans* RXLR effector AVRblb2 family targeted NbCNGC18–20 at the plasma membrane, inhibiting Ca^{2+} influx and PTI. AVRblb2 required calmodulin (CaM) and calmodulin-like (CML) proteins as co-factors to interact with *N. benthamiana* CNGCs (NbCNGCs), forming the AVRblb2-CaM/CML-NbCNGCs complex. Upon recognizing PAMPs, NbCNGC18 associated with other CNGCs, potentially providing selectivity for diverse signals to fine-tune cytosolic Ca^{2+} levels and responses. AVRblb2 suppressed the Ca^{2+} influx and oxidative burst induced by NbCNGC18. Silencing CNGC18, CNGC20, and CNGC25 compromised the effect of AVRblb2 on *P. infestans* virulence, confirming that AVRblb2 contributed to virulence by targeting CNGCs. Our findings delineated the regulatory mechanism and role of effector-targeted Ca^{2+} channels in plant innate immunity.

INTRODUCTION

The plant immune system is a sophisticated, multilayered system that protects against pathogens (Boller & Felix, 2009; Jones & Dangl, 2006). When pathogens invade, the plant immune system is activated through the recognition of conserved microbial molecules known as pathogen-associated molecular patterns (PAMPs) by pattern-recognition receptor, resulting in the activation of PAMP-triggered immunity (PTI) (Thomma et al., 2011). However, pathogens have evolved to secrete effector proteins that can disrupt PTI responses, leading to effector-triggered susceptibility (Thomma et al., 2011). To counteract this disruption, the plant immune system employs intracellular nucleotide-binding leucine-rich-repeat (NLR) receptors that recognize its cognate pathogen effectors and induce effector-triggered immunity (ETI) (Cui et al., 2015; Jones & Dangl, 2006; Kadota et al., 2019). Both PTI and ETI trigger a range of downstream responses, including calcium influx, reactive oxygen and nitrogen species production, activation of mitogen-activated protein kinase (MAPK) cascades, transcriptional reprogramming, and hormone signaling (Cui et al., 2015). PTI and ETI can also potentiate each other to provide full resistance to pathogen invasion (Yuan, Jiang, et al., 2021)

An increase in cytosolic calcium concentration is a critical early immune signaling event (Grant et al., 2000; Moeder et al., 2019). Ca^{2+} is a universal second messenger in eukaryotes, and its cytosolic levels are typically maintained low (~10^{-8} to 10^{-7} M) by sequestration in intracellular stores, such as vacuole, endoplasmic reticulum, and apoplast, via active transport (Berridge et al., 2000). Upon PAMP recognition, calcium channels at the plasma membrane are activated, leading to transient Ca^{2+} influx decoded by a variety of Ca^{2+} sensors containing EF-hand motifs, including the calmodulin (CaM) and calmodulin-like (CML) proteins. Increased Ca^{2+} influx activates respiratory burst oxidase homolog, an NADPH oxidase that generates a burst of reactive oxygen species (ROS) and triggers downstream immune responses (Xu et al., 2022).

Cyclic nucleotide-gated channels (CNGCs) are well-studied calcium channels implicated in plant immune responses. These channels have a cytosolic C-terminus with a CaM binding domain, a cyclic nucleotide-binding domain, and several phosphorylation sites (Jegla et al., 2018). Recent studies discovered regulatory mechanisms of CNGCs via the cytosolic C-terminus (DeFalco et al., 2016; Fischer et al., 2017; Tian et al., 2019). In Arabidopsis, the extensively studied AtCNGC2 and AtCNGC4 contribute to plant immunity by increasing cytosolic Ca^{2+} (Moeder et al., 2019; Wang et al., 2019).

CNGC2 and CNGC4 form a heteromeric complex kept inactive by CaM binding; however, the resting state can be released by the receptor-like cytoplasmic kinase, Botrytis-induced kinase 1, during PAMP-induced Ca^{2+} bursts (Tian et al., 2019). Furthermore, AtCNGC11/CNGC12 and AtCNGC19/20 have been linked to immunity via an autoimmune mutant that mediates constitutive Ca^{2+} influx (Yoshioka et al., 2006; Yu et al., 2019).

Plant pathogens have evolved a plethora of effectors to disrupt host defense signaling pathways and enhance their invasion. *Phytophthora infestans*, an oomycetes pathogen, secretes hundreds of effector proteins, including RXLR family members (Whisson et al., 2007; Zheng et al., 2014). Among these, the AVRblb2 gene family is particularly intriguing because it is found in all *P. infestans* isolates and is conserved in other pathogenic *Phytophthora spp.*, playing a critical role in pathogen virulence (Oliva et al., 2015). AVRblb2 and its homologs target various host proteins, including the cysteine protease C14, a potato MAPK cascade protein (StMKK1), and CaM (Bozkurt et al., 2011; Du et al., 2021; Naveed et al., 2019). Furthermore, most of the multiple copies of AVRblb2 are specifically recognized by Rpi-blb2 (Oh et al., 2009), showing the importance of this gene family in the co-evolution of *P. infestans* and their host plants. Similar to AVRblb2, several pathogen effectors directly target the main Ca^{2+} sensor protein, CaM. For example, the *P. infestans* RXLR effector

Suppressor of early flg22-induced Immune response 5 (SFI5) targets SlCaM, and the SFI5-CaM interaction is necessary for effector function (Zheng et al., 2018). Furthermore, the *Pseudomonas syringae* effector HopE1 targets the microtubule-associated protein 65 (MAP65) in a CaM-dependent manner to inhibit pathogenesis-related protein 1 (PR-1) protein secretion (Guo et al., 2016). However, the precise molecular mechanisms by which pathogens disrupt Ca^{2+} signaling to sustain their life cycles during early PTI are largely unknown.

In this study, we showed that the *P. infestans* RXLR effector AVRblb2 family could suppress PTI by targeting NbCNGCs at the plasma membrane. AVRblb2 targeted a subset of NbCNGCs (CNGC18–20) via the Ca^{2+} sensors CaM and CML36, forming the AVRblb2-CaM/CML36-CNGC complex. Molecular studies demonstrated that AVRblb2 inhibited flg22-induced Ca^{2+} influx by preventing the dissociation of CaM/CML36 and NbCNGC18. Following flg22 treatment, CNGC18 associated with other CNGCs that might be targeted by AVRblb2. AVRblb2 function was disrupted in plant silenced for CNGC3, CNGC11, CNGC18, and CNGC20 demonstrating that the function of AVRblb2 in virulence required its association with multiple CNGCs. Our findings have provided a working model for heteromeric CNGC complexes in the fine-tuning of Ca^{2+} homeostasis in plant immunity and identified how

pathogen effectors disturb PTI.

MATERIALS AND METHODS

Plant material and Agrobacterium-mediated transient overexpression

N. benthamiana plants were grown and maintained in a walk-in chamber in a controlled environment with an average temperature of 23–24°C and long day conditions (16 hr light cycle). *A. tumefaciens* GV3101 was used to deliver T-DNA constructs into *N. benthamiana* leaves. Overnight cultures of *A. tumefaciens* were centrifuged at 3500 × g for 10 min, and suspensions were adjusted to a final OD_{600} of 0.3 in infiltration buffer (10 mM $MgCl_2$, 10 mM MES, pH 5.6, and 150 μM acetosyringone).

Plasmid construction

The AVRblb2 gene (PITG_20300) was cloned into the binary vector pCAMBIA2300-LIC using a ligation-independent cloning method (Oh et al., 2010). NbCaM, NbCML36, and all candidate NbCNGC genes were amplified from *N. benthamiana* cDNA and cloned into pCAMBIA2300-LIC containing a C-terminal GFP or HAx3 tag. The recombinant plasmids were introduced into *A. tumefaciens* strain GV3101.

Ca^{2+} concentration measurements

The monitoring of changes in cytosolic calcium concentration was performed using transgenic *N. benthamiana* plants expressing YC3.6 under the control of the cauliflower mosaic virus promoter 35S. Leaf disks from YC3.6 *N. benthamiana* transgenic line were transferred to a 96-well black plate and incubated in dH_2O at 25℃ for 12 h, followed by treatment with 1 μM flg22. FRET fluorescence was measured immediately upon treatment using a multi-label plate reader (Varioskan LUX, ThermoFisher, USA) with an excitation at 440 nm and emission detection at 520 nm. Measurements were recorded at 1 min intervals. The FRET-based cpVenus/ECFP ratio was used for the ratio (R) calculation (440/520) and normalized to the initial ratio (R0). The data were plotted versus time (ΔR/R0). Experiments were repeated ten times.

Hairpin RNA-mediated gene silencing

The NbCNGC silencing fragment was amplified from *N. benthamiana* cDNA using the primers listed in Table 2-1. The specificity of the silencing fragment was analyzed using the *N. benthamiana* genome sequence and associated gene silencing target prediction tool (SGN VIGS tool: https://vigs.solgenomics.net). The purified amplicon was cloned into the pRNAi-GG vector as previously described (91). *N. benthamiana* leaves were infiltrated with Agrobacterium carrying pRNAi-GUS or various pRNAi-CNGC constructs at a final OD_{600} of

0.3.

Protein extraction and immunoblotting

N. benthamiana leaves were ground in liquid nitrogen and mixed with protein extraction buffer (10% [v/v] glycerol, 25 mM Tris-HCl [pH 7.5], 1 mM EDTA, 150 mM NaCl, 1% [w/v] polyvinylpolypyrrolidone, and 1× protease inhibitor cocktail). Suspensions were mixed and centrifuged at 12,000 × g for 15 min at 4°C. Total proteins were separated on 10% or 12% sodium dodecyl sulfate (SDS)-polyacrylamide gels and transferred to Immobilon-PSQ polyvinylidene difluoride membranes. The membranes were washed with PBST (PBS with 0.1% Tween 20) for 3 min and then blocked in 5% non-fat milk for 1 h. The membranes were then incubated with rabbit monoclonal anti-GFP (1:12000, Invitrogen, A10260) or anti-FLAG (1:12000, Sigma-Aldrich, F3165) antibody for 2 h, followed by three washes with PBST. The membranes were then incubated with PBST for 10 min each before the addition of the secondary anti-mouse Ig-horseradish peroxidase (HRP) (1: 15,000, Abcam, ab6708) or anti-rabbit Ig-HRP (1:15,000, Abcam, ab6702) antibody for 1 h. After three washes with PBST, the blots were developed using enhanced chemiluminescence (Thermo Scientific, USA).

Co-immunoprecipitation (co-IP)

Proteins were extracted from two *N. benthamiana* leaves at 1.5 days post-agroinfiltration by homogenizing the leaves in GTEN extraction buffer (10% [v/v] glycerol, 25 mM Tris-HCl [pH 7.5], 1 mM EDTA, 150 mM NaCl, 1% [w/v] polyvinylpolypyrrolidone, and 1× protease inhibitor cocktail) and centrifuging the homogenates at 12,000 × g for 15 min. For co-IP, total protein extract (1 mg) was mixed with 10 µl GFP-Trap®-A agarose beads (Chromatek, Munich, Germany), anti-FLAG agarose beads (A7470, Sigma-Aldrich), or anti-HA affinity matrix beads (Roche) and incubated end-over-end for 2 h at 4°C. Beads were washed five times with immunoprecipitation wash buffer (GTEN extraction buffer with 0.015% [v/v] Triton X-100 [Sigma-Aldrich]) and resuspended in 20 µl SDS loading dye. Proteins were eluted from the beads by heating for 10 min at 50°C for GFP or 95°C for FLAG or HA). The immunoprecipitates and input proteins were separated by SDS-PAGE and transferred onto polyvinylidene difluoride membranes using the Trans-Blot Turbo Transfer System (Bio-Rad, Munich), according to the manufacturer's instructions. Blots were blocked with 5% skim milk in tris-buffered saline containing Tween20 for a minimum of 1 h at room temperature. The immunoprecipitated proteins and input proteins were analyzed by immunoblotting with specific antibodies. Protein staining was imaged using the ImageQuant LAS 4000 luminescent imager (GE Healthcare Life Sciences,

Piscataway, NJ).

In vitro pull-down assay

Codon-optimized His:AVRblb2, CaM:GST, and CML36:GST were expressed in the BL21 (DE3) strain (RBC, Taiwan). The His:AVRblb2 protein was induced with 1 mM isopropyl β-D-1-thiogalactopyranoside (IPTG) at 37°C for 3 h. The cells were centrifuged at 3,000 rpm for 15 min, resuspended in His-binding buffer (50 mM Tris-HCl [pH 8.0], 30 mM imidazole, 300 mM NaCl, 0.1 mM EDTA), and lysed by sonication. The lysate was centrifuged at 12,000 rpm for 10 min and filtered through a 0.45-μm syringe filter. The soluble proteins were purified using HisPur™ Cobalt Resin (Thermo Scientific, USA) and eluted in His-elution buffer (50 mM Tris-HCl [pH 8.0], 50 mM NaCl, 300 mM imidazole, and 0.1 mM EDTA). The purified protein was dialyzed in PBS buffer overnight. The CaM:GST and CML36:GST proteins were induced with 1 mM IPTG at 30°C overnight. The cells were centrifuged at 3,000 rpm for 15 min, resuspended in GST-binding buffer (50 mM Tris-HCl [pH 8.0], 150 mM NaCl, 0.1 mM EDTA), and lysed by sonication. The soluble proteins were purified using Glutathione Agarose (Thermo Scientific, USA) and eluted in GST-binding buffer containing 10 mM reduced glutathione. For the pull-down assay, His:AVRblb2 (2.5 μg) and GST-

tagged prey protein (CaM or CML36, 2.5 μg each) were incubated in equilibrium buffer (20 mM Tris-HCl, [pH 7.5], 250 mM NaCl) containing 2 mM $CaCl_2$ or 1 mM EDTA for 2.5 h at 4°C with agitation. The bait protein alone served as a negative control. The incubated bait and prey proteins were added to a Ni-NTA agarose bead-containing column and incubated for 10 min on ice. The column was washed four times with equilibrium buffer containing 20 mM imidazole. The pull-down protein was eluted with elution buffer. Different concentrations of calcium were added to study the dependence of the pull-down affinity on calcium concentration.

Quantitative polymerase chain reaction (qPCR)

Total RNA was extracted from *N. benthamiana* leaves using TRIzol reagent (MRC, USA), and cDNA was generated using SuperScript III reverse transcriptase (Invitrogen, USA) and oligo (dT) primer following RNase-free DNase I treatment. Quantitative RT-PCR assays were conducted using PowerUP SYBR green master mix (Thermo, USA), according to the manufacturer's instructions. PCR was performed using the primers listed in Table 2-1. The *N. benthamiana EF1α* gene was used as the internal reference gene for calculating the relative gene expression levels, which were calculated using the $2^{-\Delta\Delta Ct}$ algorithm (Rao et al., 2013).

ROS measurements

ROS measurements were performed as previously described [46]. Four-week-old *N. benthamiana* plants for each genotype were excised into leaf discs (5-mm diameter) and floated 16 h in 200 μl water in a 96-well plate. Leaf discs were soaked in 50 mM luminol containing 10 mg/ml horseradish peroxidase and 1 μM flg22 or water control. Beginning immediately after adding the luminol solution, luminescence was measured over a 45 min period using a multi-label plate reader (Varioskan LUX, ThermoFisher, USA). Data were analyzed using company software and Microsoft Excel.

Pathogen inoculation

P. infestans T30-4 was grown on rye sucrose agar medium at 16°C in the dark. Zoospores were collected from 10 to 14-day-old cultures by flooding with cold water and incubating at 4°C for 60–90 min. For detached leaves, *P. infestans* infection assays were performed on the abaxial surface using droplet inoculation of zoospore suspensions (10 μl; 50,000 spores/ml). The phenotype was monitored for 7 days. Lesions were photographed 7 days post-inoculation using the Cy5 and Cy3 channels of the Azure 400 (Azure Biosystems, USA), and autofluorescent areas were analyzed using ImageJ software. At least three independent experiments were performed for this assay.

Yeast two hybrid (Y2H) assay

The Y2H assay was performed using the Matchmaker Gold system (Takara Bio, USA). Individual pGADT7 constructs or pGADT7 empty vector were introduced into the yeast strain Y187, and the cloned pGBKT7 plasmids were introduced into yeast strain Y2HGold. The yeast colonies containing both pGADT7 and pGBKT7 were selected on a synthetic defined (SD) medium without leucine and tryptophan (SD-L-T). The interactions were tested on SD medium without histidine, leucine, and tryptophan (SD-H-L-T) supplemented with 0.2% adenine. Plates were incubated for 3 to 6 days at 28°C and then imaged. Each experiment was repeated a minimum of three times, yielding similar results. Commercial yeast constructs were used as positive (pGBKT7-53/pGADT7-T) and negative (pGBKT7-Lam/pGADT7-T) controls (Clontech, USA).

Bimolecular fluorescence complementation(BiFC) assay

The full-length coding sequences of CNGCs and AVRblb2 were amplified and inserted into the pVYNE-35S or pSCYCE-35S vector using gateway cloning method. Agrobacterium strain GV3101 was transformed with the destination vectors before infiltrating four-week-old *N. benthamiana* leaves. Two days after infiltration, the samples were visualized using the Leica SP8 X

(USA) confocal microscope equipped with a 40× water immersion objective. Fluorescence intensity was visualized using excitation at 488 nm and emission between 455 and 480 nm. Images were captured in multichannel mode with brightfield and processed using LAS X microscope software.

Split-luciferase complementation assay

The split-luciferase complementation assay was performed as previously described (Luker & Luker, 2011). Briefly, cell suspensions of *A. tumefaciens* GV3101 carrying constrcuts were mixed in induction buffer (10 mM MES pH 5.7, 10 mM $MgCl_2$, and 150 μM acetosyringone) at an OD_{600} of 0.5. Bacteria were infiltrated into *N. benthamiana* leaves, and the plants were grown in growth chamber for 2 days. Whole leaves or leaf disks were incubated with 1 mM luciferin. Luminescence was recorded using a microplate reader (Varioskan LUX, ThermoFisher, USA), and luminescence was quantified from twelve replicates of each sample. Representative images from three independent experiments are presented.

Virus-induced gene silencing (VIGS)

VIGS was performed in *N. benthamiana* as previously described (Chung et al., 2004). Suspensions of *A. tumefaciens* strain GV3101 carrying TRV-RNA1 and TRV-RNA2 containing the corresponding fragments from NbCNGC18,

CaM, or CML36 were mixed in a 2:1 ratio in infiltration buffer (10 mM 2-[N-morpholine]ethanesulfonic acid [MES]; 10 mM $MgCl_2$; and 150 μM acetosyringone, pH 5.6) to a final OD_{600} of 0.25. Two-week-old *N. benthamiana* plants were infiltrated with *A. tumefaciens*, and the upper leaves were used two to three weeks later for further assays.

Table 2-1. Primers used in this study

Name	**Sequence (5'-> 3')**
pc2300-NbCNGC2-F	CGACGACAAGACCCTATGCTTGCCAGTCATGTA
pc2300-NbCNGC2-R	GAGGAGAAGAGCCCTCTTATCTTCTGCAGTAAAATC
pc2300-NbCNGC3-F	CGACGACAAGACCCTATGCTTGCCAGCCATGTA
pc2300-NbCNGC3-R	GAGGAGAAGAGCCCTTTTATCTTCAGCAGTAAAATCT
pc2300-NbCNGC4-F	CGACGACAAGACCCTATGACGTTTCTCAATCAAGAAA
pc2300-NbCNGC4-R	GAGGAGAAGAGCCCTGGAGCTAAAATCAGGTTCA
pc2300-NbCNGC7-F	CGACGACAAGACCCTATGTTTGGTAATTACAAGTCTC
pc2300-NbCNGC7-R	GAGGAGAAGAGCCCTACGTGGTCGCTCCGG
pc2300-NbCNGC8-F	CGACGACAAGACCCTATGGAAGCTTTTAGACATTCT
pc2300-NbCNGC8-R	GAGGAGAAGAGCCCTCTCAGTATCTTCACTGAAATCA
pc2300-NbCNGC11-F	CGACGACAAGACCCTATGTTCGACTGTGGTTCCA
pc2300-NbCNGC11-R	GAGGAGAAGAGCCCTATCTGCATCTGCACTAAAA
pc2300-NbCNGC12-F	CGACGACAAGACCCTATGGCTTATGGTAATTCCAGA
pc2300-NbCNGC12-R	GAGGAGAAGAGCCCTCTCTTCTTCAACTGAGAAATCA
pc2300-NbCNGC15-F	CGACGACAAGACCCTATGAAGAATGACGAACAAAC
pc2300-NbCNGC15-R	GAGGAGAAGAGCCCTAGTAGGAGCAGTAGTAGGGT
pc2300-NbCNGC18-F	CGACGACAAGACCCTATGATGGAGTTCAAGAAAGA
pc2300-NbCNGC18-R	GAGGAGAAGAGCCCTGTCATCATCTGGCTCAGC
pc2300-NbCNGC20-F	CGACGACAAGACCCTATGGCAAAGTACTTCTATTG
pc2300-NbCNGC20-R	GAGGAGAAGAGCCCTGTCATCAGGCTCAGCTGAA
pc2300-NbCNGC21-F	CGACGACAAGACCCTATGGTTATCTGGTTTATTATACC
pc2300-NbCNGC21-R	GAGGAGAAGAGCCCTGTCATCAGGCTCAGCTGAAA
pc2300-NbCNGC23-F	CGACGACAAGACCCTATGTCTTCTCGCCAAGAC
pc2300-NbCNGC23-R	GAGGAGAAGAGCCCTCTCAAGATGATCATGTGGC
pc2300-NbCNGC25-F	CGACGACAAGACCCTATGGCTAGTCATATAGAACTTG
pc2300-NbCNGC25-R	GAGGAGAAGAGCCCTAAAATCAAAATCATCCTGATTCG
pc2300-CML36-F	CGACGACAAGACCCTATGAAGCTCATCAAAAACTTG
pc2300-CML36-R	GAGGAGAAGAGCCCTTCTCTGCTGTTCCATCATA
pc2300-CaM-F	CGACGACAAGACCCTATGGCGGATCAGCTGACT

pc2300-CaM-R	GAGGAGAAGAGCCCTCTTGGCCATCATGACCTTG
pc2300-CNGC18CT-F	CGACGACAAGACCCTATGAACATGCAGACATACTTACAA
pc2300-CNGC18CT-R	GAGGAGAAGAGCCCTGTCATCATCTGGCTCAGC
qRT-Nbactin-F	AAAGACCAGCTCATCCGTGGAGAA
qRT-Nbactin-R	TGTGGTTTCATGAATGCCAGCAGC
qRT-NbICS1-F	AAGGAAGTTCAGTTATTGCTGC
qRT-NbICS1-R	GCTTGGTCGTAAGATGCTTTA
qRT-NbAOS-F	GCGAACCCAGTTGAGACTAAG
qRT-NbAOS-R	ATCTTCATCCCGCCAAAG
qRT-NbAcre31 -F	AAGGTCCCGTCTTCGTCGGATCTTCG
qRT-NbAcre31 -R	AAGAATTCGGCCATCGTGATCTTGGTC
qRT-NbWRKY22 -F	AAGGTCCGGGATCTACATGCGGTGGT
qRT-NbWRKY22 -R	AAGAATTCCGGGTCGGATCTATTTCG
qRT-NbEF1-α-F	GACCACTGAAGTTGGATCTGTTG
qRT-NbEF1-α-R	TAGCACCAGTTGGGTCCTTCTT
qRT-CNGC12-F	GAAGAGTTCCTCTGTTTGA
qRT-CNGC12-R	GGACCAATACGACAAGAATT
qRT-CNGC18-F	TGATTGCAAGGAGGTACTT
qRT-CNGC18-R	GCAGCTTTGATAATTTGAGC
qRT-CNGC20-F	ACGAGTACATTTATCGGGGA
qRT-CNGC20-R	TGTTCCATCCACTCTTCAG
qRT-CNGC25-F	GGCTTTTTCTCCGGAAAAA
qRT-CNGC25-R	GTCGATGAAGAGGCACATA
AD-NdeI-CaM-F	AACATATGATGGCGGATCAGCTGACT
AD-SmaI-CaM-R	AACCCGGGTCACTTGGCCATCATGAC
AD-NdeI-CML36-F	AACATATGATGAAGCTCATCAAAAACTTG
AD-NdeI-CML36-R	AACCCGGGTCATCTCTGCTGTTCCATC
AD-EcoRI-CNGC18CT-F	AAGAATTCATGAACATGCAGACATACTTACAA
AD-SmaI-CNGC18CT-R	AACCCGGGCTAGTCATCATCTGGCTCA
BD-NdeI-AVRblb2-F	AACATATGATGGCAGGTATCGAGGCT
BD-SmaI-AVRblb2-R	AACCCGGGTCAAGACTTAGTCATCTTAC

RNAi-CNGC12-F	GGGGACAAGTTTGTACAAAAAAGCAGGCTTCTCCAGCAATATTACAAAGAAAT
RNAi-CNGC12-R	GGGGACCACTTTGTACAAGAAAGCTGGGTTAGTTGTTGATTGGAGATAGG
RNAi-CNGC18-F	GGGGACAAGTTTGTACAAAAAAGCAGGCTTCTTGTGGTGGGGTTTACAA
RNAi-CNGC18-R	GGGGACCACTTTGTACAAGAAAGCTGGGTTTTCTTCGTCTACTCCACG
RNAi-CNGC18/20-F	GGGGACAAGTTTGTACAAAAAAGCAGGCTTCAAGTTCTTATGGCCAGAAC
RNAi-CNGC18/20-R	GGGGACCACTTTGTACAAGAAAGCTGGGTTTGTCCTCCGCTTGTGTC
RNAi-CNGC18/20/25-F	GGGGACAAGTTTGTACAAAAAAGCAGGCTTCAAGTTCTTATGGCCAGAAC
RNAi-CNGC18/20/25-R	GGGGACCACTTTGTACAAGAAAGCTGGGTTCTAACATGCAGCAACTTTTT
TRV2-CNGC18-F	CGACGACAAGACCCTTTGTGGTGGGGTTTACAA
TRV2-CNGC18-R	GAGGAGAAGAGCCCTTTCTTCGTCTACTCCACG
TRV2-CaM-F	CGACGACAAGACCCTCTGACGATCAGATCTCTGA
TRV2-CaM-R	GAGGAGAAGAGCCCTATCCTTGTCGAACACTCTAAA
TRV2-CML36-F	CGACGACAAGACCCTAGGAGATTTCTAACTCCG
TRV2-CML36-R	GAGGAGAAGAGCCCTAAAGTATCTCTCATCTCGTCT
GW-AVRblb2-F	GGGGACAAGTTTGTACAAAAAAGCAGGCTTCATGGCAGGTATCGAGGCT
GW-AVRblb2-R	GGGGACCACTTTGTACAAGAAAGCTGGGTTAGACTTAGTCATCTTAGC
GW-NbCNGC1-F	GGGGACAAGTTTGTACAAAAAAGCAGGCTTCATGAATCACCGTCAAGAG
GW-NbCNGC1-R	GGGGACCACTTTGTACAAGAAAGCTGGGTTCTTATCTTCTGCCGTAAAATC
GW-NbCNGC2-F	GGGGACAAGTTTGTACAAAAAAGCAGGCTTCATGCTTGCCAGTCATGTA
GW-NbCNGC2-R	GGGGACCACTTTGTACAAGAAAGCTGGGTTCTTATCTTCTGCAGTAAAATC
GW-NbCNGC3-F	GGGGACAAGTTTGTACAAAAAAGCAGGCTTCATGCTTGCCAGCCATGTA
GW-NbCNGC3-R	GGGGACCACTTTGTACAAGAAAGCTGGGTTTTTATCTTCAGCAGTAAAATCT
GW-NbCNGC4-F	GGGGACAAGTTTGTACAAAAAAGCAGGCTTCATGACGTTTCTCAATCAAGAAA
GW-NbCNGC4-R	GGGGACCACTTTGTACAAGAAAGCTGGGTTGGAGCTAAAATCAGGTTCA
GW-NbCNGC11-F	GGGGACAAGTTTGTACAAAAAAGCAGGCTTCATGTTCGACTGTGGTTCCA
GW-NbCNGC11-R	GGGGACCACTTTGTACAAGAAAGCTGGGTTATCTGCATCTGCACTAAAA
GW-NbCNGC12-F	GGGGACAAGTTTGTACAAAAAAGCAGGCTTCATGGCTTATGGTAATTCCAGA

GW-NbCNGC12-R	GGGGACCACTTTGTACAAGAAAGCTGGGTTCTCTTCTTCAACTGAGAAATCA
GW-NbCNGC18-F	GGGGACAAGTTTGTACAAAAAAGCAGGCTTCATGATGGAGTTCAAGAAAGA
GW-NbCNGC18-R	GGGGACCACTTTGTACAAGAAAGCTGGGTTGTCATCATCTGGCTCAGC
GW-NbCNGC20-F	GGGGACAAGTTTGTACAAAAAAGCAGGCTTCATGGCAAAGTACTTCTATTG
GW-NbCNGC20-R	GGGGACCACTTTGTACAAGAAAGCTGGGTTGTCATCAGGCTCAGCTGAA
GW-NbCNGC25-F	GGGGACAAGTTTGTACAAAAAAGCAGGCTTCATGGCTAGTCATATAGAACTTG
GW-NbCNGC25-R	GGGGACCACTTTGTACAAGAAAGCTGGGTTAAAATCAAAATCATCCTGATTCG

RESULTS

AVRblb2 interacts with CaM and CML36

The calmodulin-binding domain (CBD, aa 78–82 in the C-terminal region of AVRblb2) of AVRblb2 is necessary for the interaction between AVRblb2 and CaM (Naveed et al., 2019). To investigate the impact of CaM binding to AVRblb2 on pathogenicity, we utilized the CBD deletion mutant (AVRblb2(S)) and the alanine substitution mutant (AVRblb2(A)) as described by Naveed et al. (Naveed et al., 2019). When *P. infestans* reference strain T30-4 was inoculated onto *N. benthamiana* leaves expressing each construct, leaves expressing 3FLAG-AVRblb2 showed significantly enhanced susceptibility to infection compared to the GST control leaves, consistent with previous findings (Bozkurt et al., 2011). However, leaves expressing 3FLAG-AVRblb2(A) and 3FLAG-AVRblb2(S) did not exhibit enhanced susceptibility relative to 3FLAG-AVRblb2, indicating that CaM binding is required for AVRblb2 to function as an effector (Fig. 2-1 A and 2-1 B).

In addition to CaM, *Solanaceae* plants possess numerous EF motif-containing calmodulin-like proteins (CMLs) in their genomes that play critical roles as

Ca^{2+} sensors. In the *N. benthamiana* genome, there are 55 annotated CML genes exhibiting structural similarity to canonical CaM (Zhao et al., 2013). To identify putative interacting host factors with AVRblb2, we performed yeast two hybrid library screening, and identified *N. benthamiana* NbCML36a/b as interact with AVRblb2 (Fig. 2-2). In the yeast two-hybrid (Y2H) system, both CaM and CML36a interacted with AVRblb2, whereas AVRblb2(A) and AVRblb2(S) did not (Fig. 2-1 C), indicating that the CBD of AVRblb2 is required for its interactions with CaM and CML36. These interactions were further confirmed by co-immunoprecipitation (co-IP). Since CaM and CML36 function as calcium sensors, we added calcium or calcium chelator EGTA to the total protein extracts and used for IP to see how calcium affected the interactions between AVRblb2 and CaM or CML36. The results showed that AVRblb2 interacted with CaM and CML only in the presence of calcium (Fig. 2-1 D). To investigate whether CML36 orthologs in *Solanaceae* plants also interacted with AVRblb2, the CML36 orthologs of pepper, tomato, and potato (CaCML36, SlCML36, and StCML36, respectively) were cloned and tested in the Y2H assay. All tested CML36s interacted with AVRblb2 in the Y2H assay, whereas NbCML36-like-1 and NbCML36-like-2 did not (Fig. 2-1 E), indicating that AVRblb2 specifically interacts with CML36 orthologues. To better understand the interactions of CaM and CML36 with AVRblb2, an *in*

vitro competition assay was performed using His-AVRblb2, CaM-GST, and CML36-GST. As results, the CaM-GST interacted strongly with the His-AVRblb2 in the presence of calcium, whereas the CML36-GST showed a weak interaction. However, in the presence of EGTA, neither CaM-GST nor CML36-GST precipitated with His-AVRblb2 (Fig. 2-1 F). Since the CML36-GST weakly associated with the His-AVRblb2 than the CaM-GST under 1 mM $CaCl_2$ treatment, we tested the binding affinity of the CaM-GST and the CML36-GST to the His-AVRblb2 in serial concentrations of $CaCl_2$. The CaM binding affinity for AVRblb2 increased as the calcium concentration-dependent manner, while the inverse effect was observed in the CML36 and AVRblb2 association (Fig. 2-1 G), suggesting that AVRblb2 has distinct roles depending on Ca^{2+} concentration.

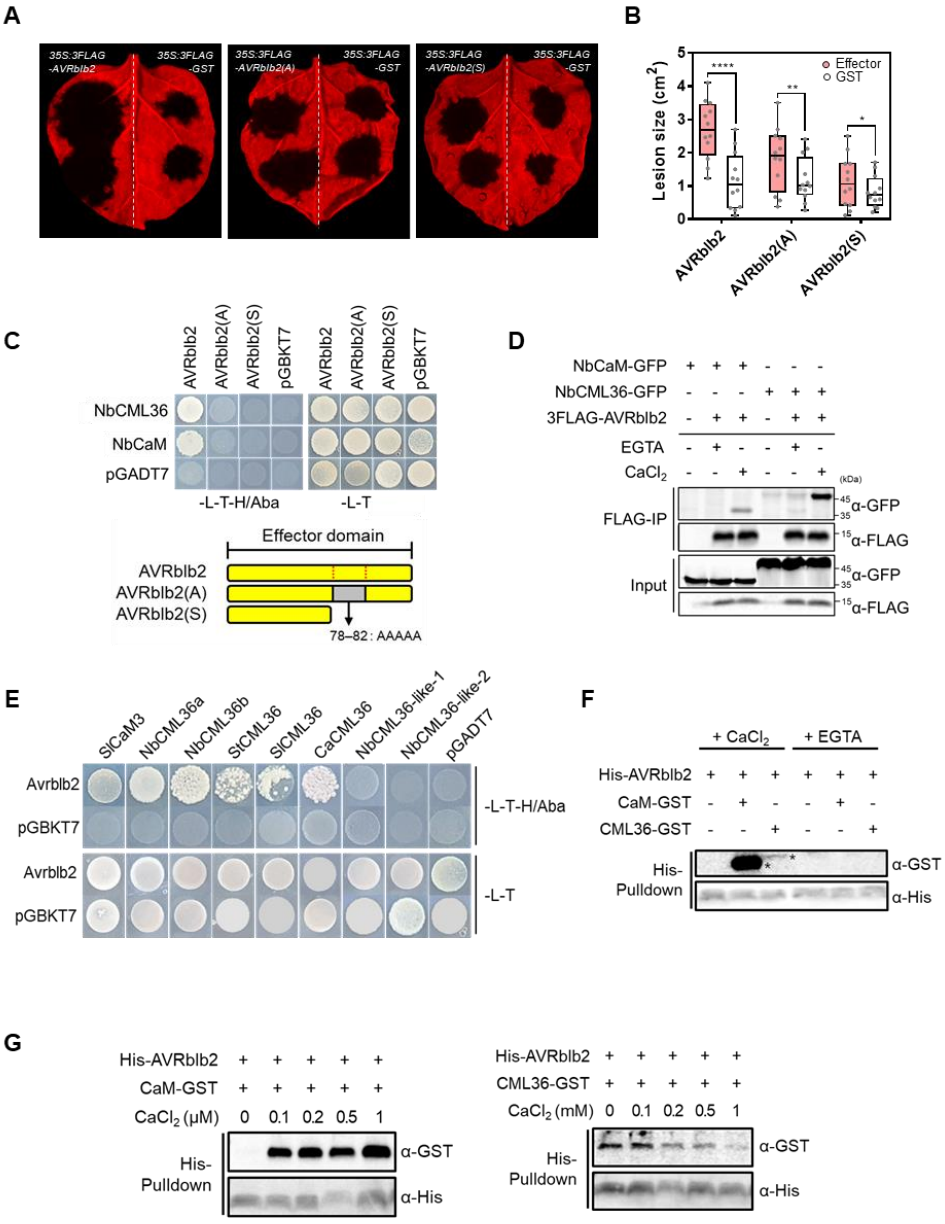

Figure 2-1. AVRblb2 interacts with NbCaM and NbCML36 in a Ca^{2+}-dependent manner. (A-B) With its CBD domain, AVRblb2 increases *P. infestans* pathogen virulence (A) *P. infestans* infection of *N. benthamiana*

leaves expressing GST, AVRblb2, AVRblb2(S), and AVRblb2(A). 3FLAG-effectors were expressed on one-half of the *N. benthamiana* leaf and 3FLAG-GST was expressed on the other half as a negative control. *P. infestans* was inoculated on the detached leaves after one day after infiltration. The photographs were taken at five days after the infection. (B) The box plots depict the lesion size of inoculation sites shown in (A). The lesion size was measured at 6 dpi. Each values in box plots are mean ± SD of the three biological replicates (n=12). The significance was determined using a t-test. ****, P < 0.0001; **, P<0.01; *, P <0.05. (C) In the Y2H assay, AVRblb2 interacts with NbCML36 and NbCaM through its CBD domain. On synthetic media, yeast cells co-expressing GAL4 BD-AVRblb2, AVRblb2(A), or AVRblb2(S) with GAL4 AD-NbCaM or -NbCML36 were grown. -L-T, medium for transformation selection; -L-T-H/Aba, medium for test of interaction. As negative controls, empty pGBKT7 and pGADT7 were used. Photos of single pots were taken 6 days after transformation (upper panel). AVRblb2 and its mutants used in (A, B and C) were depicted schematically in the lower panel. A box with red dash line in AVRblb2 indicates its CBD (aa 78-88). Avrblb2(A) was substituted the CBD to Ala. (D) AVRblb2 is associated with NbCaM and NbCML36 in the presence of calcium ion *in planta* in co-IP experiment with α-FLAG.v3FLAG-AVRblb2 and NbCaM-

GFP or NbCML36-GFP were transiently expressed in *N. benthamiana* using agro-infiltration. 3FLAG-AVRblb2 was precipitated using α-FLAG agarose in the presence of 1 mM of $CaCl_2$ or 2 mM EGTA. α-GFP was used to detect CaM/CML36 associated with AVRblb2. As input, 30 ug of total protein extract was loaded. (E) In the Y2H assays, AVRblb2 interacts with CML36 homologs from *N. benthamiana*, tomato, potato and pepper. The homologous CMLs, NbCML36-like-1 and NbCML36-like-2 were tested for AVRblb2 binding specificity to NbCML36 (F and G). *In vitro* pull-down assay of His-AVRblb2 using His-affinity resin reveals the Ca^{2+} dependent interaction with CaM-GST and CML36-GST. The physical interaction was tested in the presence of 1 mM $CaCl_2$ or 1 mM EGTA with purified His-AVRblb2 and CaM-GST or CML36-GST from *E. coli* crude extracts (F). His-AVRblb2 was pulled down with CaM-GST or CML36-GST using a series of $CaCl_2$ concentrations (G). α-GST detected pulled-down CaM-GST and CML36-GST.

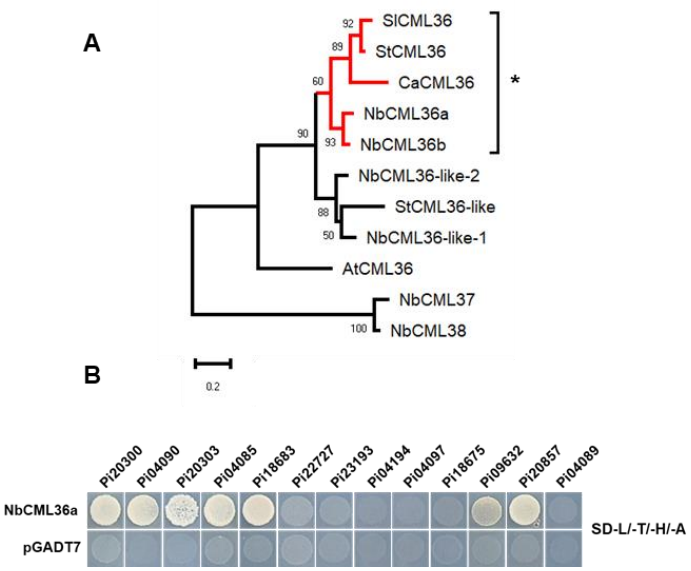

Figure 2-2. NbCML36 interacts with AVRblb2 homologs. (A) The Phylogeny of *N. benthamiana* and Tomato, potato, pepper, Arabidopsis CML36. Phylogeny of Avrblb2 homologs. Amino acids of CML36 were aligned using ClustalW and phylogenetic tree was constructed using the Maximum Likelihood (ML) method with 1000 bootstrap replication. (B) AVRblb2 homologs interacted with NbCML36a in yeast, as is shown by growth on –L-T-H-A plates. Negative control strains contained the pGADT7 vector or the pGBKT7 vector.

AVRblb2 associates with NbCNGC18 in a Ca^{2+} sensor-dependent manner

Because CaM and CML36 have been demonstrated to bind to calcium channels and modulate calcium signaling through these channels, we hypothesized that AVRblb2 might interact with calcium channels via CaM and CML36 to regulate calcium signaling. To test this hypothesis, we conducted interaction studies between AVRblb2 and CNGCs in *N. benthamiana.* Out of the 26 CNGCs in *N. benthamiana* (Saand et al., 2015), We successfully cloned nine CNGCs (NbCNGC3, 4, 5, 7, 18, 19, 20, 21 and 25) and performed co-IP assays with AVRblb2 and these cloned NbCNGCs to identify specific interactions with AVRblb2 (Fig. 2-3). The results of the co-IP experiments revealed that NbCNGC18, NbCNGC19, and NbCNGC20 specifically interacted with AVRblb2 (Fig. 2-4 A). Particularly, both NbCNGC18 and NbCNGC19 showed strong interactions with AVRblb2. Notably, NbCNGC18 and NbCNGC19 share a high degree of amino acid sequence identity of over 98%, including an identical C-terminal cytosolic region. Based on these findings, we selected NbCNGC18 for further investigation to examine the impact of AVRblb2 on the calcium channel.

Since several CNGCs are known to contain a regulatory region in their C-terminus, we focused on the C-terminal region of NbCNGC18 (NbCNGC18-

CT) to explore the potential interaction with AVRblb2 and calcium sensors. In the co-IP assays, AVRblb2 interacted with NbCNGC18-CT in the presence of Ca^{2+}, but not under EDTA treated conditions, similar to the interaction observed with CaM or CML36 (Fig. 2-4 B). NbCNGC18-CT also interacted with other members of the AVRblb2 family that share similar amino acid sequences (Fig. 2-5). Furthermore, in the Y2H system, NbCNGC18-CT interacted with CaM, CML36, and CML36-like-1, while no interaction was observed between NbCNGC18-CT and AVRblb2 (Fig. 2-4 C), indicating that AVRblb2 indirectly interacts with the C-terminal region of NbCNGC18.

To validate the interaction of AVRblb2 with calcium sensors or NbCNGC18, we performed a split-luciferase assay in *N. benthamiana*. The combination of AVRblb2 with CaM, CML36, NbCNGC18-CT successfully restored the activity of luciferase *in planta* (Fig. 2-4 D). Additionally, we investigated whether AVRblb2 forms a calcium-dependent complex with CaM/CML36 and NbCNGC18-CT. We employed CaM affinity resin to bind proteins with EF-hand motifs under CNGC18-CT and AVRblb2 or AVRblb2(A)-expressing conditions. The CaM resin precipitated both AVRblb2 and CNGC18-CT (Fig. 2-4 E), suggesting that NbCNGC18 interacts with AVRblb2, likely via CaM/CML36. These findings indicate that the association between AVRblb2 and NbCNGC18 occurs indirectly via CaM/CML36 in a Ca^{2+}-dependent

manner, suggesting that AVRblb2 may influence CNGC activity through its interaction with CaM and CML36.

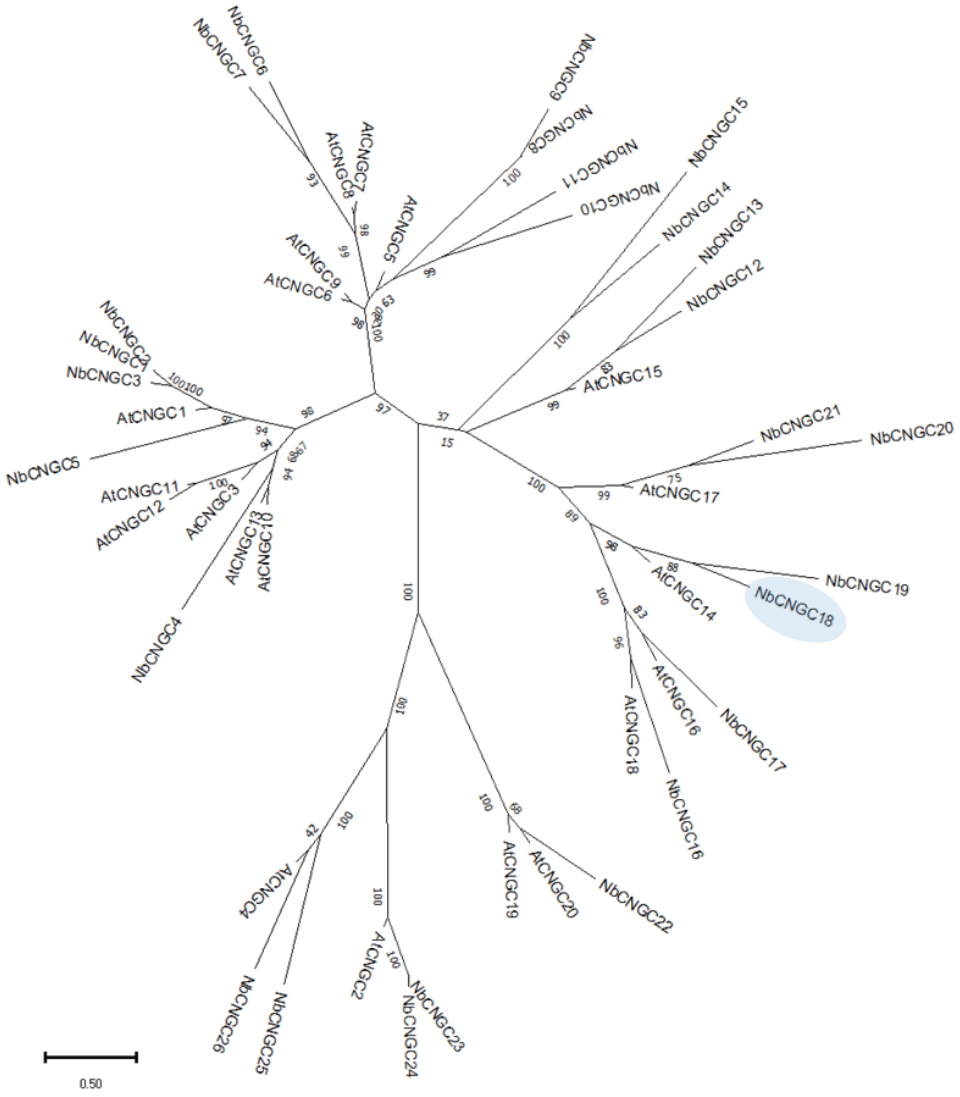

Figure 2-3. Phylogenetic tree of the NbCNGC proteins. The tree was created using Clustalx program by maxiAmino Maximum Likelihood (ML) method with 1000 bootstrap replication in MEGA7 (Tamura and Nei, 1993; Tamura et al., 2011). NbCNGC18 was shown in blue.

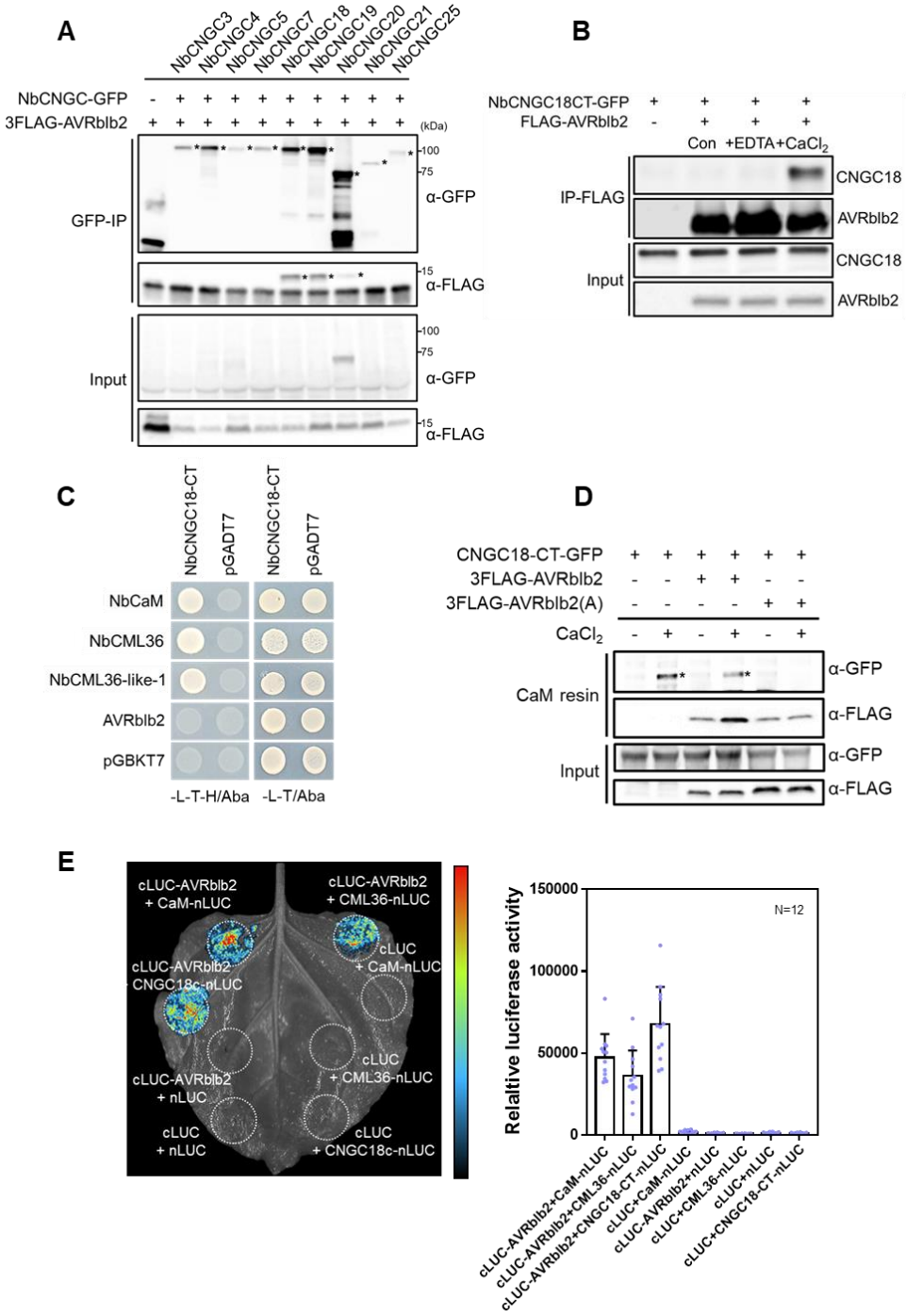
A
NbCNGC3
NbCNGC4
NbCNGC5
NbCNGC7
NbCNGC18
NbCNGC19
NbCNGC20
NbCNGC21
NbCNGC25
NbCNGC-GFP
3FLAG-AVRblb2
(kDa)
GFP-IP
α-GFP
α-FLAG
Input
B
NbCNGC18CT-GFP
FLAG-AVRblb2
Con
+EDTA
+CaCl2
IP-FLAG
CNGC18
AVRblb2
Input
C
NbCNGC18-CT
pGADT7
NbCaM
NbCML36
NbCML36-like-1
AVRblb2
pGBKT7
-L-T-H/Aba
-L-T/Aba
D
CNGC18-CT-GFP
3FLAG-AVRblb2
3FLAG-AVRblb2(A)
CaCl2
CaM resin
α-GFP
α-FLAG
Input
E
cLUC-AVRblb2
+ CaM-nLUC
cLUC-AVRblb2
+ CML36-nLUC
cLUC-AVRblb2
CNGC18c-nLUC
cLUC
+ CaM-nLUC
cLUC-AVRblb2
+ nLUC
cLUC
+ CML36-nLUC
cLUC
+ nLUC
cLUC
+ CNGC18c-nLUC
Relaltive luciferase activity
150000
100000
50000
0
N=12
cLUC-AVRblb2+CaM-nLUC
cLUC-AVRblb2+CML36-nLUC
cLUC-AVRblb2+CNGC18-CT-nLUC
cLUC+CaM-nLUC
cLUC-AVRblb2+nLUC
cLUC+CML36-nLUC
cLUC+nLUC
cLUC+CNGC18-CT-nLUC

Figure 2-4. AVRblb2 interacts with NbCNGC18 via calcium sensors. (A) Co-IP experiments show that 3FLAG-AVRblb2 associates with specific NbCNGCs-GFP in *N. benthamiana*. Total protein extract from *N. benthamiana* containing 1 mM $CaCl_2$ was precipitated with α-FLAG affinity gels and immunoblotted with α-FLAG and α-GFP. (B) 3FLAG-AVRblb2 associates with the C-terminal region of NbCNGC18 *in planta*. Co-IPs were performed using α-FLAG affinity gel and the association was tested using α-GFP in the presence of 1 mM EDTA or $CaCl_2$. (C) In the Y2H assay, the C-terminal region of NbCNGC18 physically interacts with NbCaM, NbCML36, and NbCML36-like-1, but not with AVRblb2. (D) Split-luciferase complementation assay reveals interaction between AVRblb2 and NbCML36 or NbCNGC18-CT in *N. benthamiana*. NbCaM-nLUC with cLUC-AVRblb2 was used as a positive control. The photos were taken at two days post infiltration (left panel) and the luminescence was measured by the emitted light units (right panel). The values are mean ± SD (n=12). (E) *In planta* pull-down assay using CaM resin shows that CaM/CML36 interacts with both of AVRblb2 and NbCNGC18-CT in in the presence of Ca^{2+}. Total proteins extracted from *N. benthamiana* leaves expressing CNGC18-CT-GFP and 3FLAG-AVRblb2 or 3FLAG-AVRblb2(A) were precipitated with CaM resin. α-FLAG and α-GFP were used to detect precipitated proteins.

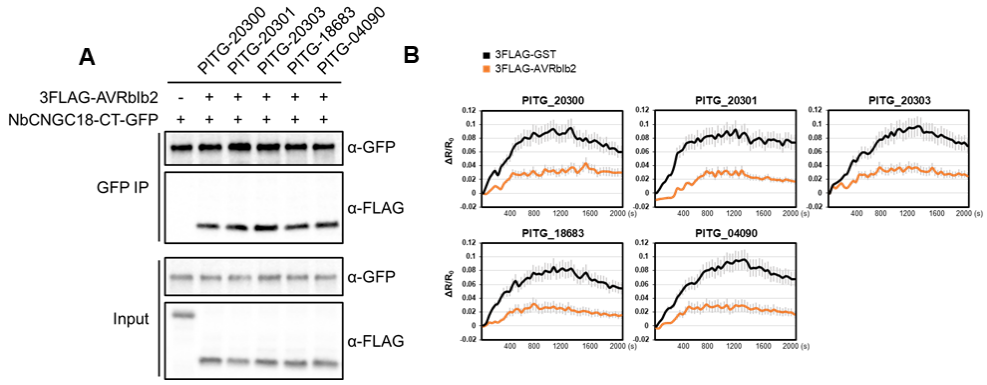

Figure 2-5. AVRblb2 paralogs associate with NbCNGC18-CT and suppress flg22-induced Ca^{2+} influx. (A) Co-IP experiments show that NbCNGC18-GFP interacts with FLAG-tagged AVRblb2 paralogs (PITG_20300, 20301, 20303, 18683, and 04090). NbCNGC18-CT was precipitated using α-GFP and associated proteins were detected by α-FLAG in the presence of 1 mM $CaCl_2$. The experiments were performed at least three times in biological replicates and the representative figure was shown. (B) Flg22-induced $[Ca^{2+}]_{cyt}$ accumulation under AVRblb2 paralogs-expressing conditions. Dynamics of $[Ca^{2+}]_{cyt}$ were monitored in time course for 30 minutes. FRET ratio ($\Delta R/R_0$) represents $[Ca^{2+}]_{cyt}$ in leaves transiently expressing indicated protein(s) in response to 1 μM flg22. ($n \geq 20$). 3FLAG-GST was used as a control. Values are mean ± SE of the three biological replicates ($n \geq 12$). Significance was determined using a t-test. ****, $P < 0.0001$.

AVRblb2 suppresses PTI-induced Ca^{2+} influx

We hypothesized that AVRblb2 could regulate the Ca^{2+} signaling induced by PAMP through its interaction with NbCNGC, as several CNGCs contribute to the transient Ca^{2+} influx induced by PTI and ETI (Zhao et al., 2021). To investigate this, we monitored cytosolic Ca^{2+} dynamics in *N. benthamiana* plants expressing the fluorescent protein-based Ca^{2+} sensor YC3.6 in response to flg22 treatment (Monshausen et al., 2008).

In the GST-expressing conditions, cytoplasmic Ca^{2+} levels peaked at 15 to 20 min after flg22 treatment and gradually declined. However, in AVRblb2-expressed conditions, flg22-induced Ca^{2+} influx was strongly inhibited, whereas the effect of AVRblb2(A) was moderate (Fig. 2-6 A and 2-6 B). Similar to AVRblb2, other members of AVRblb2 family also exhibited the ability to suppress the Ca^{2+} influx induced by flg22 (Fig. 2-7). Furthermore, AVRblb2 broadly suppressed elevated cytosolic Ca^{2+} levels induced by other PAMPs such as elf18 and chitin (Fig. 2-8), indicating that AVRblb2-inhibited Ca^{2+} influx is not pathogen-specific but disrupts the general PTI response.

We further examined the involvement of NbCNGC18 in PAMP-triggered calcium signaling by analyzing Ca^{2+} influx under NbCNGC18-expressing conditions. Overexpression of NbCNGC18 led to a significant increase in Ca^{2+}

influx after flg22 treatment, while NbCNGC18-silenced plants showed an impaired response (Fig. 2-6 A, 2-6 B and Fig. 2-9), indicating that NbCNGC18 positively regulated flg22-induced Ca^{2+} influx. Additionally, the flg22-induced Ca^{2+} spike was strongly inhibited in CaM-overexpressing *N. benthamiana* leaves, whereas Ca^{2+} influx was significantly enhanced in CML36-overexpressing plants (Fig. 2-6 A and 2-6 B), demonstrating the opposite roles of CaM and CML36 in flg22-induced Ca^{2+} influx.

To investigate the effect of CaM and CML36 on NbCNGC18 activity, we measured Ca^{2+} influx in plants co-expressing NbCNGC18 and CaM or CML36. CaM significantly compromised the Ca^{2+} influx enriched by NbCNGC18, while leaves co-expressing CML36 and NbCNGC18 showed similar Ca^{2+} influx levels to those expressing NbCNGC18 alone (Fig. 2-6 A and 2-6 B). Furthermore, co-expression of CaM, CML36, and NbCNGC18 resulted in lower Ca^{2+} peaks compared to the GST control, indicating that the CaM-mediated suppression of the NbCNGC18-induced Ca^{2+} spike was not rescued by CML36 (Fig. 2-6 A and 2-6 B). Interestingly, AVRblb2 tightly inhibited flg22-induced Ca^{2+} influx in all the cases. These findings demonstrated that NbCNGC18 is involved in the flg22-induced transient Ca^{2+} influx regulated by CaM and CML36, which have opposing functions, and AVRblb2 suppresses Ca^{2+} influx to disrupt the PTI response.

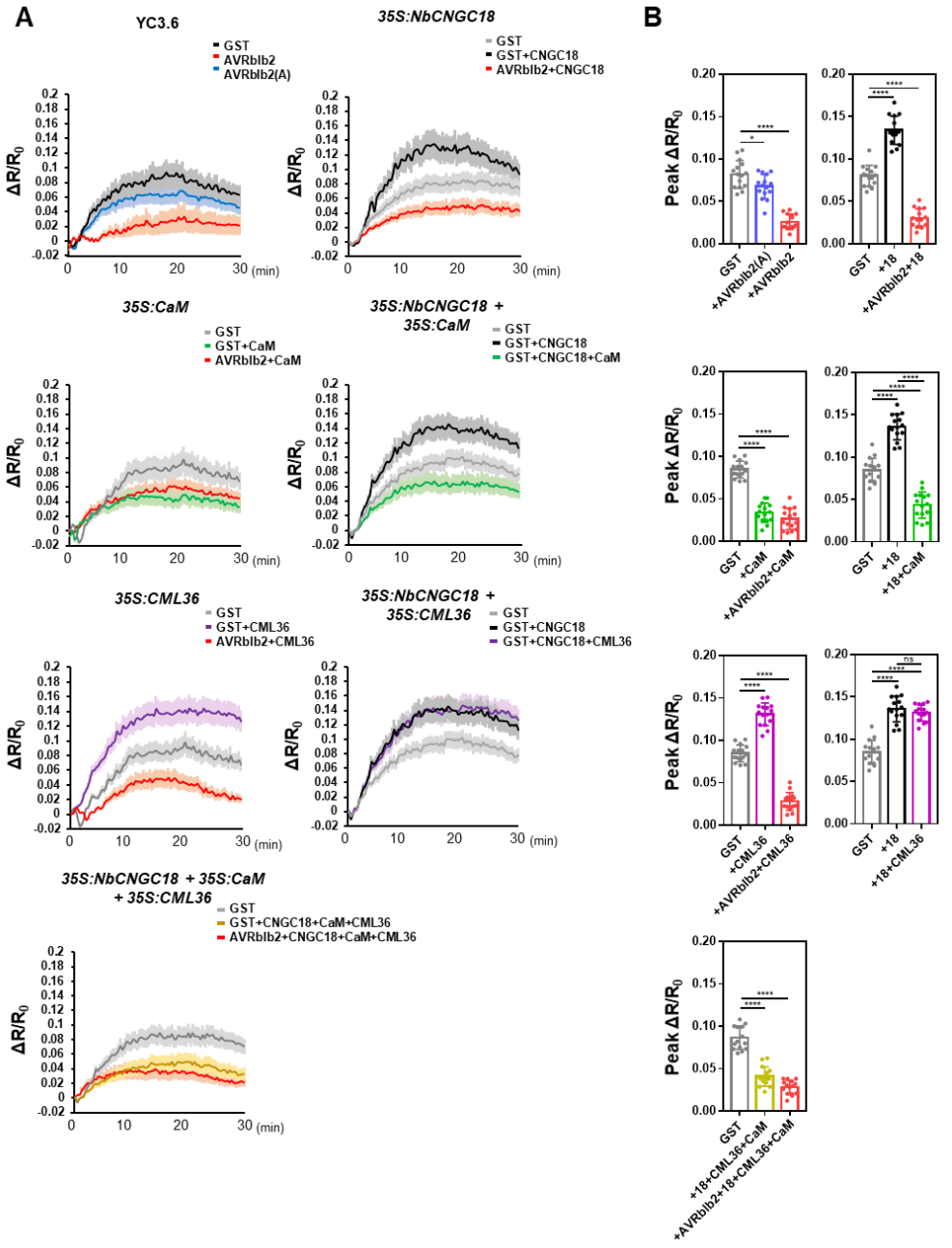

Figure 2-6. AVRblb2 suppresses the flg22-induced Ca^{2+} influx in *N. benthamiana*. (A) Calcium sensor-CNGC association affects flg22-mediated

Ca^{2+} influx in *N. benthamiana*. Dynamics of $[Ca2+]_{cyt}$ in the YC3.6 transgenic *N. benthamiana* leaves were monitored in time course. FRET ratio represents $[Ca2+]_{cyt}$ in leaves transiently expressing indicated protein(s) in response to 1 μM flg22 at time = 0 s. ($n \geq 20$).

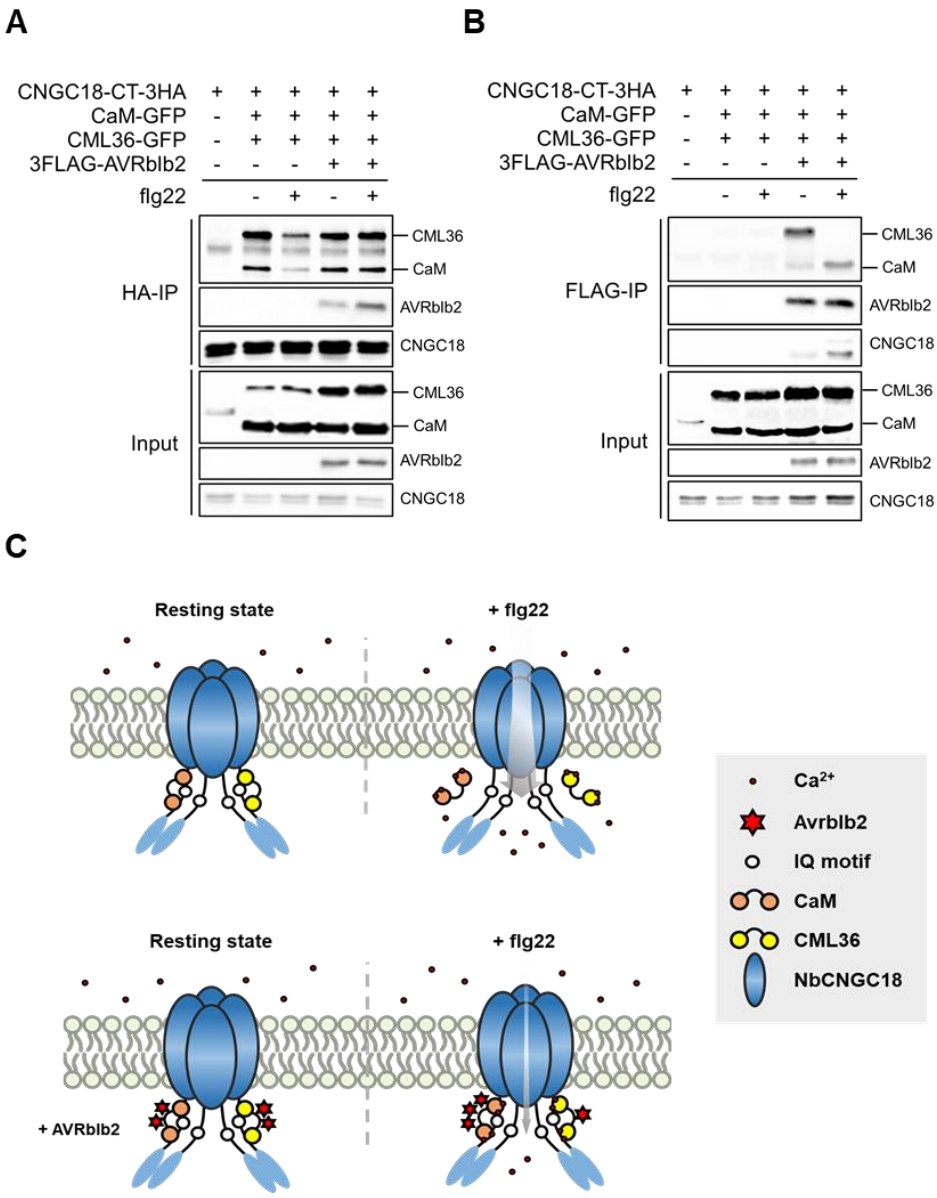

Figure 2-7. AVRblb2 regulates the activity of NbCNGC18 via calcium sensor proteins. (A) Co-IP experiments confirm that suppressed interaction between calcium sensors and CNGC18-CT in response to flg22 was restored in

presence of AVRblb2. Combinations of GFP-tagged CaM and CML36, FLAG-tagged AVRblb2 and HA-tagged CNGC18-CT were transiently expressed in *N. benthamiana* leaves by agroinfiltration, as indicated. (B) CML36 and CaM were co-IPed with AVRblb2 and CaM-AVRblb2 association is enhanced upon elicitor treatment. (C) Working model for calcium sensors and CNGC-mediated Ca^{2+} influx in response to PAMP. In the resting state, NbCNGC18 associates with CaM and CML36. Upon perception of PAMP, CaM and CML36 are separated from NbCNGC18, which results in activation of NbCNGC18 to induce Ca^{2+} influx. When PTI is suppressed in presence of AVRblb2, disassociation of CaM/CML36-NbCNGC18 is inhibited by formation of complex AVRblb2-calcium sensors-CNGC18.

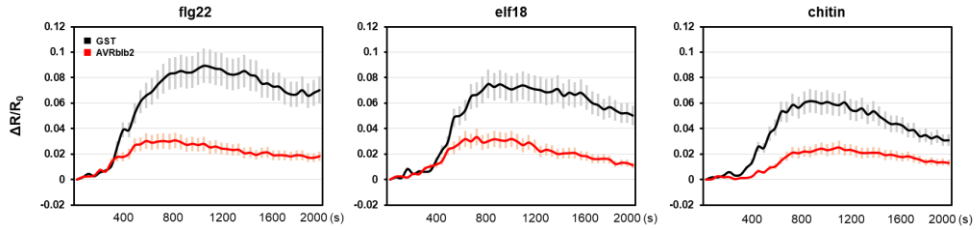

Figure 2-8. AVRblb2 suppresses Ca^{2+} influx induced by diverse PAMPs in *N. benthamiana*. Calcium elevation upon flg22, elf18 or chitin treatment is monitored in time course for 30 minutes under AVRblb2 or GST-expressing conditions using YC3.6-expressing *N. benthamiana* transgenic leaves. Values are mean ± SE of the three biological replicates (n=12). Significance was determined using a t-test. ****, $P < 0.0001$.

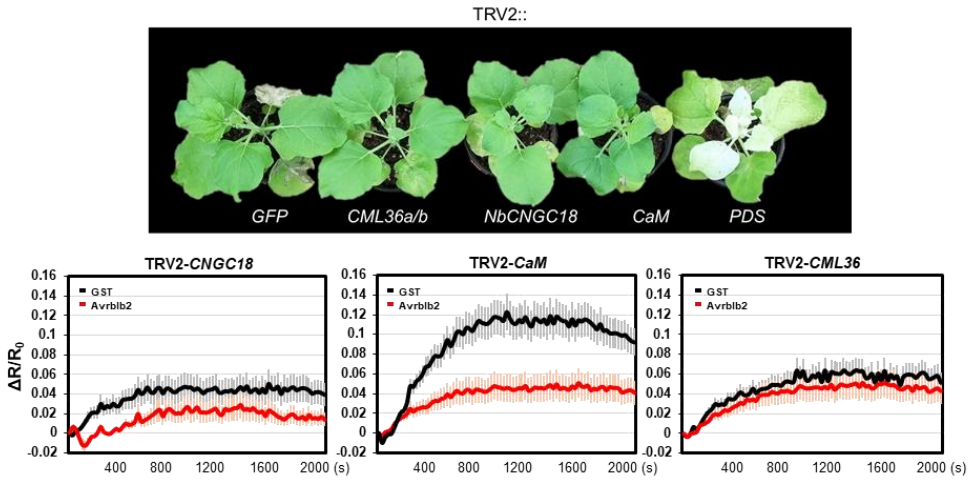

Figure 2-9. Activity of AVRblb2 in Ca^{2+} influx after flg22 treatment in NbCNGC18, CaM, or CML36-silenced plants. Morphology of CaM, CML36, and NbCNGC18-slienced plants compared to GFP and PDS-silenced plants (upper panel). CML36, CaM, or NbCNGC18 was silenced using VIGS in YC3.6 transgenic plants. GFP was used as a negative control of silencing; PDS was used as a control for efficient silencing. Three weeks later after VIGS, GST or AVRblb2 was transiently expressed using agrobacterium, and $[Ca^{2+}]_{cyt}$ accumulation was monitored for 30 minutes after flg22 treatment (lower panel). Values are mean ± SE of the three biological replicates ($n \geq 12$). Significance was determined using a t-test. ****, $P < 0.0001$; *, $P<0.05$, ns, not significant.

AVRblb2 prevents the dissociation of CaM/CML36 from NbCNGC18

Given that CaM and CML36 have different binding affinities for AVRblb2 (Fig. 2-1 F) and exert opposite effects on NbCNGC18 activity (Fig. 2-6 A), we hypothesized that AVRblb2 might suppress NbCNGC18 activity by regulating the binding affinity of CaM and CML36 to NbCNGC18. To test this hypothesis, we conducted co-IP experiments to investigate the binding affinity between NbCNGC18 and CaM or CML36 in response to flg22 treatment. In the resting state, CaM and CML36 were both associated with NbCNGC18. However, flg22 treatment significantly reduced their binding to NbCNGC18 (Fig. 2-7 A, lane 2 and 3). In the presence of AVRblb2, CaM and CML36 were unable to dissociate from NbCNGC18 after flg22 treatment (Fig. 2-7 A, lane 4 and 5). This finding suggests that AVRblb2 may regulate NbCNGC18 activity by preventing the dissociation of CaM or CML36 from NbCNGC18.

Since the binding affinities of CaM and CML36 to AVRblb2 differed in response to Ca^{2+} (Fig 2-1 F), we examined the binding affinity of CaM and CML36 to AVRblb2 in response to flg22. In the resting state, AVRblb2 predominantly interacted with CML36, but it bound to CaM after flg22 treatment (Fig. 2-7 B), consistent with the *in vitro* pull-down data. This indicates that AVRblb2 primarily associates with CaM in the presence of high

Ca^{2+}levels both *in vitro* and *in planta*, but interacts with CML36 under low Ca^{2+} conditions. These findings demonstrate that changes in the dynamics of the interactions between CaM, CML36, and NbCNGC18 are early events in PAMP perception. They also suggest that AVRblb2 primarily utilizes CaM to suppress NbCNGC18 activity and disrupt the PTI response (Fig. 2-7 C).

Phosphorylation at the C-terminus is a major regulatory mechanism for CNGC activity (Curran et al., 2011; Zhou et al., 2014), and recent studies have revealed that some CNGCs are activated through phosphorylation by receptor kinases or receptor-like kinases upon pathogen attack (Ladwig et al., 2015; Tian et al., 2019; Wang et al., 2019; Yu et al., 2019). To assess if AVRblb2 regulates NbCNGC18 activity by mediating its phosphorylation, we examined the levels of NbCNGC18 phosphorylation using p-Thr and p-Ser antibodies, which detect phosphorylated threonine and serine, respectively. We also utilized Phos-tag, which detects overall phosphorylation. We observed an increase in NbCNGC18-CT phosphorylation, particularly on Thr and Ser, in flg22-treated leaves (Fig. 2-10). However, there was no difference in Thr and Ser phosphorylation in the presence of AVRblb2. Additionally, the overall level of phosphorylation in NbCNGC18-CT was similar to that in absence of AVRblb2, suggesting that AVRblb2 does not affect the phosphorylation status of NbCNGC18.

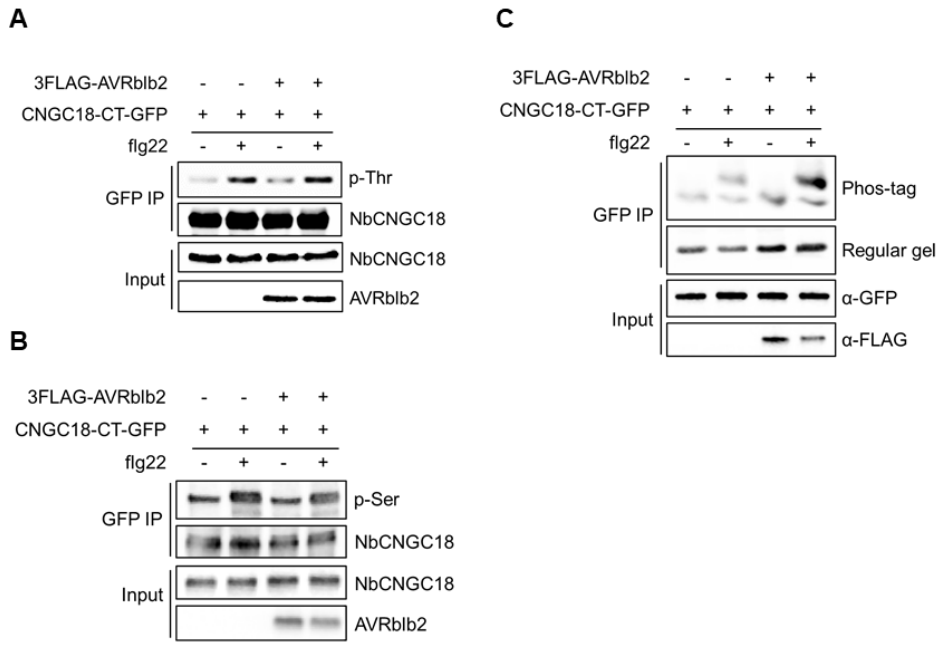

Figure 2-10. AVRblb2 does not affect NbCNGC18 phosphorylation. **(A**-C) Co-IP experiments show that CNGC18-CT is phosphorylated after flg22 treatment, but is not affected by AVRblb2. (A, B) NbCNGC18-CT was precipitated using α-GFP affinity gel and its phosphorylation was detected using α-Thr (anti-p-threonine) and α-Ser (anti-p-serine) upon flg22 treatment. 30 ug of total protein extract was loaded as input and immunoblotted to confirm the expression of NbCNGC18 and AVRblb2 using α-GFP and α-FLAG, respectively. (C) NbCNGC18-CT was precipitated using α-GFP affinity gel and its phosphorylation was detected α-GFP in a Phos-tag gel which shows phosphorylated Tyr, Thr, and Ser by shifting bands and in a SDS-

PAGE gel. 30 ug of total protein extract was loaded as input and immunoblotted to confirm the expression of NbCNGC18 and AVRblb2 using α-GFP and α-FLAG, respectively.

AVRblb2 suppresses the activity of other CNGCs by interacting with CNGC18

Plant CNGCs have the ability to form homomeric or heteromeric complexes that influence channel activity under specific conditions (Brost et al., 2019; Chin et al., 2013; Dietrich et al., 2020; Pan et al., 2019; Tian et al., 2019; Tian et al., 2020). In order to investigate the CNGC candidates that interact with NbCNGC18 during flg22-induced PTI, we conducted co-IP and liquid chromatography-tandem mass spectrometry (LC-MS/MS) analysis of NbCNGC18-expressing leaves after flg22 treatment. We identified NbCNGC3, NbCNGC11, NbCNGC20, and NbCNGC25 as potential interactors of NbCNGC18. These interactions were confirmed through co-IP experiments in response to flg22 treatment. NbCNGC3, NbCNGC20, and NbCNGC25 exhibited strong binding to NbCNGC18 upon flg22 treatment, while the interaction between NbCNGC11 and NbCNGC18 remained unchanged (Fig. 2-11 A). Furthermore, the self-association of NbCNGC18 was reduced in response to flg22 (Fig. 2-1 A), indicating that NbCNGC18 functions as part of a complex with other CNGCs in the presence of flg22 rather than functioning alone.

To validate the interactions of NbCNGC18 with other CNGCs, we utilized

bimolecular fluorescence complementation (BiFC). Consistent with the co-IP results, NbCNGC3, NbCNGC11, NbCNGC20, and NbCNGC25 interacted with NbCNGC18 *in planta*, while NbCNGC1, NbCNGC2, and NbCNGC12 did not (Fig. 2-13). BiFC was also utilized to investigate whether these interacting CNGCs could interact with AVRblb2. In addition to NbCNGC19 and NbCNGC20, which belong to the same clade as NbCNGC18 (Fig. 2-3), NbCNGC3 and NbCNGC4 were identified as interact with AVRblb2 (Fig. 2-14). Interestingly, NbCNGC11 and NbCNGC25 did not interact with AVRblb2, despite showing a fluorescence signal in BiFC with NbCNGC18 (Fig. 2-13, 2-14). These findings indicate that NbCNGC18 can associate with other CNGCs upon PAMP perception and suggest that AVRblb2 forms specific heteromeric CNGC complexes via NbCNGC18 and potentially other NbCNGCs to suppress Ca^{2+}-influx during early PTI (Fig. 2-11 B).

To determine which heteromeric NbCNGC complex is involved in the flg22-induced PTI response with NbCNGC18, we co-expressed NbCNGC18 with each NbCNGC along with RNAi GUS as a negative control for a hairpin RNA interference (RNAi), and measured Ca^{2+} influx under flg22 treatment. Flg22-induced Ca^{2+} influx significantly increased when NbCNGC18 was co-expressed with NbCNGC3, NbCNGC20, or NbCNGC25 (Fig. 2-12 A, grey line). Next, we generated an RNAi construct targeting NbCNGC18 under the

control of the CaMV 35S promoter (35S:dsNbCNGC18) and co-expressed it with each NbCNGC (Fig 2-12 A, yellow line). In NbCNGC18-silenced conditions, Ca^{2+} influx was significantly decreased compared to RNAi:GUS control, even when the NbCNGC3, NbCNGC20, or NbCNGC25 were overexpressed. However, the expression of a codon-shuffled NbCNGC18 (NbCNGC18(M)) designed to avoid RNAi complementation restored the impaired Ca^{2+} influx by 35S:dsNbCNGC18 (Fig. 2-12 A and B). These results indicate that NbCNGC3/20/25 function through NbCNGC18 in flg22-induced Ca^{2+} influx. On the other hand, when NbCNGC11 or NbCNGC12 was overexpressed, Ca^{2+} influx was not affected by NbCNGC18-silencing (Fig. 2-12 A, 2-12 B and 2-15), consistent with the co-IP results (Fig. 2-11 A). Taken together, these findings support a working model (Fig. 2-11 B) in which NbCNGC18 selectively forms heteromeric complexes with other NbCNGCs during flg22-induced PTI.

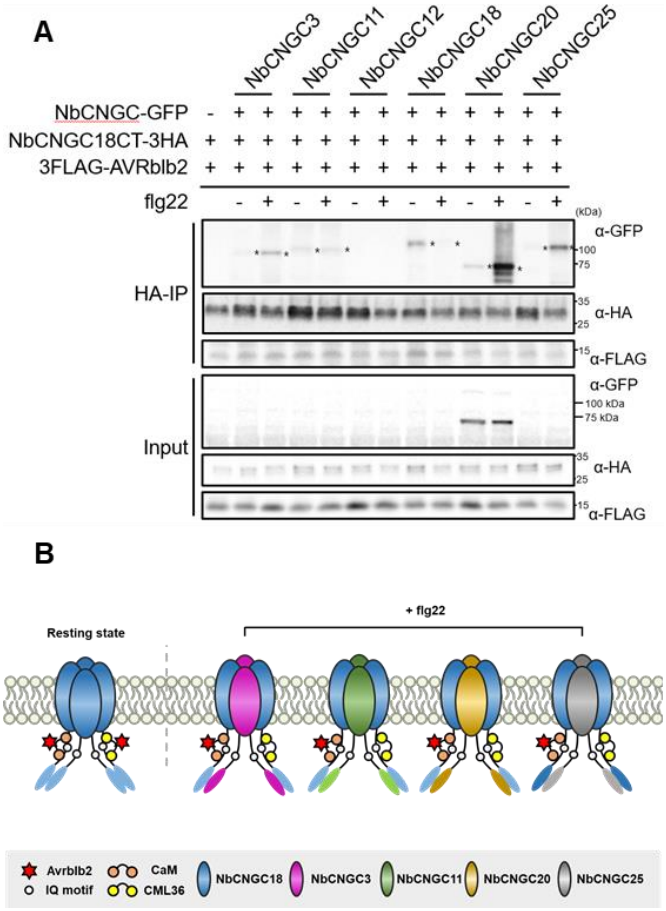

Figure 2-11. NbCNGC18 forms a complex with other CNGCs during PTI response. NbCNGC18 forms heterotetrameric complex with other CNGCs during PTI response. (A) NbCNGC18 interacts with CNGC3/20/25 after flg22 treatment. NbCNGC18-CT-3HA, NbCNGCs-GFP and 3FLAG-AVRblb2 were co-expressed in *N. benthamiana* by Agroinfiltration. Collected leave samples treated with H2O or 1 μm flg22 for 10 min were subjected to co-IP experiments. (B) Schematic model of NbCNGC18 heteromeric channels

induced by flg22.

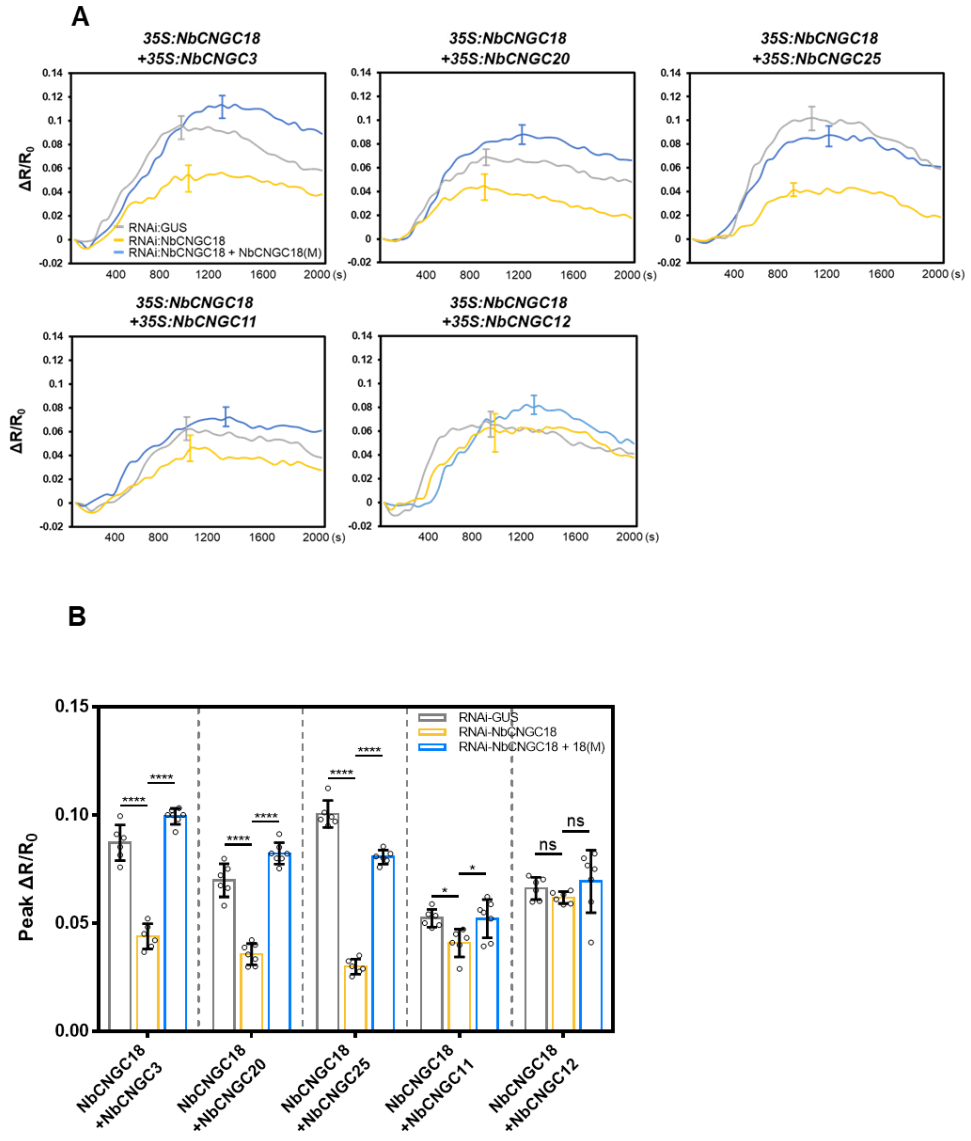

Figure 2-12. NbCNGC3/20/25 function through NbCNGC18 in flg22-

induced Ca2+ influx. (A) Co-overexpression of NbCNGC18 with NbCNGC3/20/25, but not NbCNGC11/12, enhanced Ca2+ influx upon flg22 treatment. (B) Peak value of cytosolic Ca2+ influx in leaf discs used in (A). Means ± standard deviation of the peak value are given from 18 replicates. (two-way ANOVA; Tukey's HSD; $P < 0.05$). (C) Quantitative RT-PCR analysis of *NbCNGC18* gene expression. NbActin was used as an internal standard. Results shown are mean ± SE from triplicate technical replicates from one of three representative experiments with similar results. P-values were calculated using t-tests (*$p < 0.005$).

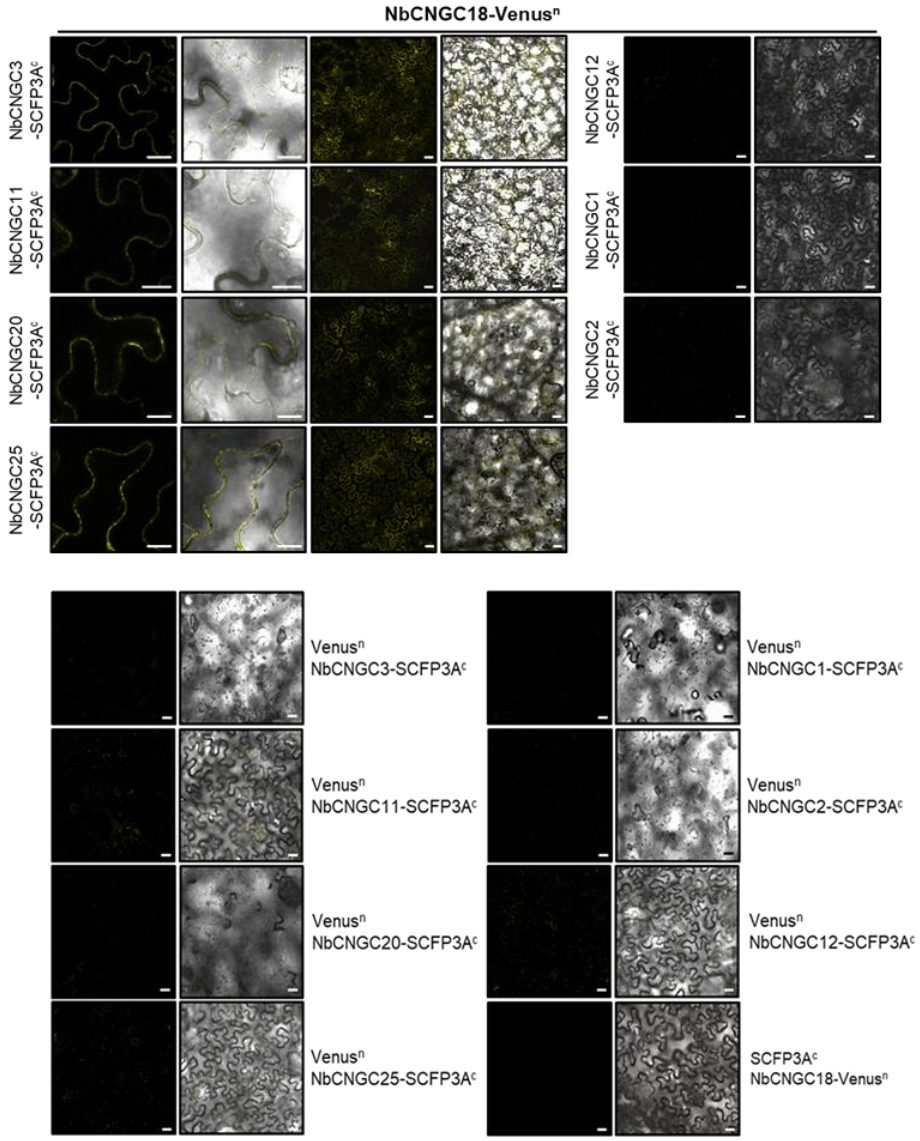

Figure 2-13. NbCNGC18 forms heteromeric complex with other NbCNGCs. *In planta* BiFC assays showing interaction of AVRblb2 fused to YFPn with NbCNGCs fused to SCFPc. NbCNGC3/4/18/19/20 show interaction with AVRblb2 and give yellow fluorescence.

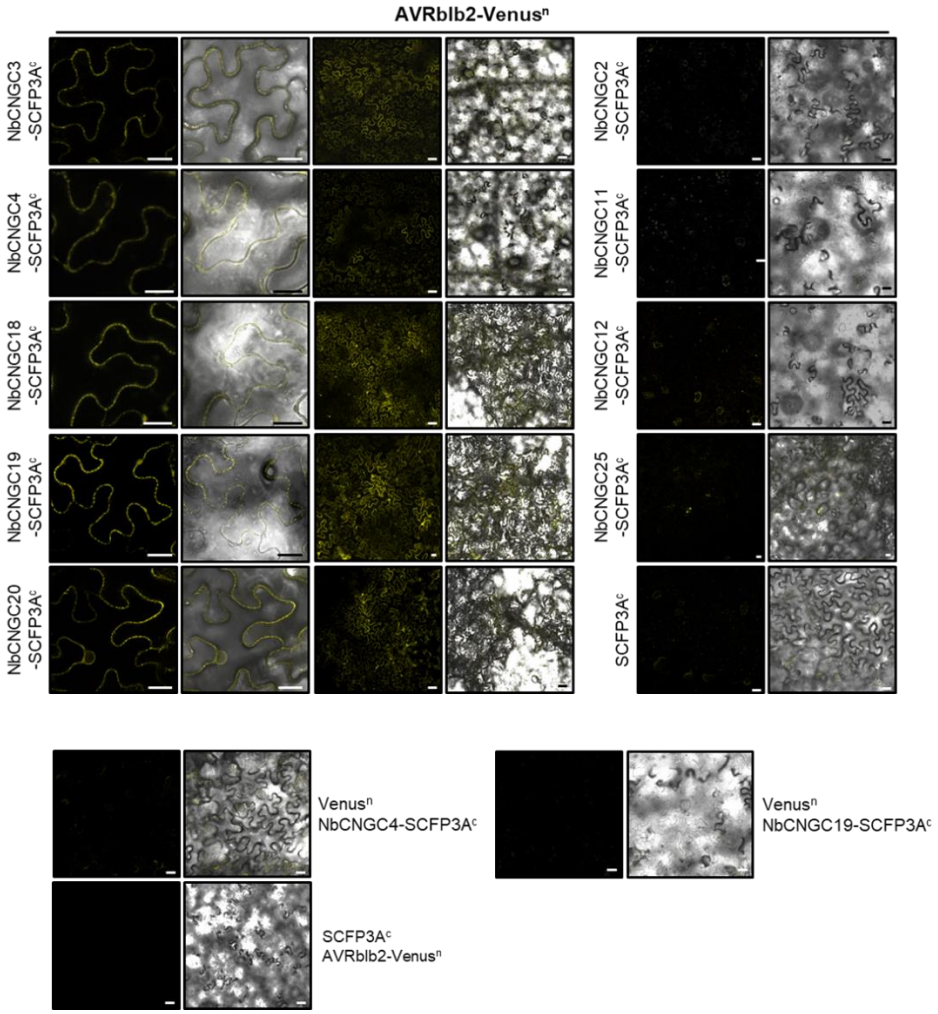

Figure 2-14. AVRblb2 associates with NbCNGCs including NbCNGC18. NbCNGC18 interact with NbCNGCs *in planta*. BiFC analyses were carried out using 4 weeks-old *N. benthamiana* leaves. Scale bar represents 20 μm, and the confocal images were taken after 2 dpi.

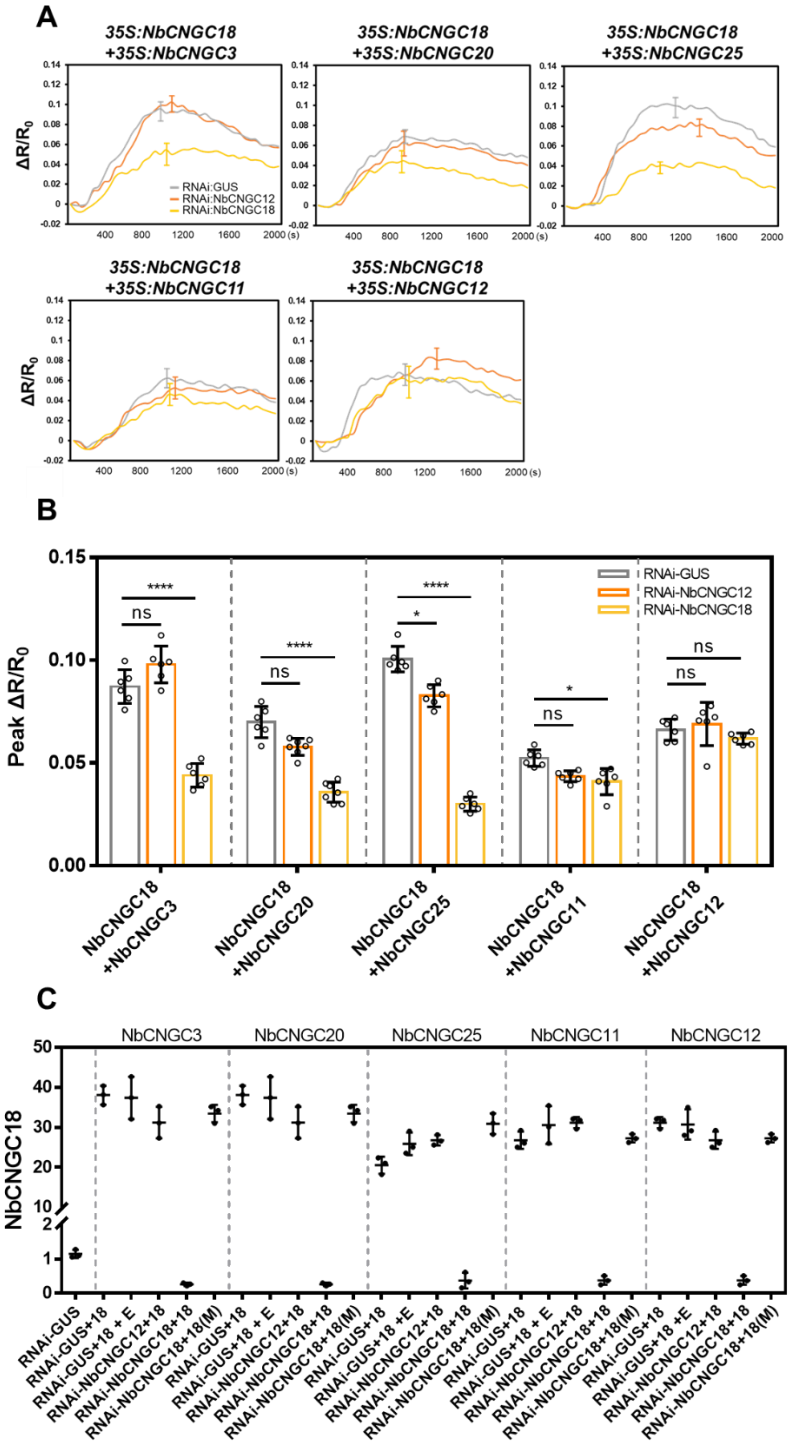
A
35S:NbCNGC18 +35S:NbCNGC3
35S:NbCNGC18 +35S:NbCNGC20
35S:NbCNGC18 +35S:NbCNGC25
35S:NbCNGC18 +35S:NbCNGC11
35S:NbCNGC18 +35S:NbCNGC12
ΔR/R0
RNAi:GUS
RNAi:NbCNGC12
RNAi:NbCNGC18
B
Peak ΔR/R0
RNAi-GUS
RNAi-NbCNGC12
RNAi-NbCNGC18
NbCNGC18 +NbCNGC3
NbCNGC18 +NbCNGC20
NbCNGC18 +NbCNGC25
NbCNGC18 +NbCNGC11
NbCNGC18 +NbCNGC12
C
NbCNGC18
NbCNGC3
NbCNGC20
NbCNGC25
NbCNGC11
NbCNGC12
RNAi-GUS
RNAi-GUS+18
RNAi-GUS+18 + E
RNAi-NbCNGC12+18
RNAi-NbCNGC18+18
RNAi-NbCNGC18+18(M)

Figure 2-15. NbCNGC18 heteromerically mediates flg22-induced Ca^{2+} influx. (a) Flg22-induced $[Ca^{2+}]_{cyt}$ accumulation in *N. benthamiana* using YC3.6. $\Delta R/R_0$ represents $[Ca^{2+}]_{cyt}$ in leaves transiently expressing indicated protein(s) in response to 1 μM flg22. Dynamics of $[Ca^{2+}]_{cyt}$ were monitored in time course for 30 minutes (n=18). RNAi:NbCNGC18 or RNAi:NbCNGC12 was co-expressed with NbCNGCs for gene silencing, and RNAi:GUS was used as a negative control of RNAi. Error bars represent the highest value of $\Delta R/R_0$. (b) Bar graphs are depicted the highest value of $\Delta R/R_0$ shown in (a). The significance was determined using a t-test. ****, $P < 0.0001$; *, $P < 0.05$; ns, not significant. (c) Quantitative RT-PCR analysis of *NbCNGC18* gene expression. *NbActin* was used as an internal standard. Results shown are mean ± SE from triplicate technical replicates from one of three representative experiments with similar results.

AVRblb2 suppresses the PTI response and enhances virulence by regulating CNGCs

To investigate the impact of AVRblb2 on downstream immune responses mediated by calcium signaling activation during PTI, we examined its effect on ROS production, expression of PTI-related genes, and MAPK activation. Our results demonstrated that AVRblb2 significantly reduced flg22-induced ROS burst compared to the control condition, while AVRblb2(A) showed a partial reduction (Fig. 2-16 A). Furthermore, qRT-PCR analysis was performed to assess the expression of PTI-related genes (*ICS1*, *PR1*, *Acre31*, and *WRKY22* (Heese et al., 2007)) under AVRblb2 or AVRblb2(A)-expressing conditions. The results showed that AVRblb2 effectively suppressed the expression of PTI marker genes, whereas AVRblb2(A) demonstrated a lesser or no degree of suppression (Fig. 2-16 B). Additionally, immunodetection assays revealed that the phosphorylated SIPK and WIPK, indicating MAPK activation, was reduced when AVRblb2 was expressed compared to the control condition (Fig. 2-16 C). Collectively, these results indicate that AVRblb2 suppresses the overall PTI response (Fig. 2-16 A-C).

To explore the effects of NbCNGCs and AVRblb2 on flg22-induced ROS burst, we measured ROS levels under NbCNGCs and/or AVRblb2-expressing

conditions. Consistent with the pattern of Ca^{2+} influx, NbCNGC18 alone increased ROS products; however, when co-expressed with AVRblb2, it failed to activate ROS burst. In contrast, co-expression of NbCNGC18/20 and NbCNGC18/20/25 resulted in additive activation of ROS burst, although the presence of AVRblb2 attenuated ROS production (Fig. 2-17 B). Interestingly, co-expression of NbCNGC18/20/25 and AVRblb2 led to an accumulation of ROS compared to the control condition (Fig. 2-17 B, filled green dots), suggesting that NbCNGC25 may influence ROS burst in conjunction with other CNGCs, including NbCNGC18.

Furthermore, pathogen infection assays were conducted to investigate the effect of NbCNGCs on pathogenic resistance. Leaves co-expressing NbCNGC18, NbCNGC20, and NbCNGC25 exhibited increased resistance to *P. infestans*, indicating that the overexpression of multiple NbCNGCs and subsequent Ca^{2+} influx enhanced PTI (Fig. 2-18). However, leaves expressing AVRblb2 showed increased susceptibility when NbCNGC12, NbCNGC20 or multiple CNGCs were co-expressed compared to the GST control, indicating that AVRblb2 could suppress the resistance induced by overexpression of NbCNGCs. This observation was consistent with the results of ROS assay (Fig. 2-17 A and 2-17 B). Silencing NbCNGC18 using RNAi constructs did not diminish the virulent activity of AVRblb2, suggesting functional redundancy

between NbCNGC18, NbCNGC19, and NbCNGC20, or a combination thereof (Fig. 2-17 C and 2-17 D). However, AVRblb2 failed to enhance susceptibility to *P. infestans* in the leaves of NbCNGC18, NbCNGC20, and NbCNGC25-silenced plants (Fig. 2-17 C and 2-17 D). These results suggest that the presence of multiple CNGCs has an additive effect in boosting immune defense against pathogens through the formation of heteromeric complexes involving NbCNGC18. Overall, AVRblb2 disrupts PTI response to enhance pathogen virulence by regulating NbCNGC18.

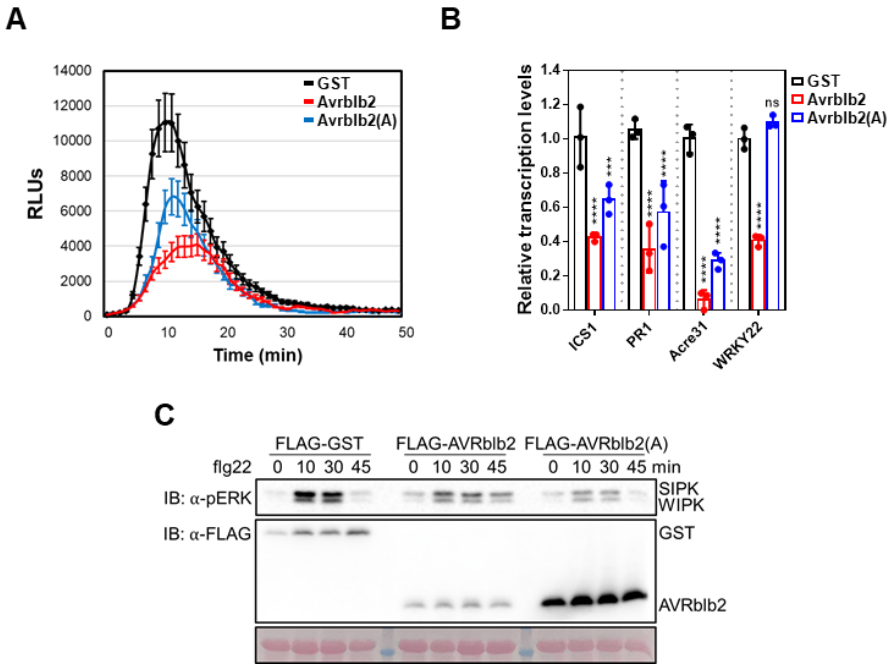

Figure 2-16. AVRblb2 suppresses the PTI response. (A) The flg22-induced ROS burst is significantly reduced in AVRblb2 expressed leaves. ROS burst was measured using a chemi-luminescence assay for 50 minutes after treatment with 1 μM flg22. The results shown are the mean of six replicates ± SE (n=6). (B) Transcriptional induction of defense related genes by flg22 in AVRblb2- or AVRblb2(A)-expressed leaves. The gene expression of *NbICS1*, *NbPR1*, *NbAcre31* and *NbWRKY22* in *N. benthamiana* was measured using qRT-PCR after flg22 treatment. Values are means ± SD (n=3, compared to GST expressed conditions). The significance was determined using a t-test; ****, P < 0.0001; ***, P<0.001; ns, not significant. The graph shown is

representative of three biological replicates. (C) Activation of MPK in *N. benthamiana* expressing AVRblb2 or AVRblb2(A) in response to flg22 treatment. Following flg22 treatment, samples were collected in a time series. Immunoblot analysis using an anti-pERK antibody reveals the kinetics of kinase activation.

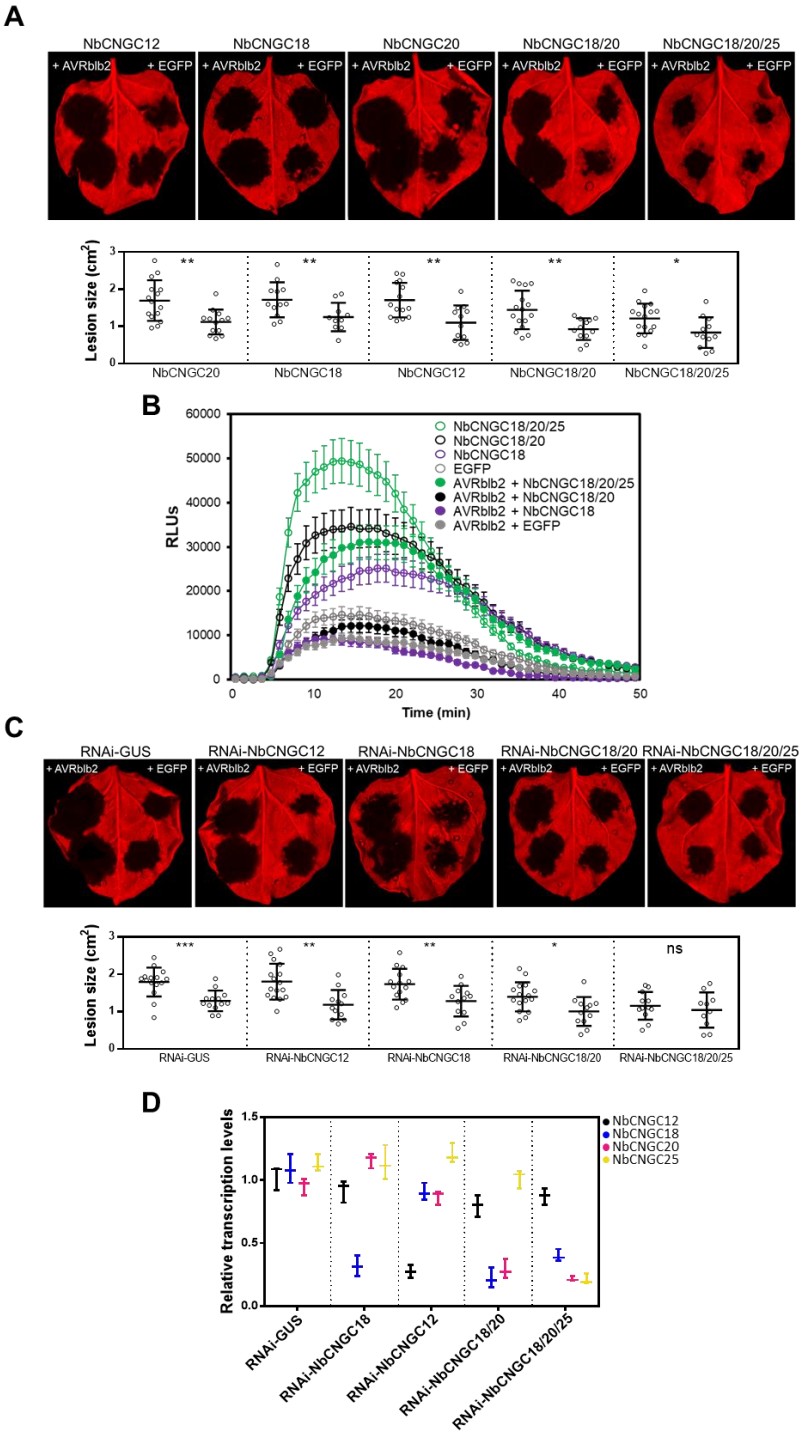
A
NbCNGC12
NbCNGC18
NbCNGC20
NbCNGC18/20
NbCNGC18/20/25
+ AVRblb2
+ EGFP
Lesion size (cm²)
NbCNGC20
NbCNGC18
NbCNGC12
NbCNGC18/20
NbCNGC18/20/25
B
RLUs
Time (min)
NbCNGC18/20/25
NbCNGC18/20
NbCNGC18
EGFP
AVRblb2 + NbCNGC18/20/25
AVRblb2 + NbCNGC18/20
AVRblb2 + NbCNGC18
AVRblb2 + EGFP
C
RNAi-GUS
RNAi-NbCNGC12
RNAi-NbCNGC18
RNAi-NbCNGC18/20
RNAi-NbCNGC18/20/25
ns
D
Relative transcription levels
NbCNGC12
NbCNGC18
NbCNGC20
NbCNGC25

Figure 2-17. AVRblb2 promotes the virulence of *P. infestans* by regulating the activity of multiple NbCNGCs. (A) *P. infestans* infection assay on *N. benthamiana* leaves expressing EGFP or AVRblb2 along with CNGCs. In the NbCNGCs-expressing *N. benthamiana*, 3FLAG-AVRblb2 was expressed on one-half of leaf and EGFP expressed on the other half as a negative control. EGFP was used as negative control. *P. infestans* was inoculated on the detached leaves after one day after infiltration. The photographs were taken six days after the infection (upper panel). The corresponding lesion sizes are shown in the lower panel. The lesion size was measured at 6 dpi. The values are the mean ± SD of the three biological replicates (n=15). The significance was determined using a t-test. **, $P < 0.01$; *, $P < 0.05$. (B) Flg22-induced ROS burst in NbCNGCs-overexpressed (unfilled dots) and NbCNGCs and AVRblb2-expressed (filled dots) plants. EGFP was used as a negative control. ROS burst was measured using chemi-luminescence assay for 50 minutes after treatment with 1 μM flg22. The results shown are the mean of six replicates ± SE (n=6). (C) *P. infestans* infection assay on *N. benthamiana* leaves expressing EGFP or AVRblb2 under NbCNGCs-silenced conditions. In the RNAi-NbCNGCs expressing *N. benthamiana*, 3FLAG-AVRblb2 was expressed on one-half of the leaf and EGFP was expressed on the other half as a negative control. EGFP was used as negative control. RNAi-GUS was used as a

negative control for the RNAi construct. *P. infestans* was inoculated on the detached leaves after one day after infiltration. The photographs were taken at six days after the infection (upper panel). Corresponding lesion sizes were shown in lower panel respectively. The lesion size was measured at 6 dpi. The values are the mean ± SD of the three biological replicates (n=15). The significance was determined using a t-test. ***, $P < 0.001$; **, $P < 0.01$; *, $P < 0.05$; ns, not significant. (D) Quantitative RT-PCR analysis of NbCNGCs gene expression in RNAi-plants. *NbActin* was used as an internal standard. The results shown are the mean ± SD of three technical replicates.

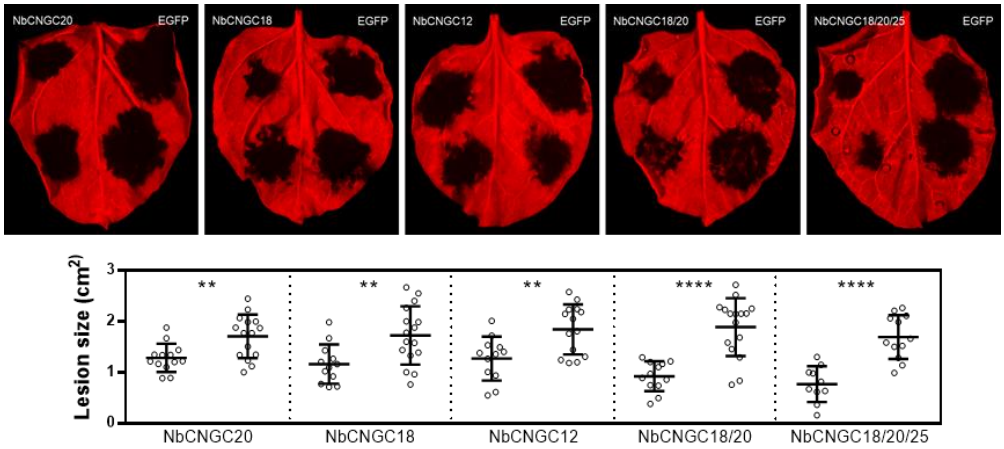

Figure 2-18. NbCNGCs additively enhance resistance against *P. infestans*. Assay of *P. infestans* infection on *N. benthamiana* leaves expressing indicated NbCNGCs (upper panel). NbCNGCs were expressed on one-half of the *N. benthamiana* leave and EGFP expressed on the other half as a negative control. *P. infestans* was inoculated on the detached leaves after one day after infiltration. Pictures were taken at 6 days after infection. The box plots show the lesion size of inoculation sites shown in upper panel. Lesion size was measured at 6 dpi. Values are mean ± SD of the three biological replicates (n=18). Significance was determined using a t-test. ****, $P < 0.0001$; **, $P<0.01$.

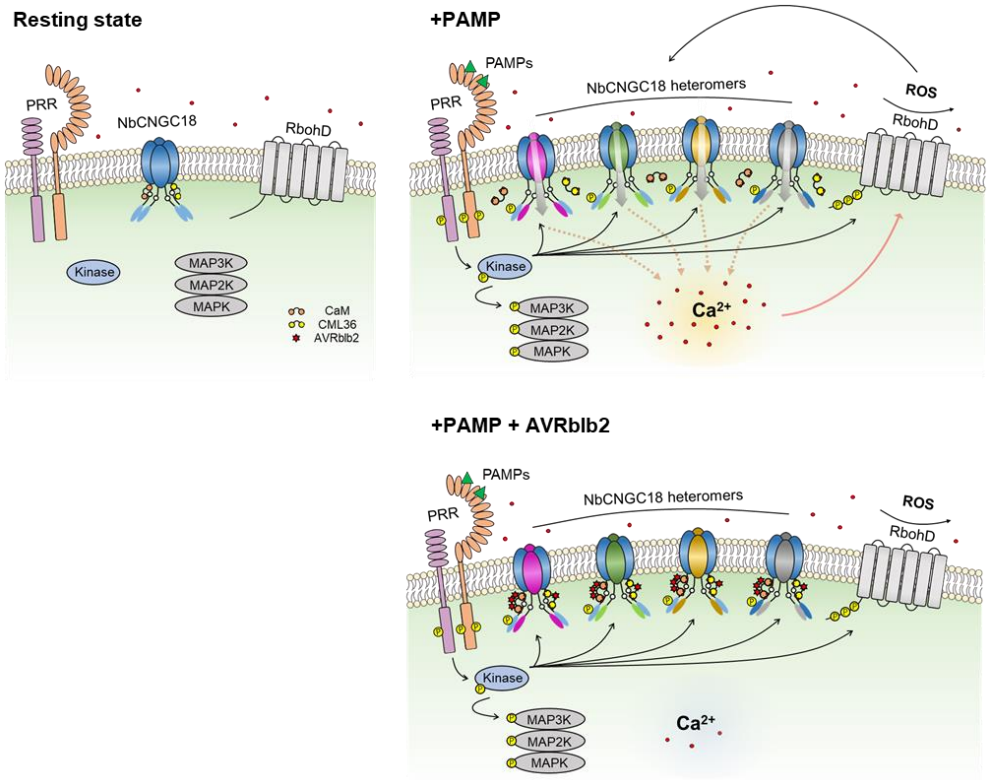

Figure 2-19. Proposed model for the role of AVRblb2 and NbCNGC18 heteromeric complex in the calcium-based PTI signaling pathway in *N. benthamiana*. In the resting state, NbCNGC18 mostly forms homomeric complex to sustain $[Ca^{2+}]_{cyt}$ homeostasis. After PAMP recognition, NbCNGC18 forms a heteromeric complex with several different NbCNGCs to increase $[Ca^{2+}]_{cyt}$ and subsequently activates PTI. However, against PTI response, AVRblb2 targets a subset of NbCNGCs (CNGC2, CNGC18, CNGC19, and CNGC20) via calcium sensors and forms AVRblb2-

CaM/CML36-CNGC complexes to suppresses PAMP-induced Ca^{2+} influx by blocking the dissociation between CaM/CML36 and NbCNGC18.

DISCUSSION

Rapid elevation of cytosolic free Ca^{2+} levels in plant cells is an important early event in immune signaling. Previous research found that calcium sensors regulate CNGCs, which function as calcium channels for Ca^{2+} influx through the plasma membrane in response to PAMP (Tian et al., 2019; Yoshioka et al., 2006; Yu et al., 2019). However, it is unknown how pathogen effectors disrupt calcium signaling to suppress PTI. Here, we shown that the *P. infestans* effector AVRblb2 targeted NbCNGCs via the Ca^{2+} sensors CaM and CML36 to disrupt the PTI response by suppressing calcium influx, allowing successful colonization of the pathogen in host plant. AVRblb2 and all tested AVRblb2 homologs interacted with NbCNGC18-CT in the presence of calcium and suppressed PAMP-induced calcium influx, indicating that they were functionally redundant with respect to *P. infestans* virulence.

CaM and CML36 likely have opposite roles in calcium channel regulation and calcium signaling in response to pathogens. CaM is released from NbCNGC18 in response to flg22 treatment, likely leading to the NbCNGC18 activation and increased calcium influx. However, in the presence of flg22, AVRblb2 increased the binding affinity of CaM for NbCNGC18 and disrupted

their dissociation, resulting in suppressed calcium influx (Fig. 2-19). In contrast, CML36 increased calcium influx while interacting primarily with AVRblb2 under normal conditions. AVRblb2 family members are recognized by the broad-spectrum resistance protein Rpi-blb2, causing hypersensitive responses (HRs). We confirmed an enhanced Rpi-blb2-AVRblb2-mediated HR cell death when CML36 was co-expressed (data not shown), indicating that CML36 may monitor the interactions between AVRblb2 and CaM; upon recognition by Rpi-blb2, robust calcium influx leads to HR. However, how Rpi-blb2 recognizes AVRblb2 activity during calcium signaling needs further investigation.

Plant CNGCs form heteromeric complexes, and the combination of CNGCs varies depending on the signal. A previous study demonstrated heterotetrameric channel formation by AtCNGC2-AtCNGC4, AtCNGC7 or AtCNGC8-AtCNGC18 and AtCNGC19-AtCNGC20 *in planta*. However, it is unclear whether those CNGC-CNGC combinations are constitutive or dynamically regulated, depending on the context (Chin et al., 2013; Pan et al., 2019; Zhao et al., 2021). In this study, we discovered that NbCNGC18 existed as a homomeric complex in the resting state but associated with other specific CNGCs in response to PTI. Furthermore, AVRblb2 interacted with NbCNGC18 to suppress calcium channel activity, disrupting the PTI response.

AVRblb2 still exhibited virulence-enhancing activity under NbCNGC18-silenced conditions, implying that NbCNGC19 and NbCNGC20, which interact with AVRblb2, likely share functional redundancy with NbCNGC18. Indeed, AVRblb2 appeared to lose its virulence-enhancing activity when NbCNGC18, NbCNGC20, and NbCNGC25 were silenced. However, we cannot rule out the possibility that other effectors work with yet-identified other calcium channels in the immune response. Given the expanded number of CNGC, CaM and CML gene family members in *N. benthamiana*, the vast array of CNGC combinations with calcium sensors could explain the generation of the almost unlimited number of stimulus-specific Ca^{2+} oscillations.

In summary, in the current study, we identified members of the defense-related Ca^{2+} channels as targets of a pathogen effector (AVRblb2) in *N. benthamiana* and developed a working mechanism for PAMP perception. Furthermore, we deciphered the role of this *P. infestans* effector in suppressing PAMP-induced Ca^{2+} influx during early PTI responses. Our findings could have far-reaching implications for future studies of Ca^{2+} signaling in plant immunity and understanding a pathogen's strategy for manipulating early plant immune responses.

REFERENCES

Boller, T. and G. Felix (2009). "A renaissance of elicitors: perception of microbe-associated molecular patterns and danger signals by pattern-recognition receptors." Annu. Rev. Plant Biol. 60: 379-406.

Bozkurt, T. O., S. Schornack, J. Win, T. Shindo, M. Ilyas, R. Oliva, L. M. Cano, A. M. Jones, E. Huitema, R. A. van der Hoorn and S. Kamoun (2011). “Phytophthora infestans effector AVRblb2 prevents secretion of a plant immune protease at the haustorial interface." Proc. Natl. Acad. Sci. U.S.A. 108(51): 20832-20837.

Brost, C., T. Studtrucker, R. Reimann, P. Denninger, J. Czekalla, M. Krebs, B. Fabry, K. Schumacher, G. Grossmann and P. Dietrich (2019). "Multiple cyclic nucleotide-gated channels coordinate calcium oscillations and polar growth of root hairs." Plant J. 99(5): 910-923.

Chin, K., T. A. DeFalco, W. Moeder and K. Yoshioka (2013). "The Arabidopsis cyclic nucleotide-gated ion channels AtCNGC2 and AtCNGC4 work in the same signaling pathway to regulate pathogen defense and floral transition." Plant Physiol. 163(2): 611-624.

Chung, E., E. Seong, Y. C. Kim, E. J. Chung, S. K. Oh, S. Lee and D. Choi (2004). "A Method of High Frequency Virus-induced Gene Silencing in Chili Pepper." Mol. Cells 17(2): 377-380.

Cui, H., K. Tsuda and J. E. Parker (2015). "Effector-triggered immunity: from pathogen perception to robust defense." Annu. Rev. Plant Biol. 66: 487-511.

Curran, A., I. F. Chang, C. L. Chang, S. Garg, R. M. Miguel, Y. D. Barron, Y. Li, S. Romanowsky, J. C. Cushman, M. Gribskov, A. C. Harmon and J. F. Harper (2011). "Calcium-dependent protein kinases from Arabidopsis show substrate specificity differences in an analysis of 103 substrates." Front. Plant Sci. 2: 36.

DeFalco, T. A., C. B. Marshall, K. Munro, H. G. Kang, W. Moeder, M. Ikura, W. A.

Snedden and K. Yoshioka (2016). "Multiple Calmodulin-Binding Sites Positively and Negatively Regulate Arabidopsis CYCLIC NUCLEOTIDE-GATED CHANNEL12." Plant Cell 28(7): 1738-1751.

Dietrich, P., W. Moeder and K. Yoshioka (2020). "Plant Cyclic Nucleotide-Gated Channels: New Insights on Their Functions and Regulation." Plant Physiol. 184(1): 27-38.

Du, Y., X. Chen, Y. Guo, X. Zhang, H. Zhang, F. Li, G. Huang, Y. Meng and W. Shan (2021). "Phytophthora infestans RXLR effector PITG20303 targets a potato MKK1 protein to suppress plant immunity." New Phytol. 229(1): 501-515.

Fischer, C., T. A. DeFalco, P. Karia, W. A. Snedden, W. Moeder, K. Yoshioka and P. Dietrich (2017). "Calmodulin as a Ca2+-Sensing Subunit of Arabidopsis Cyclic Nucleotide-Gated Channel Complexes." Plant Cell Physiol. 58(7): 1208-1221.

Grant, M., I. Brown, S. Adams, M. Knight, A. Ainslie and J. Mansfield (2000). "The RPM1 plant disease resistance gene facilitates a rapid and sustained increase in cytosolic calcium that is necessary for the oxidative burst and hypersensitive cell death." Plant J. 23(4): 441-450.

Guo, M., P. Kim, G. Li, C. G. Elowsky and J. R. Alfano (2016). "A Bacterial Effector Co-opts Calmodulin to Target the Plant Microtubule Network." Cell Host Microbe 19(1): 67-78.

Heese, A., D. R. Hann, Gimenez-Ibanez, J. S., A. M., K. He, J. Li and J. P. Rathjen (2007). "The receptor-like kinase SERK3/BAK1 is a central regulator of innate immunity in plants." Proc. Natl. Acad. Sci. U.S.A. 104(29): 12217-12222.

Jones, J. D. and J. L. Dangl (2006). "The plant immune system." Nature 444(7117): 323-329.

Kadota, Y., T. W. H. Liebrand, Y. Goto, J. Sklenar, P. Derbyshire, F. L. H. Menke, M. A. Torres, A. Molina, C. Zipfel, G. Coaker and K. Shirasu (2019). "Quantitative phosphoproteomic analysis reveals common regulatory mechanisms between effector- and PAMP-triggered immunity in plants." New Phytol. 221(4): 2160-2175.

Ladwig, F., R. I. Dahlke, N. Stuhrwohldt, J. Hartmann, K. Harter and M. Sauter (2015). "Phytosulfokine Regulates Growth in Arabidopsis through a Response Module at the Plasma Membrane That Includes CYCLIC NUCLEOTIDE-GATED CHANNEL17, H+-ATPase, and BAK1." Plant Cell 27(6): 1718-1729.

Luker, G. D. and K. E. Luker (2011). "Luciferase protein complementation assays for bioluminescence imaging of cells and mice." Methods Mol. Biol. 680: 29-43.

Moeder, W., V. Phan and K. Yoshioka (2019). "Ca(2+) to the rescue - Ca(2+)channels and signaling in plant immunity." Plant Sci. 279: 19-26.

Naveed, Z. A., S. Bibi and G. S. Ali (2019). "The Phytophthora RXLR Effector Avrblb2 Modulates Plant Immunity by Interfering With Ca(2+) Signaling Pathway." Front. Plant Sci. 10: 374.

Oh, S. K., C. Young, M. Lee, R. Oliva, T. O. Bozkurt, L. M. Cano, J. Win, J. I. Bos, H. Y. Liu, M. van Damme, W. Morgan, D. Choi, E. A. Van der Vossen, V. G. Vleeshouwers and S. Kamoun (2009). "In planta expression screens of Phytophthora infestans RXLR effectors reveal diverse phenotypes, including activation of the Solanum bulbocastanum disease resistance protein Rpi-blb2." Plant Cell 21(9): 2928-2947.

Oliva, R. F., L. M. Cano, S. Raffaele, J. Win, T. O. Bozkurt, K. Belhaj, S. K. Oh, M. Thines and S. Kamoun (2015). "A Recent Expansion of the RXLR Effector Gene Avrblb2 Is Maintained in Global Populations of Phytophthora infestans Indicating Different Contributions to Virulence." Mol. Plant-Microbe Interact. 28(8): 901-912.

Pan, Y., X. Chai, Q. Gao, L. Zhou, S. Zhang, L. Li and S. Luan (2019). "Dynamic Interactions of Plant CNGC Subunits and Calmodulins Drive Oscillatory Ca(2+) Channel Activities." Dev. Cell 48(5): 710-725 e715.

Rao, X., X. Huang, Z. Zhou and X. Lin (2013). "An improvement of the 2ˆ (–delta delta CT) method for quantitative real-time polymerase chain reaction data analysis." Biostat. bioinforma. biomath. 3(3): 71.

Saand, M. A., Y. P. Xu, W. Li, J. P. Wang and X. Z. Cai (2015). "Cyclic nucleotide gated

channel gene family in tomato: genome-wide identification and functional analyses in disease resistance." Front. Plant Sci. 6: 303.

Tamura, K., D. Peterson, N. Peterson, G. Stecher, M. Nei and S. Kumar (2011). "MEGA5: molecular evolutionary genetics analysis using maximum likelihood, evolutionary distance, and maximum parsimony methods." Mol. Biol. Evol. 28(10): 2731-2739.

Tian, W., C. Hou, Z. Ren, C. Wang, F. Zhao, D. Dahlbeck, S. Hu, L. Zhang, Q. Niu, L. Li, B. J. Staskawicz and S. Luan (2019). "A calmodulin-gated calcium channel links pathogen patterns to plant immunity." Nature 572(7767): 131-135.

Tian, W., C. Wang, Q. Gao, L. Li and S. Luan (2020). "Calcium spikes, waves and oscillations in plant development and biotic interactions." Nat. Plants 6(7): 750-759.

Wang, J., X. Liu, A. Zhang, Y. Ren, F. Wu, G. Wang, Y. Xu, C. Lei, S. Zhu, T. Pan, Y. Wang, H. Zhang, F. Wang, Y. Q. Tan, Y. Wang, X. Jin, S. Luo, C. Zhou, X. Zhang, J. Liu, S. Wang, L. Meng, Y. Wang, X. Chen, Q. Lin, X. Zhang, X. Guo, Z. Cheng, J. Wang, Y. Tian, S. Liu, L. Jiang, C. Wu, E. Wang, J. M. Zhou, Y. F. Wang, H. Wang and J. Wan (2019). "A cyclic nucleotide-gated channel mediates cytoplasmic calcium elevation and disease resistance in rice." Cell Res. 29(10): 820-831.

Whisson, S. C., P. C. Boevink, L. Moleleki, A. O. Avrova, J. G. Morales, E. M. Gilroy, M. R. Armstrong, S. Grouffaud, P. van West, S. Chapman, I. Hein, I. K. Toth, L. Pritchard and P. R. Birch (2007). "A translocation signal for delivery of oomycete effector proteins into host plant cells." Nature 450(7166): 115-118.

Xu, G., W. Moeder, K. Yoshioka and L. Shan (2022). "A Tale of Many Families: Calcium Channels in Plant Immunity." Plant Cell 34(5): 1551-1567.

Yoshioka, K., W. Moeder, H. G. Kang, P. Kachroo, K. Masmoudi, G. Berkowitz and D. F. Klessig (2006). "The chimeric Arabidopsis CYCLIC NUCLEOTIDE-GATED ION CHANNEL11/12 activates multiple pathogen resistance responses." Plant Cell 18(3): 747-763.

Yu, X., G. Xu, B. Li, L. de Souza Vespoli, H. Liu, W. Moeder, S. Chen, M. V. V. de Oliveira, S. Ariadina de Souza, W. Shao, B. Rodrigues, Y. Ma, S. Chhajed, S. Xue, G. A. Berkowitz, K. Yoshioka, P. He and L. Shan (2019). "The Receptor Kinases BAK1/SERK4 Regulate Ca(2+) Channel-Mediated Cellular Homeostasis for Cell Death Containment." Cur. Biol. 29(22): 3778-3790 e3778.

Yuan, M., Z. Jiang, G. Bi, K. Nomura, M. Liu, Y. Wang, B. Cai, J. M. Zhou, S. Y. He and X. F. Xin (2021). "Pattern-recognition receptors are required for NLR-mediated plant immunity." Nature 592(7852): 105-109.

Zhao, C., Y. Tang, J. Wang, Y. Zeng, H. Sun, Z. Zheng, R. Su, K. Schneeberger, J. E. Parker and H. Cui (2021). "A mis-regulated cyclic nucleotide-gated channel mediates cytosolic calcium elevation and activates immunity in Arabidopsis." New Phytol. 230(3): 1078-1094.

Zhao, Y., W. Liu, Y. P. Xu, J. Y. Cao and J. C. Braam, X. Z. (2013). "Genome-wide identification and functional analyses of calmodulin genes in Solanaceousspecies." BMC Plant Biol. 13(1): 1-15.

Zheng, X., H. McLellan, M. Fraiture, X. Liu, P. C. Boevink, E. M. Gilroy, Y. Chen, K. Kandel, G. Sessa, P. R. Birch and F. Brunner (2014). "Functionally redundant RXLR effectors from Phytophthora infestans act at different steps to suppress early flg22-triggered immunity." PLoS Pathog. 10(4): e1004057.

Zheng, X., N. Wagener, H. McLellan, P. C. Boevink, C. Hua, P. R. J. Birch and F. Brunner (2018). "Phytophthora infestans RXLR effector SFI5 requires association with calmodulin for PTI/MTI suppressing activity." New Phytol. 219(4): 1433-1446.

Zhou, L., W. Lan, Y. Jiang, W. Fang and S. Luan (2014). "A calcium-dependent protein kinase interacts with and activates a calcium channel to regulate pollen tube growth." Mol. Plant 7(2): 369-376.

ABSTRACT IN KOREAN

식물은 다양한 병원균들에 의한 침입에 노출되어 있으며 진화를 통해 이를 방어하기 위한 물리적, 화학적 장벽을 발달시켜왔다. 이에 대응하여 여러 병원균들은 식물의 면역 장벽을 무너뜨리기 위해 이펙터 단백질을 분비하도록 진화되었으며 이는 식물 세포에서 유도되는 면역반응을 저해하며 동시에 병원균의 생장에 필요한 영양분을 얻어 성공적으로 감염을 시키기 위함이다. 감자역병균은 전세계적으로 심각한 역병을 일으키는 난균류로써 반활물기생 생활사를 가지는 것으로 알려져 있다. 감자역병균은 감염 시 적절한 생활사의 운용을 위해 수백 개의 RXLR 이펙터 단백질을 분비 한다고 알려져 있다. 이에 현재까지 RXLR 이펙터들의 작용기작 또는 감자역병균의 생활사에 있어서 RXLR 이펙터들의 역할 등을 이해하고자 많은 연구가 이루어지고 있다. 해당 연구에서는 감자역병균 감염 시 활물기생에서 사물기생 단계로 전환되는 때에 식물 세포 내 핵 인의 크기가 비정상적으로 증가하는 현상을 관찰하였다. 이와 유사하게 감자역병균 이펙터 중 Pi23226 RXLR 이펙터 과발현 시 기주 식물인 담배 세포의 핵 인의 크기를 비정상적으로 증가시키고 세포사멸을 일으키는 것을 확인할 수 있었다. 이를 통해 Pi23226이 핵 인에서 특정 단백질과 결합하여 작용할 가능성을 생각해 볼 수 있었으며, Pi23226이 핵 인에서 25r RNA 전구체와 직접적으로 결합하여 정상적인 rRNA 형성과정을 저해하고 최종적으로 핵 인 스트레스를 유발하는 것을 실험적으로 확인하였다. 이와 동시에 Pi23226이 세포질에서 리보솜 단백질과도 결합하여 전체적인 단백질 합성과정을 저해하는 것 또한 확인할 수 있었다. 또한

병 접종 실험을 통해 Pi23226이 감자역병균의 병원성을 유의미하게 증가시키는 것을 결과를 얻을 수 있었고 이는 Pi23226에 의해 유도되는 스트레스 및 세포사멸 반응이 감자역병균의 병원성에 긍정적으로 작용한다고 해석할 수 있다. 한편, 감자역병균 감염 시에 세포 막 부근에서 병원균을 감지했을 때 순간적으로 유도되는 칼슘 이온농도의 증가는 식물의 초기 면역반응에 있어서 매우 중요하다고 알려져 있다. 해당 연구에서는 기주 식물인 담배에 Pi20300 이펙터를 과발현 시킬 경우 병원균 감지 시에 유도되는 칼슘이온의 증가가 억제되고 나아가 하위로 유도되는 저항성반응까지 저해되는 것을 관찰 할 수 있었다. 이에 Pi20300의 기능 연구를 위한 기주 세포 내 타겟 단백질 스크리닝이 진행 되었고 이를 통해 담배의 세포 막에 존재하는 칼슘 채널 단백질 CNGC18/19/20을 찾을 수 있었다. 또한 Pi20300이 CaM 및 CML 단백질 의존적으로 칼슘 채널 단백질과 결합하고 결과적으로 CNGC의 활성을 조절할 수 있음을 실험적으로 확인하였다. 추가적으로 담배에서는 CNGC18의 경우 병원균을 감지했을 때 여러 다른 CNGC들과 복합체를 이루는 것을 확인할 수 있었으며, 접종 실험을 통해 해당 CNGC 복합체들이 Pi20300에 의한 감자역병균의 병원성 증가에 중요하다는 것을 확인하였다. 위의 결과들을 통하여 기존에 보고되지 않았던 감자역병균 감염 시 기주 세포의 변화들을 밝힐 수 있었다. 또한 해당 결과들을 통하여 감자역병균 RXLR 이펙터들의 새로운 기작에 대한 정보를 제공함으로써 감염 시 다양한 이펙터들의 역할에 대한 이해도를 높이는 데 기여하고, 더 나아가 이를 활용한 식물의 병 저항성 연구에도 이바지할 수 있을 것으로 기대된다.